The effects of environment on catch and effort for the commercial fishery of Lake Winnipeg, Canada

by

Jeffery Duncan Speers

A Thesis submitted to the Faculty of Graduate Studies of

The University of Manitoba

in partial fulfillment of the requirements of the degree of

MASTER OF SCIENCE

Department of Zoology

University of Manitoba

Winnipeg

Abstract

Environmental factors affect fish distribution and fisher behavior. These factors are seldom included in stock assessment models, resulting in potentially inaccurate fish abundance estimates. This study determined the impact of these factors using the commercial catch rate of sauger (*Sander canadensis*) and walleye (*Sander vitreus*) in Lake Winnipeg by: (1) the use of satellite data to monitor turbidity and its impact on catch via simple linear regression and (2) the effect of environment on catch and effort using generalized linear models. No statistically significant relationship was found between catch and turbidity; a result which may be due to small sample sizes, the fish species' examined, and variable turbidity at depth. Decreased effort was correlated with harsh weather and decreased walleye catch. Increased walleye catch was correlated with low temperature and low Red River discharge. Increased sauger catch was correlated with high temperature, high cloud opacity, and average Red River discharge.

Acknowledgements

My gratitude to those who have provided data and insight: Bruce Benson, Dave Bergunder and Ellen Smith at the Freshwater Fish Marketing Corporation, Warren Coughlan and Walt Lysack at Manitoba Conservation, Terry Miles at Manitoba Hydro, and Ken Stewart. I am especially grateful to my advisor, Darren Gillis, for his novel perspectives and excellent advice as well as to the rest of my committee members, Mark Abrahams and Norman Kenkel, for their input into this thesis.

This thesis was funded by a studentship awarded to myself by the Faculty of Science at the University of Manitoba and by a research grant provided to Darren Gillis from the Natural Sciences and Engineering Research Council of Canada.

Table of Contents

List of Tables

List of Figures

Chapter One: General Introduction

Spatial variation in the abundance of a particular species is often attributed to both spatial and temporal changes in the environment in which they exist (Ives and Klopfer 1997). This basic observation is not restricted to the terrestrial world; many studies have shown that the distributional patterns of fish are affected by numerous environmental variables such as water chemistry, nutrient concentration, wind speed, river inflows, temperature, light level, and suspended sediment load (Doan 1942; Mohr 1965; Walters and Collie 1988; Criddle et al. 1998; Pollard et al. 1998; Sundermeyer et al. 2005). For example, the incorporation of environmental variables into models which described the population dynamics of walleye pollock (*Theragra chalcogramma*) significantly improved their predictive power (Criddle et al. 1998). Similarly, European whitefish (*Coregonus lavaretus* L.) are thought to move into deeper water to avoid high temperatures and bright light levels (Mayr 2002). The impact of turbidity on aquatic ecosystems is of special concern, as the introduction of sediment into water bodies by human activities is widespread in North America and influences aquatic biota in many different ways (Pollard et al. 1998; Reid et al. 1999). Turbidity is often highly variable on both a spatial and temporal scale in lacustrine environments (Abrahams and Kattenfeld 1997).

In general, turbidity reduces the ability of fish to visually detect both predator and prey (Hayes et al. 1992; Abrahams and Kattenfeld 1997) by scattering light and consequently reducing the apparent contrast between objects and their background (Heege and Appenzeller 1998). In highly turbid waters, fish may congregate at the water's surface in order to increase their efficiency as visual predators at the risk of

exposing themselves to unfavorably high temperatures and an increased probability of depredation by visual predators (Doan 1942). For example, visual predators such as largemouth bass (*Micropterus salmoides*) (Kawamura and Kishimoto 2002) exhibited a reduction in encounter rates with piscine prey in turbid waters (Reid et al. 1999). In addition, predator avoidance behaviours such as schooling, startle, and escape responses are all reduced in turbid water (Reid et al. 1999). These same predator avoidance behaviours are also less effective in turbid water (Abrahams and Kattenfeld 1997; Reid et al. 1999). Thus it is not surprising that many fish species are known to avoid areas of high turbidity (Borgström et al. 1992; Dörgeloh 1995; Reid et al. 1999) with the exception of those who are adapted to turbid conditions (Lester et al. 2004).

The spatial variation observed in the distributional patterns of fish species resulting from these environmental factors is reflected in fisheries research when data derived from commercial catch records are used. For example, the efficiency of fishing gear is affected by environmental conditions such as turbidity and temperature (Borgström et al. 1992; Buijse et al. 1992). These apparent changes in production are often indistinguishable from changes in distribution (Walters and Collie 1988) or abundance. Surprisingly, this spatial variability is often ignored and this leads to inaccurate estimates of abundance (Walters and Collie 1988; Booth 2000). In addition, these fish assessment models rarely take into consideration the dynamic decisions of the fishers, who decide where, when, and how often fishing takes place (Salas and Gaertner 2004). The objective of this project was to determine the impact of the environment on both the effort allocation of the fishers and on the commercial catch rate of sauger (*Sander canadensis*) and walleye (*Sander vitreus*).

Walleye habitat is dependant upon lake bathymetry, thermocline depth, climate, and water clarity (Lester et al. 2004). A Secchi depth between 1-3 m is preferred as the fish are negatively phototrophic (Ryder 1977; Lester et al. 2004). This allows the fish to feed during the day, as opposed to the crepuscular or nocturnal feeding which occurs in less turbid waters (Vandenbyllaardt et al. 1991). Walleye are piscivores after their first year (Mathias and Li 1982). Sauger are similar in their habitat (Ryder 1977; Amadio et al. 2005) and diet requirements (Swenson and Smith 1976), although they prefer more turbid waters than walleye (Nelson and Walburg 1977). Both species are visual predators (Ali et al. 1977; Ryder 1977).

The water clarity values used for the prediction of changes in the catch rate of walleye and sauger were inferred from satellite imagery. Traditionally, ground-based monitoring methods were used to determine these values. However, these techniques are expensive and often sacrificed spatial coverage for greater temporal resolution (Kloiber et al. 2002). The use of satellite imagery for this purpose offers several advantages. The solar reflectance derived from satellite images is known to be correlated with many measures of water clarity, including turbidity (Heege and Appenzeller 1998; Kloiber et al. 2002). In addition to being more cost-effective than traditional methods, this technique also allows continuous examination of larger areas in comparison to ground-based methods (Cox et al. 1998; Kloiber et al. 2002).

The following chapter establishes the relationship between satellite reflectance and water clarity. The water clarity values are then examined for their ability to predict the catch rate of walleye and sauger. Chapter 3 examines the impact of meteorology on both the effort allocation of fishers and, once again, the catch rate of both species stated

previously. Chapter 4 summarizes the results of the previous two chapters and suggests some areas which would benefit from future study.

References

Abrahams, M., and Kattenfeld, M. 1997. The role of turbidity as a constraint on predator-prey interactions in aquatic environments. Behav. Ecol. Sociobiol. **40**: 169-174.

Ali, M.A., Ryder, R.A., and Anctil, M. 1977. Photoreceptors and visual pigments as related to behavioral responses and preferred habitats of perches (*Perca* spp.) and pikeperches (*Stizostedion* spp.). J. Fish. Res. Board Can. **34**: 1475-1480.

Amadio, C.J., Hubert, W.A., Johnson, K., Oberlie, D., and Dufek, D. 2005. Factors affecting the occurrence of saugers in small, high-elevation rivers near the western edge of the species' natural distribution. T. Am. Fish. Soc. **134**: 160-171.

Booth, A.J. 2000. Incorporating the spatial component of fisheries data into stock assessment models. ICES J. Mar. Sci. **57**: 858-865.

Borgström, R., Brabrand, Å., and Solheim, J.T. 1992. Effects of siltation on resource utilization and dynamics of allopatric brown trout, *Salmo trutta*, in a reservoir. Environ. Biol. Fishes **34**: 247-255.

Buijse, A.D., Schaap, L.A., and Bult, T.P. 1992. Influence of water clarity on the catchability of six freshwater fish species in bottom trawls. Can. J. Fish. Aquat. Sci. **49**: 885-893.

Cox, R.M. Jr., Forsythe, R.D., Vaughan, G.E., and Olmsted, L.L. 1998. Assessing water quality in Catawba River reservoirs using Landsat thematic mapper satellite data. Lake and Reserv. Manage. **14**: 405-416.

Criddle, K.R., Herrmann, M., Greenberg, J.A., and Feller, E.M. 1998. Climate fluctuation and revenue maximization in the eastern Bering Sea fishery for walleye pollock. N. Am. J. Fish. Manage. **18**: 1-10.

Doan, K.H. 1942. Some meteorological and limnological conditions as factors in the abundance of certain fishes in Lake Erie. Ecol. Monogr. **12**: 293-314.

Dörgeloh, W.G. 1995. Fish distribution in relation to turbidity gradients in a man-made, Sterkfontein dam (South Africa). Water S. A. **21**: 95-99.

Hayes, J.W., Rutledge, M.J., Chisnall, B.L., and Ward, F.J. 1992. Effects of elevated turbidity on shallow lake fish communities. Environ. Biol. Fishes. **35**: 149-168.

Heege, T., and Appenzeller, A.R. 1998. Correlations of large-scale patterns of turbidity and pelagic fish biomass using satellite and acoustic methods. Arch. Hydrobiol. Spec. Issues Advanc. Limnol. **53**: 489-503.

Ives, A.R., and Klopfer, E.D. 1997. Spatial variation in abundance created by stochastic temporal variation. Ecology **78**: 1907-1913.

Kawamura, G., and Kishimoto, T. 2002. Color vision, accommodation and visual acuity in the largemouth bass. Fisheries Sci. **68**: 1041-1046.

Kloiber, S.M., Brezonik, P.L., and Bauer, M.E. 2002. Application of Landsat imagery to regional-scale assessments of lake clarity. Water Res. **36**: 4330-4340.

Lester, N.P., Dextrase, A.J., Kushneriuk, R.S., Rawson, M.R., and Ryan, P.A. 2004. Light and temperature: Key factors affecting walleye abundance and production. T. Am. Fish. Soc. **133**: 588-605.

Mathias, J.A., and Li, S. 1982. Feeding habits of walleye larvae and juveniles: Comparative laboratory and field studies. T. Am. Fish. Soc. **111**: 722-735.

Mayr, C. 2002. The effect of water turbidity on distribution and feeding success of European whitefish (*Coregonus lavaretus* L.). Arch. Hydrobiol. Spec. Issues Advanc. Limnol. **57**: 265-275.

Mohr, H. 1965. Changes in the behaviour of fish due to environment and motivation and their influence on fishing. ICNAF Spec. Publ. **6**: 775-779.

Nelson, W.R., and Walburg, C.H. 1977. Population dynamics of yellow perch (*Perca flavescens*), sauger (*Stizostedion canadense*), and walleye (*S. vitreum vitreum*) in four main stem Missouri River reservoirs. J. Fish. Res. Board Can. **34**: 1748-1763.

Pollard, A.I., González, M.J., Vanni, M.J., and Headworth, J.L. 1998. Effects of turbidity and biotic factors on the rotifer community in an Ohio reservoir. Hydrobiologia **387/388**: 215-223.

Reid, S.M., Fox, M.G., and Whillans, T.H. 1999. Influence of turbidity on piscivory in largemouth bass (*Micropterus salmoides*). Can. J. Fish. Aquat. Sci. **56**: 1362-1369.

Ryder, R.A. 1977. Effects of ambient light variations on behavior of yearling, subadult, and adult walleyes (*Stizostedion vitreum vitreum*). J. Fish. Res. Board Can. **34**: 1481-1491.

Salas, S., and Gaertner, D. 2004. The behavioural dynamics of fishers: Management implications. Fish and Fisheries **5**: 153-167.

Sundermeyer, M.A., Rothschild, B.J., and Robinson, A.R. 2005. Using commercial landings data to identify environmental correlates with distributions of fish stocks. Fish. Oceanogr. **14**: 47-63.

Swenson, W.A., and Smith, L.L. Jr. 1976. Influence of food competition, predation, and cannibalism on walleye (*Stizostedion vitreum vitreum*) and sauger (*S. canadense*) populations in Lake of the Woods, Minnesota. J. Fish. Res. Board Can. **33**:

1946-1954.

Vandenbyllaardt, L., Ward, F.J., Braekevelt, C.R., and McIntyre, D.B. 1991. Relationships between turbidity, piscivory, and development of the retina in juvenile walleyes. T. Am. Fish. Soc. **120**: 382-390.

Walters, C.J., and Collie, J.S. 1988. Is research on environmental factors useful to fisheries management? Can. J. Fish. Aquat. Sci. **45**: 1848-1854.

Chapter Two: Influences of Satellite Image-Derived Turbidity on Catch

Abstract

The concentration of suspended sediment is known to affect the distribution of aquatic organisms. The study presented in this chapter used satellite reflectance data to monitor changes in turbidity and investigated its affects on the commercial catch rate of sauger and walleye in the south basin of Lake Winnipeg. The relationship between turbidity and the catch rate of both species was modeled using simple linear regression. No consistent statistically significant relationship between catch per unit effort and the length or complexity of the turbid/clear water boundary was found for either species. This result was attributed to small sample sizes and the nature of the fish species' examined, as well as variation in the measurements of water clarity, environmental conditions, backscattering from land, and the lack of a universal algorithm dictating the relationship between reflectance and turbidity. Variable turbidity at depth may have also hidden the relevant turbidity fronts from view.

2.1 Introduction

Many components of the aquatic environment are known to affect the distribution of aquatic organisms. Among the most important of these are differences in temperature, light, and suspended solid concentration (Ives and Klopfer 1997; Kling 1998; Pollard et al. 1998). Historically, these properties of water have been monitored using ground-based methods. Because of the high cost associated with these methods, spatial coverage is frequently sacrificed in favor of higher temporal coverage (Cox et al. 1998; Kloiber et al. 2002). Similarly, the historic use of satellites has been generally restricted to land-based and oceanographic disciplines (Cox et al. 1998; Miller and McKee 2004). However, the use of satellite data for monitoring lakes has several advantages, including lower cost, greater spatial coverage, and the examination of water parameters as a continuum both regionally and within the same water body (Cox et al. 1998; Kloiber et al. 2002). Specifically, the solar radiance reflectance measured by satellites is known to be correlated with several measures of water clarity, including humic color, suspended solids, and Secchi depth (Kloiber et al. 2002). This study used the solar radiance reflectance (abbreviated to 'reflectance') measured by the Moderate Resolution Imaging Spectroradiometer - Terra (abbreviated as 'MODIS') satellite to calculate another measure of water clarity: turbidity. Changes in the spatial and temporal gradients of turbidity as dictated by the satellite were then compared to fluctuations in fish catch rate.

Turbidity is defined as the cloudiness of water resulting from the intense scattering of light by fine particles (Davies-Colley and Smith 2001). Increases in turbidity affect the light regime of aquatic environments in two ways; increasing light attenuation and reducing contrast (De Robertis et al. 2003). However, water clarity is often more

environmentally relevant than turbidity (Davies-Colley and Smith 2001). Consequently, water clarity as measured by the maximum sighting distance of a perfectly black disk, viewed horizontally (Davies-Colley and Smith 2001) (hereafter simply referred to as 'visibility') was implemented in this study to determine the relevant turbidity and satellite reflectance values. Given that visibility is nearly equivalent to the more common Secchi depth measure of water clarity (Steel and Neuhausser 2002), the two were used interchangeably in this study. Secchi depth is defined as the point at which a black-and-white disc lowered into standing water is judged to disappear (Davies-Colley and Smith 2001). Visibility could not be calculated directly from reflectance because the necessary data were not available (described in greater detail on page 21).

The effects of turbidity on different fish species are variable. Piscivorous fish are in general less efficient predators in turbid water (Abrahams and Kattenfeld 1997; Reid et al. 1999; De Robertis et al. 2003). In contrast, the feeding efficiency of planktivorous fish are less affected by increases in turbidity as plankton can only be seen at relatively small distances, regardless of turbidity (Heege and Appenzeller 1998; De Robertis et al. 2003). In addition, plankton are typically concentrated near the surface in turbid waters (Doan 1942; Burdloff et al. 2000), which allows planktivores to become more efficient feeders. However, predator avoidance techniques such as escape responses, schooling behavior, and the avoidance of areas with a high risk of predation are all reduced in turbid water; behavior modifications which may make fish in turbid waters more susceptible to capture once located by piscivorous fishes (Abrahams and Kattenfeld 1997; Reid et al. 1999; De Robertis et al. 2003).

Study Site and Background

Lake Winnipeg is located between 50.0 and 54.0 degrees latitude in southern Manitoba, Canada - separating the prairies from the Canadian shield (Torigai et al. 2000). The lake is the eleventh largest in the world by surface area (Todd et al. 1998) and is divided into a north basin and a south basin. This study examined the south basin of Lake Winnipeg (see Figure 2.1); a region with a surface area of 3 600 km^2 and an average depth of 12 m (Torigai et al. 2000). The basin itself is turbid and unstratified, generally having a Secchi depth of less than 1.0 m (Brunskill et al. 1979) with 70-90 % of the suspended sediment composed of clay and silt (Allan and Brunskill 1977; Torigai et al. 2000). The south basin is the discharge basin of two major rivers; the Red and the Winnipeg. Most of the suspended sediment in the south basin originates from the Red River, while most of the water originates from the Winnipeg (Allan and Brunskill 1977). The convergence of turbid water from the Red River with the clear water of the Winnipeg River results in distinct spatially and temporally variable zones of turbidity (Burbidge and Schröder-Adams 1998; Kling 1998), the boundaries of which are referred to as 'turbidity fronts' in this study.

The lake in its entirety supports a prominent commercial fishing industry worth over $25 million in catch value alone (Manitoba Conservation 2003). Sauger (*Sander canadensis*) and walleye (*Sander vitreus*) represent the most economically important species in the lake, comprising approximately 52 % of the biomass caught in 1997. There are five commercial fishery licensing regions in the south basin: Gimli, Riverton, Selkirk, Traverse Bay, and Wanipigow (see Figure 2.1), with each licensing region based around a central delivery location within a major town. The fishery is comprised of small fishing

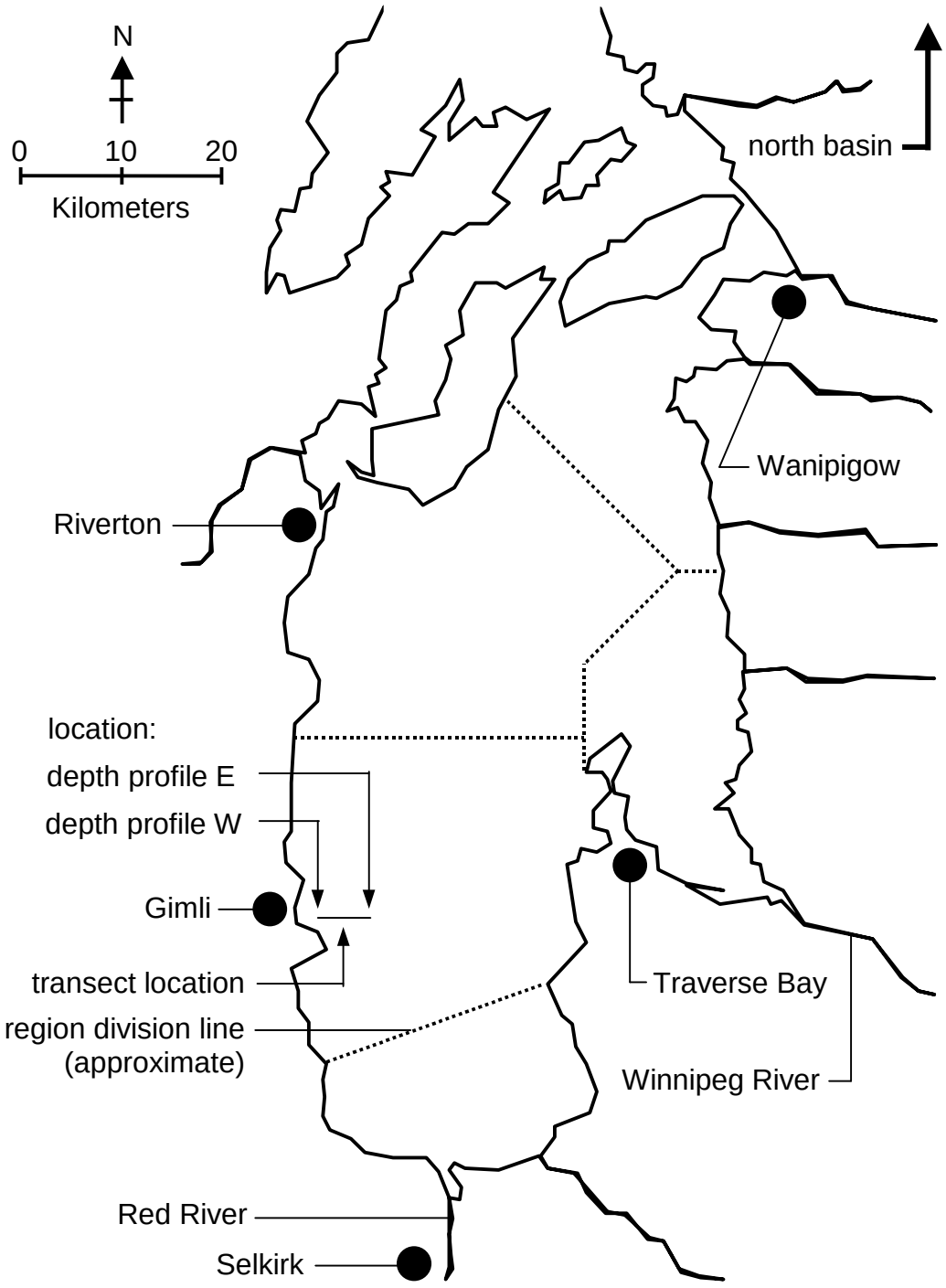

Figure 2.1 The south basin of Lake Winnipeg; located in southern Manitoba, Canada. Regional delivery sites are symbolized by a bullet (●). The depth profiles labeled 'E' and 'W' correspond to the east and west depth profiles, respectively.

vessels (less than 10 meters in length) utilizing gill nets of regulated mesh size (Lysack 1995), representing a constant fishing power throughout the fishing season. Gill nets are a passive fishing gear (Olin et al. 2004), with no ability to discriminate among species.

The south basin possesses favorable conditions for both walleye and sauger (Allan and Brunskill 1977; Ryder 1977; Brunskill et al. 1979; Torigai et al. 2000). The turbid nature of the south basin reduces light intensity, restricting the feeding and forage times of many competing species (Ryder 1977; Brunskill et al. 1979; Vandenbyllaardt et al. 1991). A specialized retinal structure present in both walleye and sauger (known as the *Tapetum lucidum*) amplifies existing light, allowing for superior prey detection in turbid water with reduced light availability (Ali et al. 1977; Lester et al. 2004). Closely packed bundles of retinal cells (known as macroreceptors) increase visual contrast (Vandenbyllaardt et al. 1991), another property which is degraded in turbid water (De Robertis et al. 2003). The preferred range of Secchi depth for walleye is 1-3 m (Ryder 1977), and a Secchi depth of 2 m is considered ideal (Lester et al. 2004). The ideal Secchi depth for sauger is currently unknown, although it is likely less than that of walleye given that sauger prefer more turbid water (Nelson and Walburg 1977). Both walleye and sauger are known to consume planktivorous prey such as the emerald shiner (*Notropis atherinoides*) (Smith and Pycha 1960; Wahl and Nielsen 1985). Such planktivorous prey may relax predator avoidance behaviors (Vandenbyllaardt et al. 1991) and forage more frequently in areas with a higher risk of predation when the water is turbid, even though mortality rates may be the same in both turbid and clear waters (Abrahams and Kattenfeld 1997). In addition, walleye are known to move to areas of preferred turbidity and avoid areas of turbidities beyond their preferred range (Ryder 1977; Lake Winnipeg

Research Consortium 2001). Thus walleye and sauger may congregate around turbidity fronts waiting for reductions in turbidity which may expose planktivorous prey congregated in the area exploiting the potentially high concentrations of plankton.

I hypothesized that increases in the relative abundance of walleye and sauger in different regions of the south basin could be predicted by increases in turbidity front length and complexity. Changes in relative abundance took the form of changes in abundance between regions. Catch was used as a proxy for abundance as performed by Ryder (1977) using walleye. Three visibility thresholds were used in the construction of the turbidity front boundaries: 1.00 m, 0.50 m, and 0.25 m. The 1.00 m threshold was chosen because it is within the preferred range for walleye habitat (Ryder 1977), while the 0.50 m and 0.25 m thresholds were chosen as an estimate of sauger's preferred Secchi depth and a Secchi depth beyond the range of preference for both species, respectively. These final two thresholds were also chosen as a way of simply breaking up the visibility range between 1.0 m and 0.0 m. The complexity of the turbidity fronts was established using the fractal dimension of the front itself. In order for the turbidity fronts to have any meaning, it was assumed that turbidity was constant throughout the water column; a reasonable assumption given that the south basin is not stratified (Brunskill et al. 1979).

2.2 Materials and Methods

Detailed commercial fishery data were available for the years of 1996-2004 in the form of both catch and effort. Delivery records from a particular region were assumed to represent catch from that specific region, with no catch originating from outside the region. This assumption was deemed valid due to the fact that the fishing vessels were

small, the occupants were exposed to the elements, and there was little means to preserve catch (personal observation). Thus the long distance trips required to travel to the delivery location in a different region were unlikely to occur without special arrangements. The regional boundaries were set by determining the approximate location from which the distance between one delivery location (around which the regions were centered) and its nearest neighbor were equal.

Daily catch records obtained from the Freshwater Fish Marketing Corporation (located in Winnipeg, Canada) contained the catch and effort data used in the analyses where appropriate. The data uniquely identified each fisher to his or her total number of deliveries (effort) and total round weight caught for each species of interest per day (catch). However, the data lacked the licensing area under which each fisher was assumed to operate - a crucial detail if changes in catch under different hydrological conditions were to be compared between regions. To rectify this problem, data were obtained from Manitoba Conservation (the Interlake regional office located in Gimli, Canada) which uniquely identified each fisher operating in the south basin of Lake Winnipeg and their corresponding licensing area. Once these two data sets were combined, sums of daily catch and effort values were created using all fishers associated with each region. The entire south basin was also examined as a single region in order to obtain a basin-wide perspective on the relationship between hydrology and catch. In order to minimize the effect of annual variation in effort on the analyses, only those fishers who actively fished in all years under examination were retained. From the catch and effort sums, daily catch per unit effort (CPUE) values for each region were obtained

in the form of round weight per delivery. CPUE was chosen as the measure of catch in order to eliminate the effect of any seasonal variation in effort on catch.

I) Choice and Refinement of Satellite Images

Satellite data were obtained as a hierarchical data format (HDF) computer file from the National Aeronautics and Space Administration for the years of 2003 and 2004. The data chosen for this study recorded solar light reflectance from the earth in the 620-670 nm wavelength range with a maximum resolution of 250 m $\cdot$ pixel^{-1} (Miller and McKee 2004). This bandwidth was chosen because it contained the wavelengths typically used to measure turbidity (Harrington et al. 1992; Heege and Appenzeller 1998; Miller and McKee 2004). The orbit of MODIS is sun-synchronous (Xiong et al. 2003); meaning that the sun was in the same approximate position relative to the earth's surface when spatially identical images of the earth were recorded on different dates (Capderou and Forget 2004). This reduced variation in reflectance due to variations in the angle at which the sun struck the earth's surface (Capderou and Forget 2004). The MODIS data were also subjected to earth-sun distance, radiometric, sensor decline, spectral, spatial, and sun-angle calibration by equipment on-board MODIS (Xiong et al. 2003). To be included in the analyses, the satellite image must have been taken on a day when fishing was known to occur and when ice was absent from the entire south basin (as evident from the satellite image itself; ice was always absent throughout the entire south basin prior to the start of the fishing season for all years examined). In addition, only satellite images in which the south basin appeared in the approximate center of the image were included in

the analyses. The reasoning behind the incorporation of only these images is presented in a later section.

Each satellite image contained some degree of error in both the reported location of each pixel on the surface of the earth (georeferencing) and in the actual display of the image data itself. Because the establishment of the turbidity fronts required spatial and temporal matching of reflectance to turbidity and Secchi depth measurements made in the field (described later), both types of error were corrected. In addition, the georeferencing portion of the satellite data had a maximum resolution of only 1 000 $m \cdot pixel^{-1}$ (Guenther et al. 1998). This resolution was increased to match that of the image data (at a maximum of 250 $m \cdot pixel^{-1}$) via a bicubic interpolation procedure; a process which takes into consideration all neighboring low resolution values when calculating each high resolution value. Image error was present as uniformly spaced, duplicated zones of latitude (see Figure 2.2). These zones were deleted from each image. In order to increase the ease with which distances were measured and expressed, the original geodetic georeferencing system was projected onto a Universal Transverse Mercator (UTM) grid. Any irregularities in the georeferencing system resulting from the deletion of the duplicated zones was eliminated by selecting non-distorted georeferencing regions from which to base the UTM projection (see Figure 2.3). The accuracy of the georeferencing system was assessed by the selection of 5 points of known location on the satellite image (ground truthing points) and comparing the reported location of these points against the known location of these points. Any consistent discrepancies between these values for all 5 ground truthing points were removed by shifting the UTM grid in such a way that the average difference between the reported and known location of all 5 ground truthing

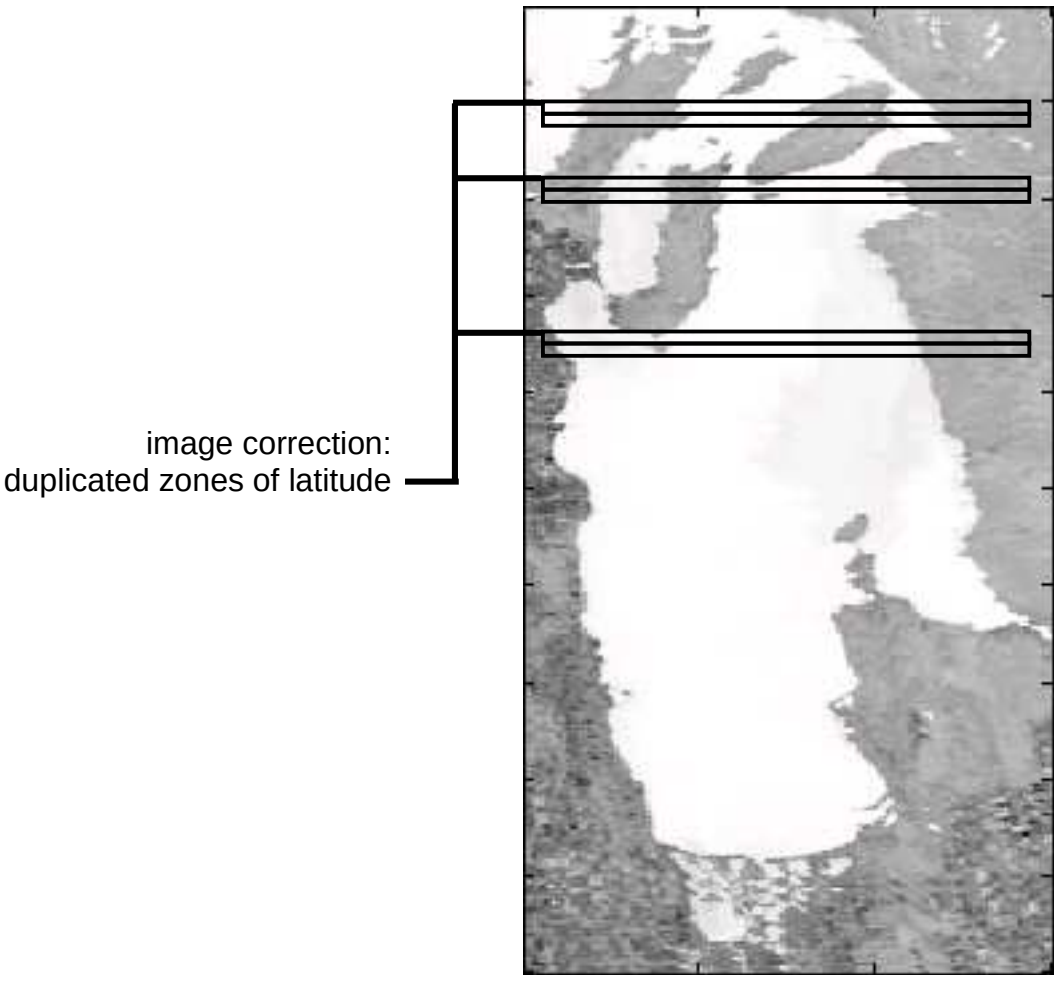

Figure 2.2 A typical image of the south basin showing image error. Image error was present in the form of duplicated zones of latitude at regular intervals (obvious examples of duplicated pairs enclosed by adjacent rectangles). These duplicated zones were removed prior to the establishment of the turbidity fronts. The functions used to remove image error are supplied in Appendix 1.

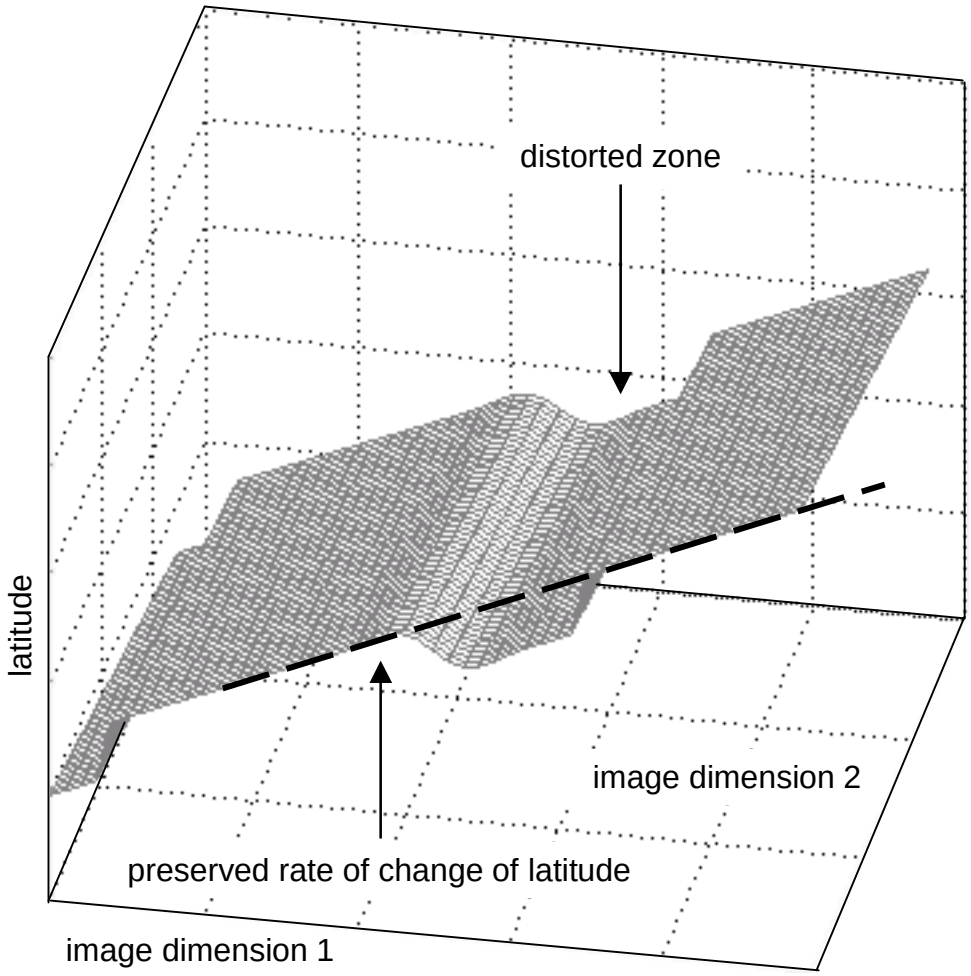

Figure 2.3 A typical image of geodetic distortion. The distorted zones were removed by selecting values on the non-distorted zones and extrapolating a constant rate of change along the image axis in which the distortion was present (labeled as 'image dimension 1' above). Note that the perpendicular axis (labeled 'image dimension 2') does not have distorted zones because the rate of change is constant along that axis. The functions used to remove geodetic distortion are supplied in Appendix 1.

points was zero (Miller and McKee 2004). The location of the ground truthing points and the functions used to manipulate the satellite images as described above are given in Appendix 1, Table A1.1.

II) Turbidity Front Definition and CPUE Modeling

In order to infer visibility from reflectance it was necessary to create relationships between visibility in meters and turbidity in nephelometric turbidity units (NTU, the standard unit of measure for turbidity) and between turbidity and reflectance. Visibility and reflectance could not be related directly because only turbidity data were available from hydrological surveys of the south basin. The relationship between visibility and turbidity was taken from Davies-Colley and Smith (2001) and subsequently verified by field measurements made in the south basin. This relationship (equation 2.1) was constructed using data from waters in which clay was the main component of the

$$\text{visibility} = 4.09 \cdot \text{turbidity}^{-0.76} \quad (2.1)$$

suspended particles (Davies-Colley and Smith 2001), similar to the composition of the suspended sediment within the south basin (Torigai et al. 2000). The relationship between turbidity and reflectance was generated by spatially and temporally matching turbidity data from the hydrological surveys to the survey coordinates on the satellite image captured the same day. The reflectance at the survey coordinates was thus assumed to be the reflectance resulting from the recorded turbidity. Change in reflectance from the image minimum reflectance (hereafter simply referred to as 'reflectance') was used to correct for atmospheric scattering effects (Lathrop 1992; Cox et al. 1998; Miller and

McKee 2004). Plotted data suggested a linear relationship between turbidity and reflectance. The coefficients were then estimated using simple linear regression. This relationship was also verified by field measurements made in the south basin.

Once the reflectance associated with each target visibility was calculated, the position at which reflectance exceeded these thresholds was mapped on each satellite image (see Figure 2.4). This formed a boundary line (or 'turbidity front') from which perimeter length and complexity measurements could be made, given that 1 pixel dimension on the front represented 250 m on the earth. Turbidity front pixels immediately adjacent to land were judged to exhibit false reflectance readings due to reflectance contamination from the land and were consequently discarded (Cox et al. 1998). Each pixel which composed the remaining turbidity front was attributed to a region in the south basin based upon its proximity to each landing location; each pixel was assigned to the landing location with which it had the highest proximity. The complexity of the turbidity front was quantified by calculating the fractal dimension of the turbidity front using the box counting technique; a common method for establishing the fractal dimension of two-dimensional image data representing areas of differing ecological habitats (Kenkel and Walker 1996). The fractal dimension of the turbidity front was calculated for all regions and the south basin as a whole. The functions used to generate the turbidity fronts and calculate the fractal dimension of these fronts are presented in Appendix 1. The methodology used for calculating fractal dimension using the box counting technique followed Peitgen et al. (2004).

Due to variable angles between the satellite's image capture device and the south basin on different dates the actual resolution of the satellite image fluctuated between

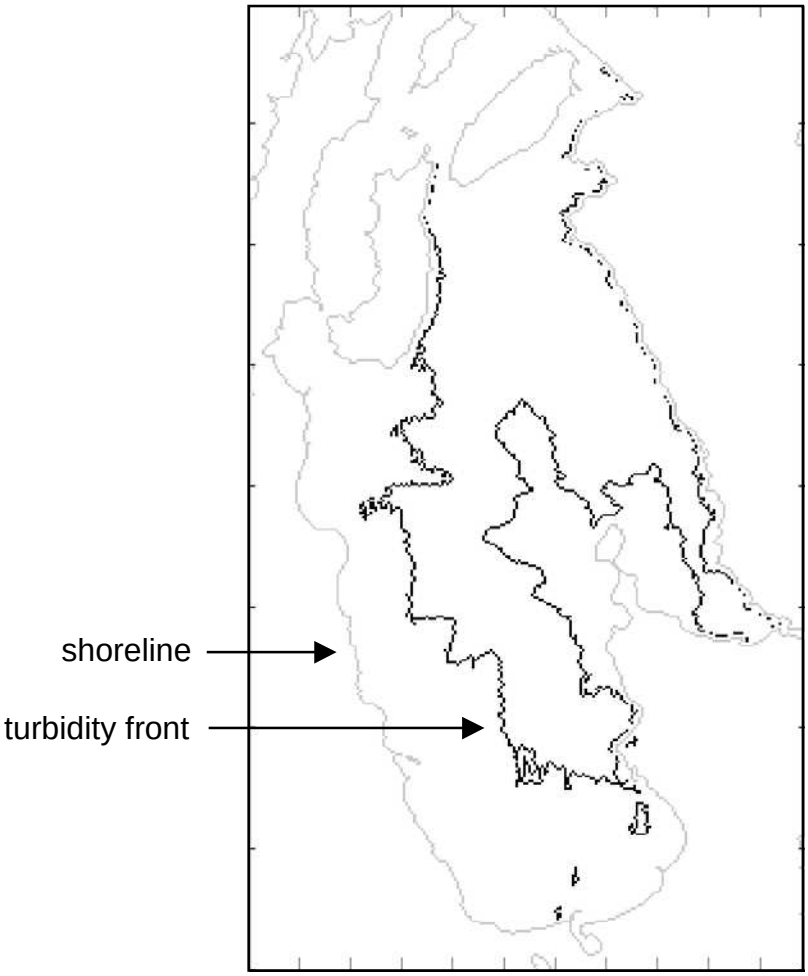

Figure 2.4 Established turbidity front (October 09 2003). The front shown above is the threshold between waters where visibility was greater than 0.25 m and where it was less than this value. Pixels which comprised the turbidity front but were adjacent to the shoreline were discarded due to presumably false visibility values generated by contamination of the pixel's reflectance value from nearby land reflectance (Cox et al. 1998); these pixels have been removed in the above image. The functions used to generate the turbidity fronts are supplied in Appendix 1.

images. To compensate for this, the reported distance between two points of known location (all pair combinations of the 5 ground truthing points; see Appendix 1, Table A1.1 for the UTM coordinates of these points) from the satellite image were compared to the known distance between the same two points. A correction factor was created by dividing the known distance by the reported distance. All turbidity front length measures were multiplied by this value in order to adjust for the variability in satellite image resolution. Satellite images with correction factors greater than 1.5 were discarded because the magnitude of the correction factor required varied over different portions of the same satellite image in these cases (as established from the magnitude of the correction factor using all pair combinations of the 5 ground truthing points). Addressing this complex variation in the magnitude of the correction factor required was beyond the scope of this thesis. Once the lengths and fractal dimensions of the turbidity fronts were calculated, the regional relationships between these two independent variables and CPUE were examined using linear regression. Statistical significance was inferred if $p < 0.05$ (by convention).

III) Field Verification of Hydrological Assumptions

In order to validate the conversion of visibility to turbidity and turbidity to reflectance, turbidity and Secchi depth (as an equivalent measure of visibility) were recorded every 250 m along a transect in the south basin east of Gimli (see Figure 2.1 for the location of this transect and Appendix 1, Table A1.1 for their UTM coordinates). Visibility could not be measured directly because the necessary equipment was not available. Turbidity measurements were made using a YSI 6600 multiparameter sonde

equipped with a YSI 6136 turbidity probe and a YSI 650 MDS data logger. The turbidity probe was calibrated using formazin and the 2-point calibration procedure described in the YSI 6-Series Environmental Monitoring Systems Operating Manual (YSI Incorporated 2001) prior to the deployment of the sonde in the field. Turbidity was measured approximately 0.25 m below the water's surface at each water sampling site. Secchi depth measurements were made using a standard Secchi disc with a diameter of 0.203 m. Horizontal movement of the sonde was reduced as much as possible while the sonde was deployed. The location of each water sampling site was matched to its counterpart on the satellite image taken at approximately the same time (+/- 30 minutes) on the same day in order to establish reflectance at the water sampling site. The relationship between Secchi depth and turbidity as well as between turbidity and reflectance using the field data was established in the same manner as the non-field relationship between turbidity and reflectance described previously. The field data were concluded to support the non-field relationships if the predicted values using the non-field data relationships fell within the 95 % prediction intervals of the field relationships at the turbidity and reflectance thresholds associated with each target visibility.

Examination of the assumption that turbidity remained constant regardless of depth was performed by the construction of two depth profiles east of Gimli (see Figure 2.1 for the location of these sites and Appendix 1, Table A1.1 for their UTM coordinates) using the same equipment and calibration procedure described in the previous paragraph. To obtain the depth profiles the sonde was lowered to the lake bottom and raised at a gradual rate (approximately 0.08 $m \cdot s^{-1}$). Turbidity was automatically measured every 3

seconds. Horizontal movement of the sonde was reduced as much as possible while the sonde was deployed.

2.3 Results

The field data supported the relationship between visibility and turbidity obtained from the primary literature; the relationship constructed using the field data was statistically significant ($F = 26.4$, degrees of freedom; numerator, denominator (d.f.) = 1,19, $p < 0.05$) and exhibited the same functional form (not shown). The 95 % prediction interval of the turbidity associated with the 1.00 m visibility / Secchi depth threshold encompassed the predicted turbidity value generated by the non-field data (see Figure 2.5). The other two visibility thresholds could not be examined as the smallest Secchi depth obtained was 0.72 m. Extrapolation beyond the extreme values of the data may produce misleading results (Kutner et al. 2005). Consequently, the turbidities associated with the 0.25 m and 0.50 m visibility thresholds were not analyzed in conjunction with the field data but were retained for the CPUE analyses.

The relationship between turbidity and reflectance exhibited a functional form most closely matched by a linear function. Alternative functional forms (such as the exponential, logarithmic, and power relationships) did not follow the trend in the data as closely as indicated by the adjusted coefficient of determination. Reflectance monotonically increased as turbidity increased (see Figure 2.6). The relationship generated using the field data was statistically significant ($F = 31.0$, d.f. = 1,18, p-value < 0.05) and supported the non-field relationship as both were most closely matched by the same functional form (not shown). However, the expected values generated using the

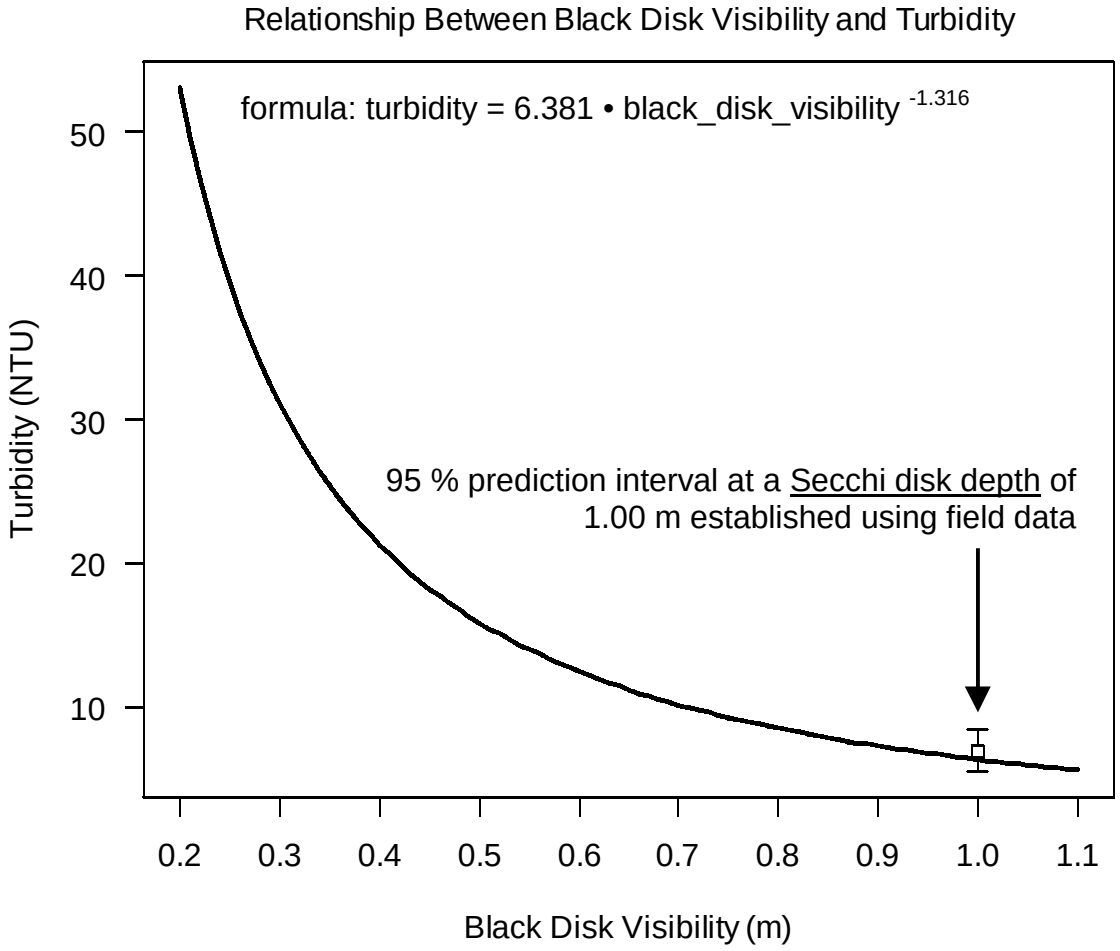

Figure 2.5 The relationship between black disk visibility (in meters) and turbidity (in nephelometric turbidity units) used in this study. The relationship was obtained from Davies-Colley and Smith (2001) as data from the south basin was not available. This relationship was verified by field measurements from the south basin; the 95 % prediction interval generated by the field data relationship encompasses the value predicted by the established relationship. Due to equipment limitations Secchi depth was measured in the field instead of black disk visibility. However, black disk visibility is nearly equivalent to Secchi depth (Steel and Neuhausser 2002).

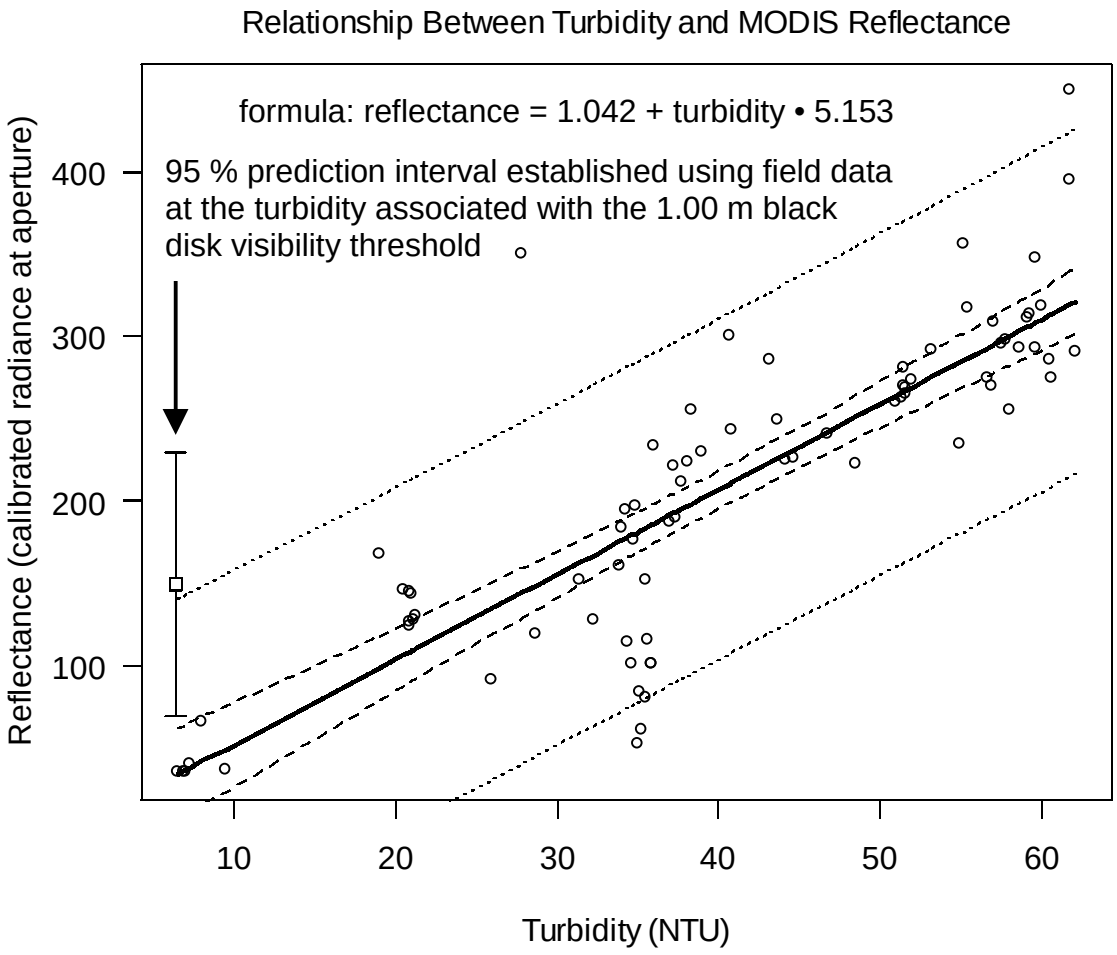

Figure 2.6 The relationship between turbidity (in nephelometric turbidity units) and solar reflectance between the wavelengths of 620-670 nm as measured by the Moderate Resolution Imaging Spectroradiometer - Terra (as calibrated at-aperture radiance measured in $W \cdot m^{-2} \cdot \mu m^{-1} \cdot sr^{-1}$, effect of atmospheric scattering removed) from the south basin of Lake Winnipeg (2003-2004). The 95 % estimation interval is represented by the dashed lines, while the 95 % prediction interval is depicted by the dotted lines. The relationship is statistically significant ($F = 187.0$, d.f. = 1,76, $p < 0.05$, not shown). The 95 % prediction interval constructed using field data at the 1.00 m black disk visibility threshold does not encompass the predicted value of the established relationship.

non-field relationship did not fall within the 95 % prediction interval of the field relationship at the 1.00 m visibility threshold (see Figure 2.6). Once again the other two visibility thresholds were not examined because extrapolation beyond the extreme values of the data would have been necessary.

The depth profiles revealed that turbidity did not remain constant at depth; the turbidity recorded in the upper water column varied from that of the lower. This change in turbidity between the upper and lower water columns was not consistent between the two depth profiles (see Figure 2.7). Using the relationship between visibility and turbidity established above, visibility at the east site decreased by 0.025 m at depth, while visibility at the west site increased by 0.069 m at depth (see Figure 2.7).

Only the turbidity fronts constructed using the 0.25 m and 0.50 m visibility thresholds were used in the analyses; front lengths greater than zero at the 1.00 m visibility threshold were absent in all but one of the satellite images examined. In addition, the fractal dimension of the portions of the front assigned to each region were not analyzed because the calculation regularly produced results less than 1. This was a nonsensical result as the fractal dimension of any line should lie between 1 and 2 and was attributed to the relatively small number of boxes occupied (Kenkel and Walker 1996) by the regional portion of each front. In contrast, the fractal dimension of the turbidity fronts for the entire south basin as a whole were consistently larger than 1.

No statistically significant relationship existed between CPUE and turbidity front length at any visibility threshold for any region, including the south basin as a whole (with the exception of sauger CPUE at the 0.25 m visibility threshold in the Wanipigow

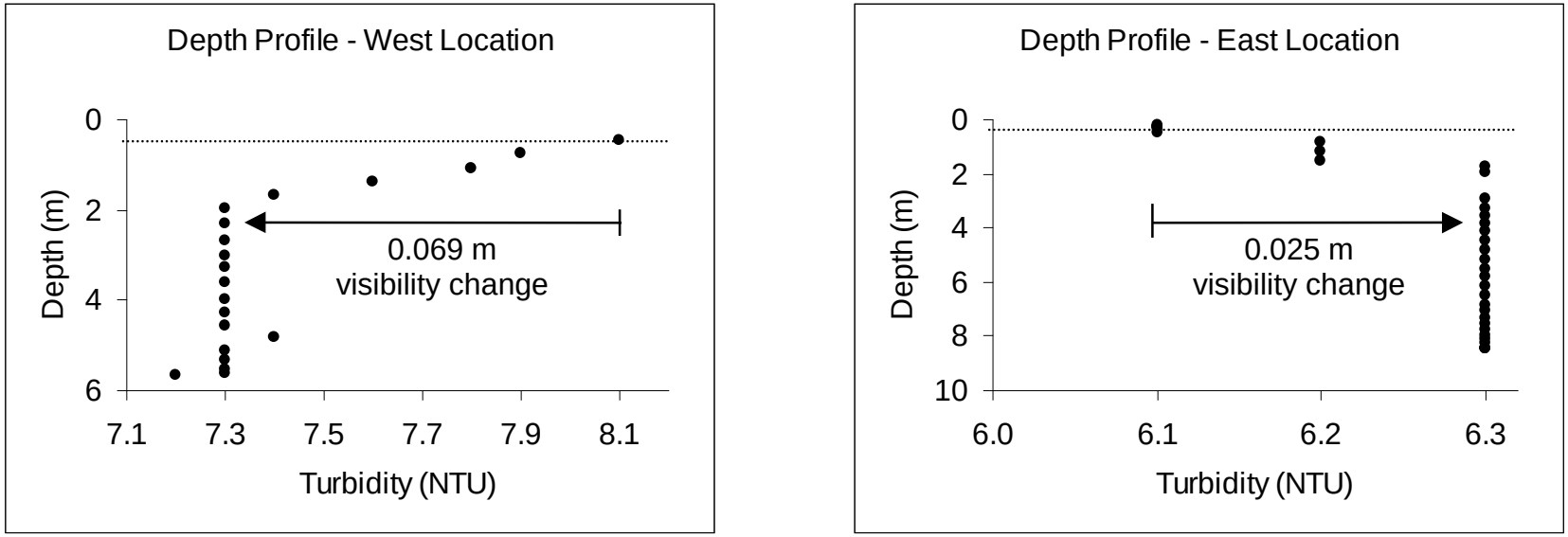

Figure 2.7 Depth profiles measured in the south basin (see Figure 2.1 for the location of these profiles and Appendix 1, Table A1.1 for their coordinates). Black disk visibility was calculated using the equation from Figure 2.5. Assuming a liberal Secchi depth of 1.00 m and the conservative estimate that a satellite can only 'see' into the water a maximum of 50 % of Secchi depth (shown as dotted lines above) (Cox et al. 1998), the satellite would not have detected the turbidity exhibited by the majority of the water column. While the change in visibility in both instances was less than 0.1 m, the prevalence and magnitude of these changes throughout the south basin were unknown.

region). In addition, the relationship between CPUE and turbidity front complexity for the entire south basin was also statistically insignificant at any visibility threshold, whether examined by itself or in conjunction with front length (see Table 2.1). The typical relationship between CPUE and turbidity front length and complexity is shown in Figure 2.8.

2.4 Discussion

The results of this study indicated that turbidity front length and complexity had no statistically significant ability to influence the catch rate of either walleye or sauger at any visibility threshold examined. This result did not support the hypothesis postulated previously; that both species will exhibit higher abundances in regions which possess relatively long and complex turbidity fronts. This conclusion was attributed to both prey dynamics and the numerous sources of variation associated with inferring the values of water quality parameters from satellite image data. The following sections describe how the distribution of prey may have made both species' more efficient predators in waters typically thought to be 'too turbid' for either species. Known sources of variation necessarily present in satellite data are also discussed; in particular the inability of satellite sensors to penetrate the water column and observe changes in turbidity at depth.

I) Impact of Turbidity Front Length and Complexity on CPUE

The general absence of a statistically significant relationship between CPUE and turbidity front length or complexity fails to support my hypothesis. While there was one case where the relationship between CPUE and turbidity front length was statistically

Table 2.1 Statistical significance of the relationship between catch per unit effort (CPUE) and turbidity front length in each region using linear regression. S.E. is standard error and n is the sample size. Only sauger CPUE in the Wanipigow region at the 0.25 m black disk visibility threshold was statistically significant (slope $p < 0.05$). Table values given below for the entire south basin are from the model in which both turbidity front length (L) and complexity (C) were included together; neither variable was statistically significant (slope $p > 0.05$) with CPUE by itself or in combination. The relationship for the Selkirk region at the 0.50 m visibility threshold could not be created because visibility in that region was never greater than 0.50 m during the time period examined.

Walleye Black Disk Visibility Threshold

	0.25 m				**0.50 m**			
Location	p-value	Slope	S.E.	n	p-value	Slope	S.E.	n
Gimli	0.233	0.599	0.475	13	0.312	-0.365	0.344	13
Riverton	0.290	0.750	0.674	13	0.451	-0.393	0.502	13
Selkirk	0.930	0.079	0.878	13	NA	NA	NA	NA
Traverse Bay	0.747	0.104	0.315	13	0.173	0.588	0.404	13
Wanipigow	0.870	-0.212	1.264	12	0.209	0.599	0.446	12
South Basin L	0.787	0.063	0.229	14	0.116	0.719	0.418	13
South Basin C	0.863	26.91	152.5	14	0.155	-344.0	223.4	13

Sauger Black Disk Visibility Threshold

	0.25 m				**0.50 m**			
Location	p-value	Slope	S.E.	n	p-value	Slope	S.E.	n
Gimli	0.866	-0.013	0.077	13	0.147	-0.078	0.050	13
Riverton	0.086	0.168	0.089	13	0.297	-0.078	0.071	13
Selkirk	0.472	-0.455	0.611	13	NA	NA	NA	NA
Traverse Bay	0.059	0.163	0.077	13	0.087	0.208	0.111	13
Wanipigow	0.041	0.180	0.077	12	0.936	0.003	0.037	12
South Basin L	0.731	-0.014	0.039	14	0.310	-0.084	0.078	13
South Basin C	0.484	18.73	25.85	14	0.374	38.84	41.78	13

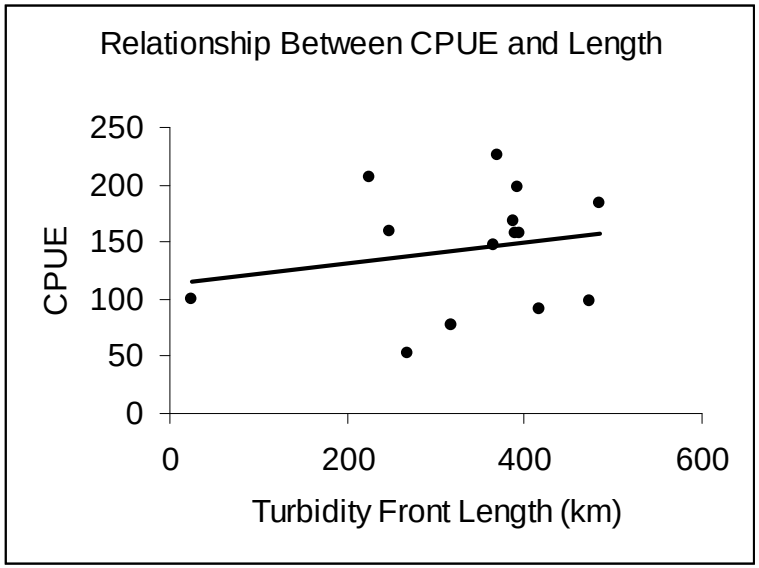

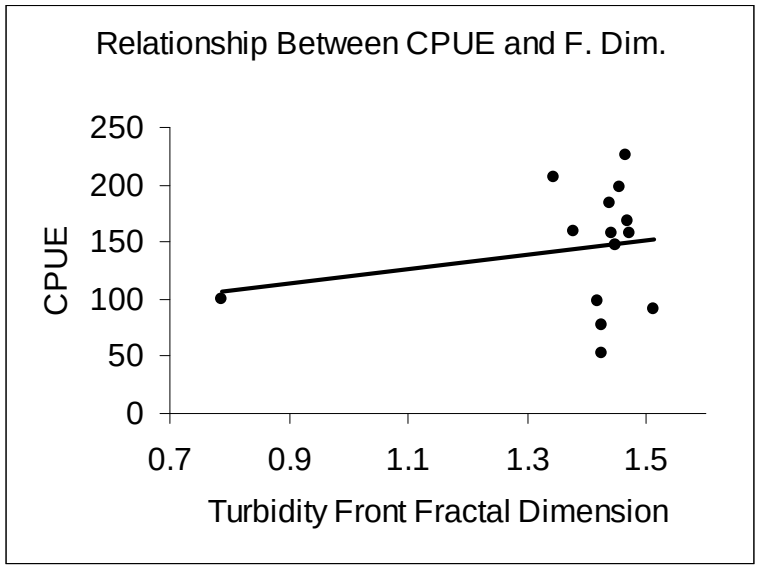

Figure 2.8 The typical relationship between catch per unit effort (CPUE) and turbidity front characteristics. Fractal dimension is abbreviated 'F. Dim.'. The relationships shown above use walleye CPUE data over the entire south basin region and the turbidity fronts established using the 0.25 m black disk visibility threshold. Neither relationship is statistically significant (slope $p > 0.05$); as was generally the case for the regional relationship between CPUE and turbidity front length (see Table 2.1).

significant, this result was likely an artifact of the number of tests and not representative of a true trend. Similarly, the relationship between CPUE and turbidity front complexity (as indicated by the fractal dimension of the turbidity front) was largely dictated by a single data point. If this point were ignored the data suggest almost no relationship between the two variables.

The general absence of a statistically significant relationship between CPUE and turbidity front length or complexity also indicated that walleye and sauger were not influenced by the structure of the turbid water found within the south basin and generally opposes the conclusions drawn in the primary literature. Specifically, it has been established that light is the major determinant of walleye activity level and consequently feeding level (Ryder 1977). Walleye feeding activity is also known to decline at higher turbidities (Vandenbyllaardt et al. 1991). If walleye and sauger had favored the less turbid side of areas with relatively long turbidity front lengths then CPUE in these regions would have been elevated, given that increases in activity result in increased encounters with passive fishing gear (Mohr 1965) such as the gill nets used in the south basin. It was possible that even the more turbid side of the turbidity level associated with the 0.25 m Secchi depth was simply not turbid enough to have had a noticeable effect on walleye and sauger catch rate. This may have been particularly relevant for sauger, which are known to prefer more turbid water than walleye (Nelson and Walburg 1977). However, given that walleye prefer waters with a Secchi depth of 2 m (Lester et al. 2004) it remained surprising that no changes in CPUE were observed. The distribution of fish can also be affected by other environmental conditions such as temperature and river inflows (Pollard et al. 1998; Lester et al. 2004). The variation in catch which may have

been produced by these environmental conditions were not accounted for and thus may have obscured the relationship between CPUE and turbidity front characteristics. It was also possible that the tests possessed insufficient statistical power to detect any trends which may have been present given the small sample sizes.

However, this apparent lack of habitat selectivity could also be partially explained by prey dynamics. Both walleye and sauger feed on planktivorous prey (Smith and Pycha 1960; Wahl and Nielsen 1985). Turbid areas have a less adverse effect on planktivorous feeding than on piscivorous feeding (Heege and Appenzeller 1998; De Robertis et al. 2003). It was possible that both species remained efficient predators simply through regular encounters with planktivorous prey items on either side of the turbidity front. If the probability of capturing prey was comparable in these 'too turbid' areas than in the less turbid areas it was unlikely either species avoided the areas with 'unsuitably' high turbidities.

II) Reliability of the Relationships Between Secchi Depth, Turbidity, and Reflectance

Although there was only 1 instance where the relationship between CPUE and turbidity front characteristics was statistically significant, it is important to note that there were numerous sources of variation which had the potential to obscure underlying trends. Foremost amongst these is the precision of measuring Secchi depth and visibility, both of which vary in accordance with observer judgment and (in the case of Secchi depth) sun angle (Cox et al. 1998). The relationship between visibility and turbidity varies between lake type and must be established for each body of water examined in order to have any environmental meaning (Davies-Colley and Smith 2001). This relationship could not be

established using south basin values because no data were available. Consequently, the data from a similar lake type were used. However, the use of south basin data would have eliminated any doubt of the applicability of the relationship, despite the fact that the limited field measurements supported the relationship.

In contrast, the relationship between turbidity and reflectance was not supported by measurements made in the field. This discrepancy was attributed to the fact that field verification of the satellite data could only be obtained from 1 satellite pass and may not have been representative of the true relationship between reflectance and turbidity. This relationship is also typically represented by an exponential function in the primary literature (Harrington et al. 1992), whereas in this study a linear function fit the data closest. However, the relationship did show increasing reflectance with increasing turbidity, a trend supported by Ruhl et al. (2001). This discrepancy was accounted for by the fact that turbidity may be highly variable in a small area (such as the area covered by a single pixel on the satellite image), with point samples not necessarily representative of the area as a whole (Ruhl et al. 2001). In addition, the poor contrast of the data may have excluded the portion of the relationship where the curvature of an exponential relationship is most pronounced, as other studies such as that performed by Kloiber et al. (2002) utilized a wide range of water clarity conditions in the generation of the relationship between turbidity and reflectance.

Uncertainty regarding the relationships between visibility, turbidity, and reflectance aside, it has been demonstrated that the measurement of water quality from satellite data is possible (Harrington et al. 1992; Lathrop 1992). However, the use of satellite imagery is not without its own complications. Meteorological conditions such as

abundant cloud cover and the presence of fog can obscure the image, while hydrological and limnological events such as waves and chlorophyll blooms can cause deviations between true turbidity and the turbidity inferred from satellite imagery (Ryder 1977; Cox et al. 1998; Ruhl et al. 2001). It was also possible that the resolution of the satellite was too coarse to detect the turbidity fronts which influenced walleye and sauger movements on a local scale, given that each pixel dimension represented 250 m on the earth. However, given the self-invariant property of fractals found in nature (Lovejoy 1982), the fractal patterns observed at the 250 m resolution should be comparable to those found at higher resolutions which are potentially more relevant to local walleye and sauger movement patterns.

Although the variation in reflectance due to changes in sun angle relative to the center of each satellite image was corrected (Xiong et al. 2003), the variation in reflectance due to the relative position of the south basin in each satellite image was not. This complex step was omitted in favor of the selection of only satellite images in which the south basin was in the approximate center of the image; thus the variation in reflectance due to the position of the south basin was minimized. Similarly, the inclusion of images in which the south basin was relatively far from the center of the image was not appropriate due to the decline in image resolution as the boundary of the satellite image is approached. As mentioned previously, these lower resolution images required complex correction techniques to extract true turbidity front length and complexity, a process which was beyond the scope of this thesis. The presence of these sources of variation reduced the sample size and may have similarly reduced the power of the tests employed to detect any relationship between turbidity front characteristics and CPUE.

Other concerns existed for inferring water quality parameters in addition to those described above. Although the ground truthing method utilized in this study is established in the primary literature (Lathrop 1992), it has been postulated that reliable results using satellite data can only be obtained from large water bodies free from reflectance contamination from adjacent land cover (Cox et al. 1998). It was possible that the 1 pixel buffer zone used in this study was inadequate and that the measured turbidity was altered in some cases by background scatter from land objects. However, the minimum size at which a given water body is unsuitable for analysis using satellites remains unknown. Similarly, there exists no universal algorithms for converting satellite data to water quality parameter values (Cox et al. 1998) and it was thus difficult to compare the relationships established in this study with those established in others. This is especially relevant when differing resolutions, sensor types, and advances in technology are considered.

The final, and potentially most relevant source of error in this study was the fact that turbidity at depth was not similar to that on the surface. It is well known that a satellite's ability to 'see' into the water column is limited, and may extend to a maximum depth of 4 m (Heege and Appenzeller 1998). Assuming a liberal Secchi depth of 1 m and using the more conservative estimate of the satellite 'seeing' only 20-50 % of Secchi depth (Cox et al. 1998) the satellite would not have been able to observe the level of turbidity the majority of the water column possessed. This is another known limitation of water quality parameters derived from satellite data (Ruhl et al. 2001) and may have arisen through a number of processes including lake stratification (if present), opposing currents, and the inflow of water of differing turbidities from different rivers (Heege and

Appenzeller 1998). While these differences in turbidity equate to a change in visibility at depth of less than 0.1 m, the prevalence, magnitude, and ecological impact of these changes in terms of walleye and sauger habitat preference for the entire south basin are unknown. It was possible that the catch rate of walleye and sauger in the south basin was strongly dictated by turbidity front characteristics but the relevant fronts were too deep to be seen. In contrast, variations in turbidity between the two depth profiles were greater than within each profile itself. Thus surface turbidity may be an appropriate indicator of turbidity at depth. However, more depth profiles are needed to support this theory.

III) Conclusions

In conclusion, no consistent statistically significant relationships between CPUE and turbidity front length or complexity were found with either walleye or sauger for any of the visibility thresholds examined. This conclusion generally opposes that found in the primary literature but may have arisen from the numerous sources of variation present in the methodology as well as the nature of the fish species examined. Both species prefer turbid water and may not have been deterred by even the most extreme visibilities examined, especially if prey concentration was high. Variation in visibility measurements and the absence of the data required to calibrate the relationship between visibility and turbidity called into question the threshold turbidities extracted, despite verification using field data. Small sample sizes, environmental conditions, backscattering from land, coarse image resolution, and the lack of a universal algorithm dictating the relationship between reflectance and turbidity may have also obscured the relationship between turbidity front characteristics and CPUE. Finally, variable turbidity at depth may have

hidden the relevant turbidity fronts from the view of the satellite and thus not conclusively eliminated the possibility that walleye and sauger catch rate were dictated by turbidity front characteristics in the south basin of Lake Winnipeg.

IV) Suggestions for Future Work

More data are needed from the south basin in the form of hydrological surveys. This will allow the generation of a Secchi depth- and visibility-turbidity relationships unique to the south basin, and has the potential to address the magnitude and prevalence of the variation in turbidity with depth uncovered in this study. More satellite data are also required in the form of higher temporal resolution in order to increase the power to detect relationships between CPUE and turbidity front characteristics examined in this study. Similarly, the use of satellite data with higher spatial resolution would allow a more detailed analysis of turbidity front length and complexity, once again increasing the power to detect the previously mentioned relationships. Finally, analysis of the area within the south basin above threshold turbidity values may allow more definite conclusions to be drawn regarding the turbidity preferences of walleye and sauger.

References

Abrahams, M., and Kattenfeld, M. 1997. The role of turbidity as a constraint on predator-prey interactions in aquatic environments. Behav. Ecol. Sociobiol. **40**: 169-174.

Ali, M.A., Ryder, R.A., and Anctil, M. 1977. Photoreceptors and visual pigments as related to behavioral responses and preferred habitats of perches (*Perca* spp.) and pikeperches (*Stizostedion* spp.). J. Fish. Res. Board Can. **34**: 1475-1480.

Allan, R.J., and Brunskill, G.J. 1977. Relative atomic variation (RAV) of elements in lake sediments: Lake Winnipeg and other Canadian lakes. Proc. Int. Symp. 1976: 108-120.

Brunskill, G.J., Schindler, D.W., Elliott, S.E.M., and Campbell, P. 1979. The attenuation of light in Lake Winnipeg Canada waters. Fish. Mar. Serv. Report 1522, Dep. Fish. Environ., Winnipeg, MB.

Burbidge, S.M., and Schröder-Adams, C.J. 1998. Thecamoebians in Lake Winnipeg: A tool for Holocene paleolimnology. J. Paleolimnol. **19**: 309-328.

Burdloff, D., Gasparini, S., Sautour, B., Etcheber, H., and Castel, J. 2000. Is the copepod egg production in a highly turbid estuary (the Gironde, France) a function of the biochemical composition of seston? Aquat. Ecol. **34**: 165-175.

Canada Department of Energy, Mines, and Resources, Canada Centre for Mapping. "Hecla, Manitoba" [map]. Edition 4. 1:250,000. Canada 1:250,000, sheet 62 P. Ottawa: Canada Centre for Mapping, 1988.

Canada Department of Energy, Mines, and Resources, Canada Centre for Mapping. "Selkirk, Manitoba" [map]. Edition 7. 1:250,000. Canada 1:250,000, sheet 62-I. Ottawa: Canada Centre for Mapping, 1994.

Capderou, M., and Forget, F. 2004. Optimal orbits for Mars atmosphere remote sensing. Plant. Space Sci. **52**: 789-798.

Cox, R.M. Jr., Forsythe, R.D., Vaughan, G.E., and Olmsted, L.L. 1998. Assessing water quality in Catawba River reservoirs using Landsat thematic mapper satellite data. Lake and Reserv. Manage. **14**: 405-416.

Davies-Colley, R.J. and Smith, D.G. 2001. Turbidity, suspended sediment, and water clarity: A review. J. Am. Water Resour. As. **37:** 1085-1101.

De Robertis, A., Ryer, C.H., Veloza, A., and Brodeur, R.D. 2003. Differential effects of turbidity on prey consumption of piscivorous and planktivorous fish. Can. J. Fish. Aquat. Sci. **60**: 1517-1526.

Doan, K.H. 1942. Some meteorological and limnological conditions as factors in the abundance of certain fishes in Lake Erie. Ecol. Monogr. **12**: 293-314.

Guenther, B., Godden, G.D., Xiong, X., Knight, E.J., Qiu, S.-Y., Montgomery, H., Hopkins, M. M., Khayat, M.G., and Hao, Z. 1998. Prelaunch algorithm and data format for the level 1 calibration products of the EOS-AM1 Moderate Resolution Imaging Spectroradiometer (MODIS). IEEE Trans. Geosci. Remote Sensing **36**: 1142-1151.

Harrington, J.A. Jr., Schiebe, F.R., and Nix, J.F. 1992. Remote Sensing of Lake Chicot, Arkansas: Monitoring suspended sediments, turbidity, and Secchi depth with Landsat MSS data. Remote Sens. Environ. **39**: 15-27.

Heege, T., and Appenzeller, A.R. 1998. Correlations of large-scale patterns of turbidity and pelagic fish biomass using satellite and acoustic methods. Arch. Hydrobiol. Spec. Issues Advanc. Limnol. **53**: 489-503.

Ives, A.R., and Klopfer, E.D. 1997. Spatial variation in abundance created by stochastic temporal variation. Ecology **78**: 1907-1913.

Kenkel, N.C., and Walker, D.J. 1996. Fractals in the biological sciences. Coenoses **11**: 77-100.

Kling, H.J. 1998. A summary of past and recent plankton of Lake Winnipeg, Canada using algal fossil remains. J. Paleolimnol. **19**: 297-307.

Kloiber, S.M., Brezonik, P.L., and Bauer, M.E. 2002. Application of Landsat imagery to regional-scale assessments of lake clarity. Water Res. **36**: 4330-4340.

Kutner, M.H., Nachtsheim, C.J., Neter, J., and Li, W. 2005. Applied Linear Statistical Models, 5th Ed. McGraw-Hill Irwin, N.Y.

Lake Winnipeg Research Consortium. 2001. Report on the Health of the Lake Winnipeg Ecosystem and the Role of the Lake Winnipeg Research Consortium. Lake Winnipeg Research Consortium, Winnipeg, MB.

Lathrop, R.G. Jr. 1992. Landsat thematic mapper monitoring of turbid inland water quality. Photogramm. Eng. Rem. S. **58**: 465-470.

Lester, N.P., Dextrase, A.J., Kushneriuk, R.S., Rawson, M.R., and Ryan, P.A. 2004. Light and temperature: Key factors affecting walleye abundance and production. T. Am. Fish. Soc. **133**: 588-605.

Lovejoy, S. 1982. Area-perimeter relation for rain and cloud areas. Science **216**: 185-187.

Lysack, W. 1995. Mesh Size Effects in Lake Winnipeg's Commercial Fisheries. Manitoba Department of Natural Resources. Fisheries Branch MS Report No. 95-02.

Manitoba Conservation. 2003. A Profile of Manitoba's Commercial Fishery, Manitoba:

Government of Manitoba.

Miller, R.L. and McKee, B.A. 2004. Using MODIS Terra 250 m imagery to map concentrations of total suspended matter in coastal waters. Remote Sens. Environ. **93**: 259-266.

Mohr, H. 1965. Changes in the behaviour of fish due to environment and motivation and their influence on fishing. ICNAF Spec. Publ. **6**: 775-779.

Nelson, W.R., and Walburg, C.H. 1977. Population dynamics of yellow perch (*Perca flavescens*), sauger (*Stizostedion canadense*), and walleye (*S. vitreum vitreum*) in four main stem Missouri River reservoirs. J. Fish. Res. Board Can. **34**: 1748-1763.

Ortiz, M., and Arocha, F. 2004. Alternative error distribution models for standardization of catch rates of non-target species from a pelagic longline fishery: Billfish species in the Venezuelan tuna longline fishery. Fish Res. **70**: 275-297.

Peitgen, H.O., Jürgens, H., and Dietmar, S. 2004. Chaos and fractals: New frontiers of science. 2nd Ed. Springer, N.Y.

Pollard, A.I., González, M.J., Vanni, M.J., and Headworth, J.L. 1998. Effects of turbidity and biotic factors on the rotifer community in an Ohio reservoir. Hydrobiologia **387/388**: 215-223.

Reid, S.M., Fox, M.G., and Whillans, T.H. 1999. Influence of turbidity on piscivory in largemouth bass (*Micropterus salmoides*). Can. J. Fish. Aquat. Sci. **56**: 1362-1369.

Ruhl, C.A., Schoellhamer, D.H., Stumpf, R.P., and Lindsay, C.L. 2001. Combined use of remote sensing and continuous monitoring to analyze the variability of

suspended-sediment concentrations in San Francisco Bay, California. Estuar. Coast. Shelf Sci. **53:** 801-812.

Ryder, R.A. 1977. Effects of ambient light variations on behavior of yearling, subadult, and adult walleyes (*Stizostedion vitreum vitreum*). J. Fish. Res. Board Can. **34**: 1481-1491.

Smith, L.L. Jr., and Pycha, R.L. 1960. First-year growth of the walleye, *Stizostedion vitreum vitreum* (Mitchill), and associated factors in the Red Lakes, Minnesota. Limnol. Oceanogr. **5**: 281-290.

Steel, E.A., and Neuhausser, S. 2002. Comparison of methods for measuring visual water clarity. J. N. Am. Benthol. Soc. **21**: 326-335.

Todd, B.J., Lewis, C.F.M., Thorleifson, L.H., Nielsen, E., and Last, W.M. 1998. Paleolimnology of Lake Winnipeg. J. Paleolimnol. **19**: 211-213.

Torigai, K., Schröder-Adams, C.J., and Burbidge, S.M. 2000. A variable lacustrine environment in Lake Winnipeg, Manitoba: Evidence from modern thecamoebian distribution. J. Paleolimnol. **23**: 305-318.

Vandenbyllaardt, L., Ward, F.J., Braekevelt, C.R., and McIntyre, D.B. 1991. Relationships between turbidity, piscivory, and development of the retina in juvenile walleyes. T. Am. Fish. Soc. **120**: 382-390.

Wahl, D.H., and Nielsen, L.A. 1985. Feeding ecology of the sauger (*Stizostedion canadense*) in a large river. Can. J. Fish. Aquat. Sci. **42**: 120-128.

Xiong, X., Sun, J., Esposito, J., Guenther, B., and Barnes, W.L. 2003. MODIS reflective solar bands calibration algorithm and on-orbit performance. Proceedings of SPIE: Optical Remote Sensing of the Atmosphere and Clouds III **4891**: 95-104.

YSI Incorporated. 2001. YSI 6-Series Environmental Monitoring Systems Operating Manual [online]. Available from http://www.ysi.com/extranet/EPGKL.nsf/447554deba0f52f2852569f500696b21/90a0378150c2d2dd85256a1f0073f295/$FILE/069300B.pdf [cited 09 January 2006].

Chapter Three: Environment, Fishing Fleet Dynamics, and Catch

Abstract

Environmental factors affect the distribution of fish. The behavior of fishers also depends upon a variety of factors. These sources of variation are seldom included in stock assessment models, resulting in potentially inaccurate estimates of fish abundance. The study presented in this chapter examined the impact of these factors on the commercial catch rate of sauger and walleye in the south basin of Lake Winnipeg. The influence of light intensity, air temperature, wave height, barometric pressure, and the discharge rate of the Red River on both fishing effort and the catch rate was determined. Both catch- and effort-environment effects were examined using generalized linear models. Decreased effort was attributed to harsh weather conditions and conditions which decreased walleye catch. Increased walleye catch was indicated by decreased temperature and low Red River discharge. Increased sauger catch was indicated by increased temperature, high cloud opacity, and average Red River discharge.

3.1 Introduction

Environmental factors are a major component in controlling the spatial variation observed in species' distributional patterns (Walters and Collie 1988; Ives and Klopfer 1997; Criddle et al. 1998). Differences in water chemistry, light intensity, and water temperature often dictate the distribution of fish and other aquatic organisms (Doan 1942; Kling 1998; Sundermeyer et al. 2005). For example, temperature is known to limit the distribution of many organisms; as a species' thermal limit is approached, abundance declines (Ives and Klopfer 1997). The severity of these environmental influences are controlled by two factors; the range of conditions encountered and the strength of its association with the target species (Stoner 2004). Due to this interaction with the environment, almost all fisheries data exhibits some spatial variation (Booth 2000). This variation is often ignored, potentially leading to inaccurate estimates of population size and distribution (Booth 2000). The purpose of this study was to determine the prevalence and extent of this environmentally-mediated spatial variation in the catch and effort of the commercial fishery located in the south basin of Lake Winnipeg, Canada.

Study Site and Background

Lake Winnipeg is located between 50.0 and 54.0 degrees latitude in southern Manitoba, Canada - separating the prairies from the Canadian shield (Torigai et al. 2000). The lake is the eleventh largest in the world by surface area (Todd et al. 1998) and is separated into a north basin and a south basin by a central channel region. This study examined the south basin of Lake Winnipeg (see Figure 3.1); a region with a surface area of 3 600 km^2 and an average depth of 12 m (Torigai et al. 2000). The basin itself is

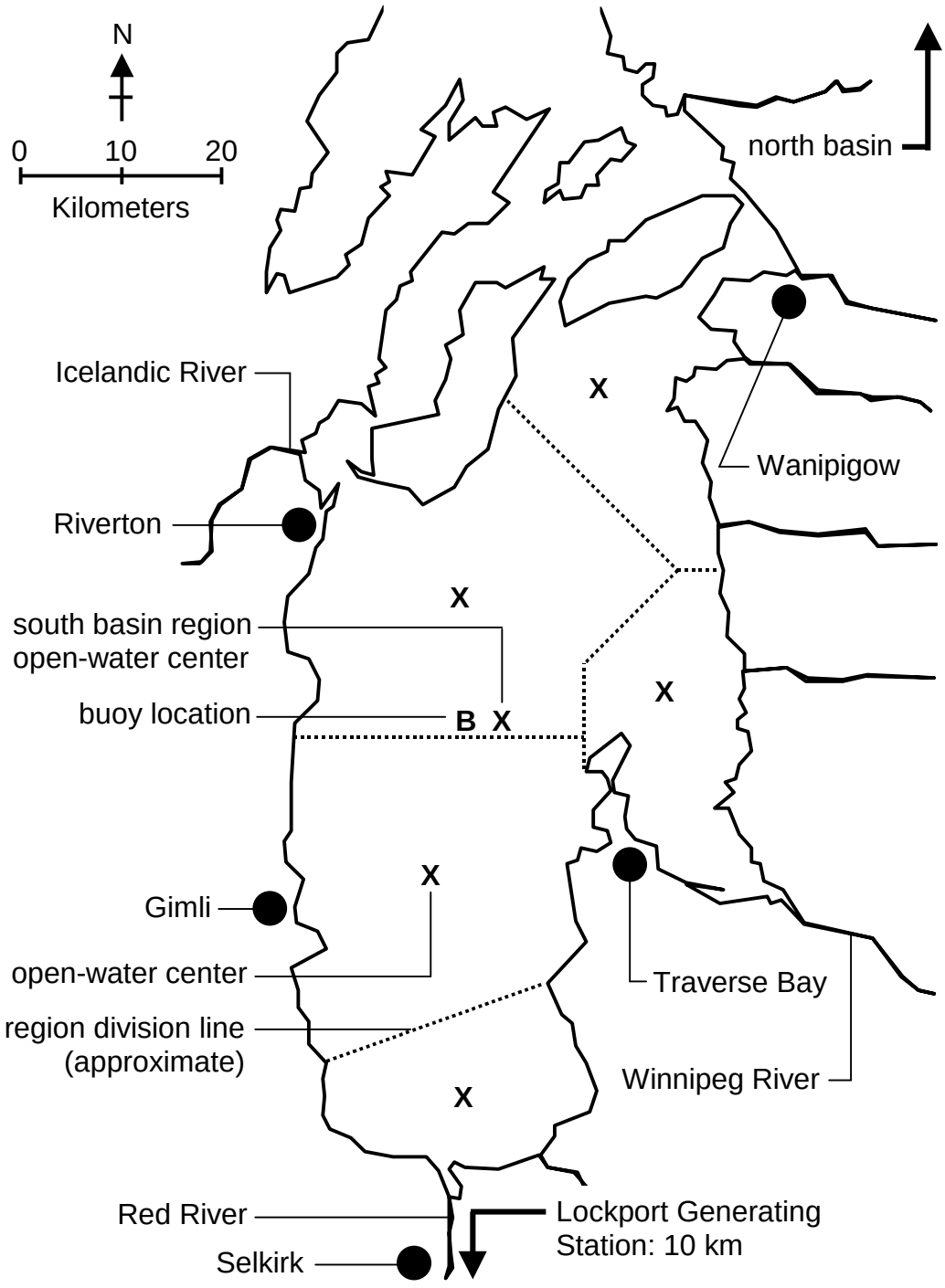

Figure 3.1 The south basin of Lake Winnipeg; located in southern Manitoba, Canada. Regional delivery sites are symbolized by a bullet (●) while the corresponding open-water centers are demarcated by an X.

turbid, generally having a Secchi depth of less than 1.0 m (Brunskill et al. 1979). The lake in its entirety supports a prominent commercial fishing industry worth over $25 million in catch value alone (Manitoba Conservation 2003). Sauger (*Sander canadensis*), and walleye (*Sander vitreus*) represent the most economically important species in the lake, comprising approximately 52 % of the biomass caught in 1997. There are five commercial fishery licensing regions in the south basin: Gimli, Riverton, Selkirk, Traverse Bay, and Wanipigow (see Figure 3.1), with each licensing region based around a central delivery location within a major town. The fishery is comprised of small fishing vessels (less than 10 meters in length) utilizing gill nets of regulated mesh size (Lysack 1995). Gill nets are a passive fishing gear (Olin et al. 2004) that discriminate based upon size and morphology rather than species.

The south basin possesses favorable conditions for both walleye and sauger (Allan and Brunskill 1977; Ryder 1977; Brunskill et al. 1979; Torigai et al. 2000). The turbid nature of the south basin reduces light intensity, restricting the feeding and forage times of many competing species (Ryder 1977; Brunskill et al. 1979; Vandenbyllaardt et al. 1991). However, a specialized retinal structure present in both walleye and sauger (known as the *Tapetum lucidum*) amplifies existing light, allowing for superior prey detection in turbid water with reduced light availability (Ali et al. 1977; Lester et al. 2004).

I hypothesized that increases in the catch rate of walleye and sauger in different regions of the south basin could be predicted by increases in temperature and decreases in light intensity. Decreased light intensity was represented by decreased visibility, increased cloud opacity, and increased wave height. This hypothesis was based on the

environmental conditions in the south basin and the fact that walleye habitat is known to depend upon water clarity and temperature (Lester et al. 2004). Wave height was included in the hypothesis because wave resuspension of bottom sediments could potentially increase turbidity and consequently reduce light intensity below the water's surface. The impact of the discharge rate of the Red River was also examined, given that discharge rate could be indicative of relative sediment loading and thus a predictor of light intensity below the water's surface. Finally, the effect of barometric pressure in the form of mean sea level pressure was examined due to its generally unknown impacts upon fish populations (Stoner 2004).

Fisher behavior was also taken into consideration in order to examine any potential bias in effort related to environmental conditions. The decision to fish is rarely included in long-term fisheries models (Salas and Gaertner 2004), despite the varying strategies a group of fishers may employ (Hilborn 1985). Each fisher is likely to express different tactics in response to varying social, cultural, and economic restraints (Salas and Gaertner 2004). Thus the decision to fish may not be absolute, especially under challenging environmental conditions such as extreme temperatures, high waves, or storm events. Based on this reasoning, I further hypothesized that decreases in fishing effort in different regions of the south basin could be predicted by increases in wave height and other conditions indicative of hostile weather conditions from a fishing perspective such as low barometric pressure (indicative of storm events).

3.2 Materials and Methods

I) Data Manipulation

Detailed commercial fishery data were available for the years of 1996-2004 in the form of both catch and effort. Delivery records from a particular region were assumed to represent catch from that specific region, with no catch originating from outside the region. This assumption was deemed valid due to the fact that the fishing vessels were small, the occupants were exposed to the elements, and there was little means to preserve catch (personal observation). Thus the long distance trips required to travel to the delivery location in a different region were unlikely to occur without special arrangements. The regional boundaries were set by determining the approximate location from which the distance between one delivery location (around which the regions were centered) and its nearest neighbor were equal.

Daily catch records obtained from the Freshwater Fish Marketing Corporation (located in Winnipeg, Canada) contained the catch and effort data used in the analyses where appropriate. Ice was always absent from the entire south basin prior to the start of the fishery in all years examined. The catch and effort data uniquely identified each fisher to his or her total number of deliveries (effort) and total round weight caught for each species of interest per day (catch). However, the data lacked the delivery location from which each fisher was assumed to operate - a crucial detail if changes in catch and effort under different meteorological conditions were to be compared between regions. To rectify this problem, data were obtained from Manitoba Conservation (the Interlake regional office located in Gimli, Canada) which uniquely identified each fisher operating in the south basin of Lake Winnipeg and their corresponding delivery location. Once

these two data sets were combined, sums of daily catch and effort values were created using all fishers associated with each region. The entire south basin was also examined in order to obtain a basin-wide perspective on the relationship of environment with catch and effort. In order to minimize the effect of annual variation in effort on the analyses, only those fishers who actively fished in all years under examination were retained. From the previously mentioned sums, daily catch per unit effort (CPUE) values for each region were obtained in the form of round weight per delivery. CPUE was chosen as a measure of catch in order to eliminate any seasonal variation in effort.

Daily Red River discharge rates were obtained from Manitoba Hydro (the corporate head office located in Winnipeg, Canada) for the Red River near the Lockport Generating Station (station number 05OJ010, see Figure 3.1 for the location of this site). Hourly meteorological conditions were obtained from Environment Canada (located in Winnipeg, Canada) using the meteorological data from the Gimli weather station (World Meteorological Organization station index number 71856). This station was chosen because it was the only weather station physically close to the south basin (see Figure 3.1 for the proximity of Gimli to the south basin). The following six meteorological variables were included in the catch and effort analyses: visibility, wind direction, wind speed, dry bulb air temperature, mean sea level pressure, and cloud opacity.

For all variables with the exception of the wind measures, daily variable values were obtained by averaging hourly values over 'daylight hours' (08:00 to 22:00). If any hourly values were missing, calculations were made using the remaining values. 'Night' values were discarded because measures of light intensity such as visibility and cloud opacity have no meaning. Daily wind direction and speed could not be calculated in this

manner due to their directional nature. Consequently, these two measures of wind were combined and recalculated in the form of maximum significant wave height which is defined as the average height of the highest one-third of the waves encountered and is the standard measure for wave height impacts (Sorensen 1997). The details of this calculation are provided in the following section.

II) Maximum Significant Wave Height Calculations

Maximum significant wave height (hereafter simply referred to as 'wave height') was calculated in accordance with Sorensen (1997) to produce wave height estimates for 'deep-water' waves (waves generated in a water depth greater than half the wavelength of the waves). This model necessarily assumes that water depth is greater than half the wavelength of the waves. Given that the average depth of the south basin is 12 meters (Torigai et al. 2000), this assumption would be violated only if wavelength exceeded 24 meters. It was possible that deep-water wave dynamics may not have been appropriate for regions such as the south shore and Traverse Bay where the average depth is approximately 4 m (Canada Department of Fisheries and Oceans 1995). However, wavelength data from the south basin required to test this assumption were not available.

Initially, the highest wave height was calculated for a given fetch assuming unlimited duration of average wind speed and constant direction (equations 3.1 and 3.2, see Appendix 2, Table A2.1 for fetches). Fetch was measured in sixteen different compass directions in order to mimic the divisions of the wind direction categories defined by the meteorological data. Fetch measurements were made from the open-water centers around each region. These centers (illustrated in Figure 3.1) represented the

approximate middle of the water-covered area around a region which lied closest to the delivery location in that particular region; where each region has only one delivery location around which the regions are centered. Further information on these centers is supplied in Appendix 2, Table A2.2. Next, the duration required to generate this wave height was calculated (equation 3.3). The final step was to compare the calculated duration with the observed duration; if the observed duration was shorter, the wave height was recalculated using this shorter duration. If the observed duration was larger than the calculated duration there was no need for recalculation as the wave height in this case was constrained by fetch. The symbols W and W_A are the wind speed and adjusted wind speed, respectively (both in $m \cdot s^{-1}$). H_{mo} is wave height (m), g the gravitational constant (9.81 $m \cdot s^{-2}$), F the fetch (m), and t_d the minimum duration (s) to reach the wave height calculated from equation 3.2.

(3.1) $$W_A = 0.71 \cdot W^{1.23}$$

(3.2) $$H_{mo} = 0.0016 \cdot (g \cdot F \cdot W_A^{-2})^{0.50} \cdot (W_A^{2} \cdot g^{-1})$$

(3.3) $$t_d = 68.8 \cdot (g \cdot F \cdot W_A^{-2})^{0.67} \cdot (W_A \cdot g^{-1})$$

Missing wind direction values were set to the wind direction value of the previous hour. Missing wind speed values were set to the average wind speed of the previous hour and the following hour. On every occasion when wind speed shifted into a new direction division, wave height was recalculated for the number of chronological hours the wind direction remained in that particular direction division. Daily wave height was calculated as the weighted average of all wave heights for a particular day. Weightings were

assigned as the total number of chronological hours the wind came from a given direction division.

Hourly data obtained from the single Environment Canada buoy in the south basin (Marine Environmental Data Services Identification Number C45140) were used to verify the accuracy of the wave height calculations described in the previous paragraph. Expected wave heights were calculated using fetches measured from the buoy's location (see Figure 3.1 and Appendix 2, Tables A2.1 and A2.2) in the same manner as described previously. These values were compared to the average daily wave heights as measured by the buoy using simple linear regression and correlation. Both variables were subjected to a natural logarithm transformation prior to analysis in order to address the resultant multiplicative relationship between the mean and the variance. Each wave height value provided by the buoy was supplied with a quality control number ranging from 1 to 4: 1 ("record appears correct"), 2 ("record is probably correct"), 3 ("record is probably erroneous"), 4 ("record appears erroneous"). Wave height observations with a quality control number of 4 were omitted from the analysis. The remaining quality control numbers were weighted equally in the analyses due to the subjective nature of the quality control number categories and the fact that the omission of any of the remaining categories did not improve the relationship between the calculated wave height and the wave height as recorded by the buoy. Multicollinearity between all environmental variables was examined using variance inflation factors and Spearman ranked correlations.

III) Data Modeling

After the extraction and manipulation of the environmental variables were complete they were set as predictor variables for the single response variable of effort or CPUE. As commercial fishing was prohibited during the month of August over the years examined (Manitoba Conservation 2006), the effort data were divided into an 'early' fishery period (from the beginning of May until the end of July) and a 'late' fishery period (from the end of August until the end of October; no fishing activities were recorded during the month of August for all of the years examined). A 'day' variable was then added to the list of potentially significant explanatory variables in the form of day of the year (where January 1 of each year was day 1, hereafter simply referred to as 'day') to further investigate the relationship between effort and day. 'Year' was also added in the form of a qualitative factor in order to address any interannual variation not accounted for by the explanatory variables.

The model was generated by fitting a generalized linear model with polynomial terms in the explanatory variables to each period of the data using a log link function and a quasipoisson distribution family (see Appendix 3 for the functions used to perform this task). Polynomial orders no larger than three were created for both simplicity and to reduce the potential for multicollinearity among the predictors. To further reduce multicollinearity among polynomial terms all original variables were centered prior to polynomial value generation. This was not done for the 'year' variable because it was expressed as a factor and not as a polynomial term. Generalized linear models are becoming customary for count data (Manly 2001). However, the typical Poisson distribution would not have been appropriate given that some of the models exhibited

overdispersion. Overdispersion is said to occur in Poisson and binomial distributions when the dispersion parameter exceeds 1 (the value assumed by these two distributions). The failure to compensate for overdispersion results in an overestimation of the precision of the coefficient estimates. The quasipoisson distribution is then required where the Poisson distribution would have been used in the absence of overdispersion, as the 'quasi' distributions estimate the value of the dispersion parameter as well (Fox 2002).

Individual polynomial orders of all variables were added and removed as necessary as dictated by a bi-directional stepwise variable selection procedure (Fox 2002). The 'year' variable was always included as the first variable in the model (regardless of statistical significance) in order to address any potential year effects (Maunder and Punt 2004). Any given variable order was deemed statistically significant if it explained at least 2 % of the null deviance (Maunder and Punt 2004). Information criterion methods typically used for this process such as Akaike's and Bayesian Information Criteria (AIC and BIC, respectively) require a maximum likelihood estimation of the dispersion parameter, a property which cannot be calculated for the 'quasi' family of distributions (McCullagh and Nelder 1989). However, the continuous portion of the CPUE data did not utilize a 'quasi' family in the modeling process (discussed below). Consequently, the final models produced using typical continuous CPUE data (walleye CPUE data from the Gimli region) under each variable selection method (AIC, BIC, and deviance threshold) were compared. This was done in order to examine the relative severity of the 2 % deviance threshold in comparison to the penalties for including variables associated with the more common AIC and BIC methods.

Formal model suitability was determined by calculating the resultant standardized studentized residuals (hereafter simply referred to as 'residuals') in accordance with McCullagh and Nelder (1989) and testing them for homoscedasticity and a normal distribution using the Breusch-Pagan and Lilliefors tests, respectively. The Breusch-Pagan test was chosen as a test for homoscedasticity because it does not involve dividing the residuals into subjective 'high' and 'low' categories (Kutner et al. 2005). The Lilliefors test was chosen as a test for the normal distribution of residuals because it does not assume a specific mean and standard deviation of the data (Conover 1980). The residual variance was calculated as an indicator of an appropriate link function; a value close to one indicates a suitable link function choice (McCullagh and Nelder 1989). The variance was judged to represent a suitable link function if it did not differ from 1.0 in a statistically detectable fashion ($p > 0.05$) from a chi-squared distribution with n-1 degrees of freedom (Bhattacharyya and Johnson 1977), where n is the sample size.

The CPUE data were divided into the same 'early' and 'late' fishery periods as the effort data in order to maintain consistency with the effort models. A 'day' variable was also added to the list of potentially significant explanatory variables in the same form as the effort 'day' variable. A 'year' variable in the form of a qualitative factor was added as well in order to address any interannual variation not accounted for by the explanatory variables. Modeling was again performed by fitting a generalized linear model to the data, but this time a delta approach was used in order to deal with the instances where CPUE was zero (Pennington 1983; Maunder and Punt 2004) (see Appendix 3 for the functions used to perform this task). This approach was chosen because the residuals produced from multiple regression using the typical south basin data did not meet the

homoscedastic and normal distribution assumptions of the model. Conventional predictor variable manipulations such as the log and box-cox transformations also failed to meet these assumptions.

The binary portion of the data (CPUE being equal to zero or set to one when CPUE exceeded zero) were modeled using a quasibinomial distribution (to address the overdispersion which was present in some of the models) with a complimentary log-log link function. The small number of CPUE = 0 records suggested an asymmetrical relationship with the variables under examination and thus required the use of the asymmetrical complimentary log-log link (Kutner et al. 2005). This choice of link function was also supported by the Hosmer-Lemeshow test for goodness-of-fit. The continuous portion of the data (CPUE > 0) were modeled using a gamma distribution with an inverse link function. The gamma distribution was chosen for modeling the portion of the data where CPUE > 0 because the mean appeared to vary with the standard deviation (McCullagh and Nelder 1989). The inverse link function was chosen based on the high proximity of the resultant residual variance to one, the informal check of link function suitability mentioned previously.

Both the binary and the continuous CPUE models were constructed in the same fashion as the effort models; the statistical significance of each variable was again dictated by the percentage of the null deviance it explained. This was done in order to maintain consistency with the effort models. The same methods used for testing the suitability of the effort models were used for testing the suitability of the continuous CPUE data models. Formal model suitability using the binary data were determined using only the Hosmer-Lemeshow test for goodness-of-fit - a common test for response

variables which are of binary form (Agresti 1996). The residual tests performed on the continuous response models were not applied to the binary data because the results would not have been informative (Ortiz and Arocha 2004).

3.3 Results

I) Wave Height Verification, Variable Multicollinearity, and Deviance Threshold Choice

The relationship between buoy wave height (response) and calculated wave height (predictor) was statistically significant ($F = 49.0$, degrees of freedom; numerator, denominator (d.f.) = 1,144, $p < 0.001$, where significance was inferred by convention when $p < 0.05$) with a coefficient of determination of 0.254. The relationship was described by a slope of 0.570 +/- 0.161 (mean +/- 2 standard errors) and an intercept of -0.239 +/- 0.293 (see Figure 3.2). The difference in mean wave height between the early and late periods for each region were not statistically significant (results from a multiple comparison test of means derived from a Kruskal-Wallis test all had p-values > 0.05). Results from analyzing multicollinearity among variables using the variance inflation factor always yielded values less than 4 (see Table 3.1). Spearman rank correlations between all variables examined are listed in Table 3.2. The 2 % null deviance threshold applied a greater penalty to the inclusion of a variable in the model than the BIC selection method using the continuous walleye CPUE data from the typical Gimli region. While the models generated using the deviance threshold and BIC methods produced similar models in terms of the type and number of variables included (see Table 3.3), the AIC selection method generated models which included more variables; some of which had p-values larger than 0.05 for the accepted variables.

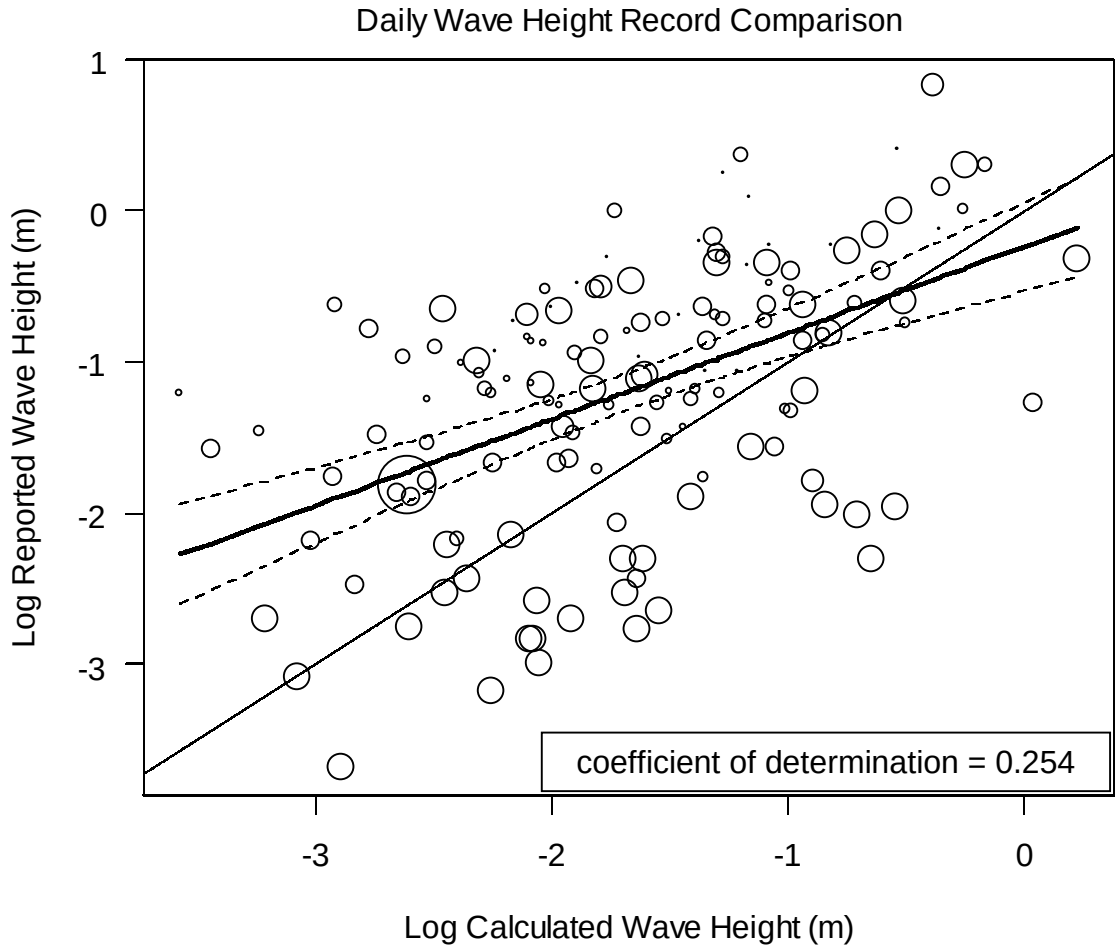

Figure 3.2 Comparison between the natural logarithm of the calculated and recorded maximum significant wave heights. Smaller circle diameter indicates a greater proportion of error in the reported data. The two measures of wave height are not equivalent given that the 95 % estimation interval of the slope (dashed lines, the thick line is the slope), does not encompasses the line y = x over most of its range (thin line). The large degree of variability not explained by the relationship (coefficient of determination = 0.254) indicated that the calculated wave height was also a poor indictor of true wave height as recorded by the buoy.

Table 3.1 Variable inflation factor (VIF) values for all of the explanatory variables used in the catch and effort modeling the process. Table values are the VIFs for the intersecting variables in each row and column. The 'all other variables' category is the calculated VIF between the variable listed in the row and all the other explanatory variables used in the modeling process. Sample size is 399 for the early period and 544 for the late period. By convention, VIF values greater than or equal to 10 indicate problematic multicollinearity between variables (Kutner et al. 2005). As all table values are less than 4 any multicollinearity among explanatory variables was judged to be insignificant.

Early Period	Variable Inflation Factor Values						
Variable	All Other Variables	Cloud Opacity	Day	Pressure	Red River Discharge	Temp.	Visibility
Cloud Opacity	2.437						
Day	1.305	1.001					
Pressure	1.455	1.078	1.004				
Red River Discharge	1.047	1.006	1.000	1.025			
Temperature	2.479	1.534	1.152	1.021	1.007		
Visibility	1.277	1.221	1.007	1.086	1.002	1.039	
Wave Height	1.087	1.012	1.010	1.052	1.000	1.003	1.001

Late Period	Variable Inflation Factor Values						
Variable	All Other Variables	Cloud Opacity	Day	Pressure	Red River Discharge	Temp.	Visibility
Cloud Opacity	1.684						
Day	2.971	1.057					
Pressure	1.457	1.003	1.020				
Red River Discharge	1.055	1.000	1.009	1.000			
Temperature	3.916	1.280	2.505	1.153	1.004		
Visibility	1.344	1.302	1.039	1.053	1.002	1.026	
Wave Height	1.102	1.014	1.018	1.040	1.001	1.006	1.019

Table 3.2 Spearman ranked correlation values for all of the explanatory variables used in the catch and effort modeling process. Table values are the correlations for the intersecting variables in each row and column. Sample size is 399 for the early period and 544 for the late period. The large magnitude of the correlation between day and temperature in both the early and late fishery periods had the potential to reduce the statistical significance of either variable when both were present in a model.

Early Period	Spearman Ranked Correlation Values					
Variable	Cloud Opacity	Day	Pressure	Red River Discharge	Temp.	Visibility
Day	0.022					
Pressure	-0.270	-0.060				
Red River Discharge	-0.074	-0.014	0.155			
Temperature	-0.590	0.363	-0.143	0.084		
Visibility	-0.425	-0.080	0.282	0.045	0.195	
Wave Height	0.110	-0.097	-0.223	0.014	-0.051	-0.028

Late Period	Spearman Ranked Correlation Values					
Variable	Cloud Opacity	Day	Pressure	Red River Discharge	Temp.	Visibility
Day	0.233					
Pressure	-0.054	0.141				
Red River Discharge	-0.005	-0.097	0.006			
Temperature	-0.468	-0.775	-0.364	0.065		
Visibility	-0.482	-0.194	0.225	-0.045	0.159	
Wave Height	0.119	0.131	-0.195	0.033	-0.080	-0.138

II) Effort Modeling

Both the early and late fishery periods of all regions exhibited a significant relationship between effort and one or more of the variables examined (proportion of the deviance explained by the variable(s) was greater than or equal to 2 %, see Table 3.3). Figure 3.3 shows the relationship between effort and day. The percentage of the deviance explained and the p-value for each of the statistically significant orders of the variables are provided in Appendix 4, Table A4.1 along with the variable addition order for each model. The mean percentage of the deviance explained in all regions was 51.367 +/- 6.962 for the early period and 33.817 +/- 9.552 for the late period. The typical relationship between the observed and expected effort for both periods is plotted in Figure 3.4; all regions displayed a similar form. The general form of the model used to generate expected effort is given in equation 3.4. See Appendix 4, Table A4.1 for the

(3.4) $$\hat{y}_i = \log_e (\beta_0 + \beta_1 x_{i1} + ... + \beta_k x_{ik})$$

relevant variables and their addition order for each model. Table 3.4 values are the percentage of the deviance explained by a given variable (all statistically significant orders); the inclusion of a value indicates that a polynomial order of the variable was statistically significant in the final model for that particular region and period.

As apparent from Table 3.4, the day variable was always statistically significant, as was the year variable with the exception of the late fishery in the south basin. Temperature and wave height were statistically significant in some regions and periods, while all other environmental variables were never statistically significant. The typical

Table 3.3 Models generated with different variable selection techniques (AIC, BIC, and deviance threshold) using the continuous walleye catch per unit effort data from the typical Gimli region. The inclusion of a value in the table indicates the variable was selected by the corresponding variable selection technique. With the exception of year, the number following a variable indicates the polynomial order of the variable (no number = order 1). The specific year is listed after the year variable (no polynomial order was used as it was a factor variable). AIC included variables with $p > 0.05$ while the other two methods did not. The 2 % deviance threshold method selected an identical set of variables in the early period, but was more conservative than the BIC method in the late period. This latter point is evident in the table where the percent null deviance (% Dev) is less than 2 % for Day2 and Red_Flow, both of which were selected by BIC.

Early Period (sample size = 373)

Variable	AIC	BIC	Dev Threshold	
	p-value	p-value	p-value	% Dev
Intercept	< 0.001	< 0.001	< 0.001	0
Day	< 0.001	< 0.001	< 0.001	26.21
Day3	0.006	0.002	0.002	2.51
Pressure	0.014			
Pressure2	0.086			
Pressure3	0.011			
Temp2	0.125			
Temp3	< 0.001			
Year_1997	0.694			
Year_1998	0.211			
Year_1999	0.199			
Year_2000	0.072			
Year_2001	0.014			
Year_2002	0.171			
Year_2003	0.602			
Year_2004	0.004			

Late Period (sample size = 530)

Variable	AIC	BIC	Dev Threshold	
	p-value	p-value	p-value	% Dev
Intercept	< 0.001	< 0.001	< 0.001	0
C_Opacity2	0.053			
Day	< 0.001	< 0.001	< 0.001	18.79
Day2	0.005	0.002	0.002	1.82
Pressure	0.050			
Red_Flow	0.084	< 0.001	< 0.001	1.90
Red_Flow3	0.171			
Temp3	< 0.001			
Visibility	0.138			
Year_1997	0.004			
Year_1998	0.022			
Year_1999	< 0.001			
Year_2000	< 0.001			
Year_2001	0.003			
Year_2002	0.017			
Year_2003	0.002			
Year_2004	0.016			

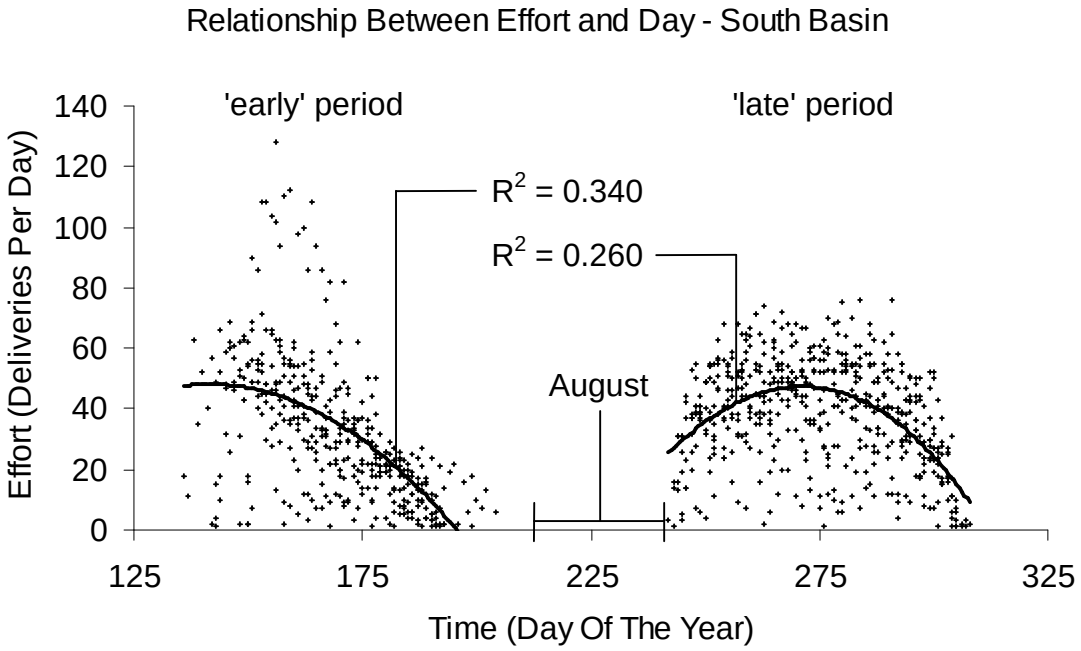

Figure 3.3 The relationship between day and fishing effort for the entire south basin region (1996-2004). Day was defined as the day of the year (where January 1 of each year was day 1). Other sub-regions within the south basin had similar functional forms but are not displayed for simplicity. The strength of this relationship lead to the inclusion of a 'day' variable when environmental impacts on effort were modeled in order to increase the explanatory power of the model. Effort data were divided into an 'early' and 'late' fishery period because fishing was prohibited during the month of August (day 213-243) for all of the years examined (Manitoba Conservation 2006). The coefficient of determination (R^2) for each period is labeled on the figure.

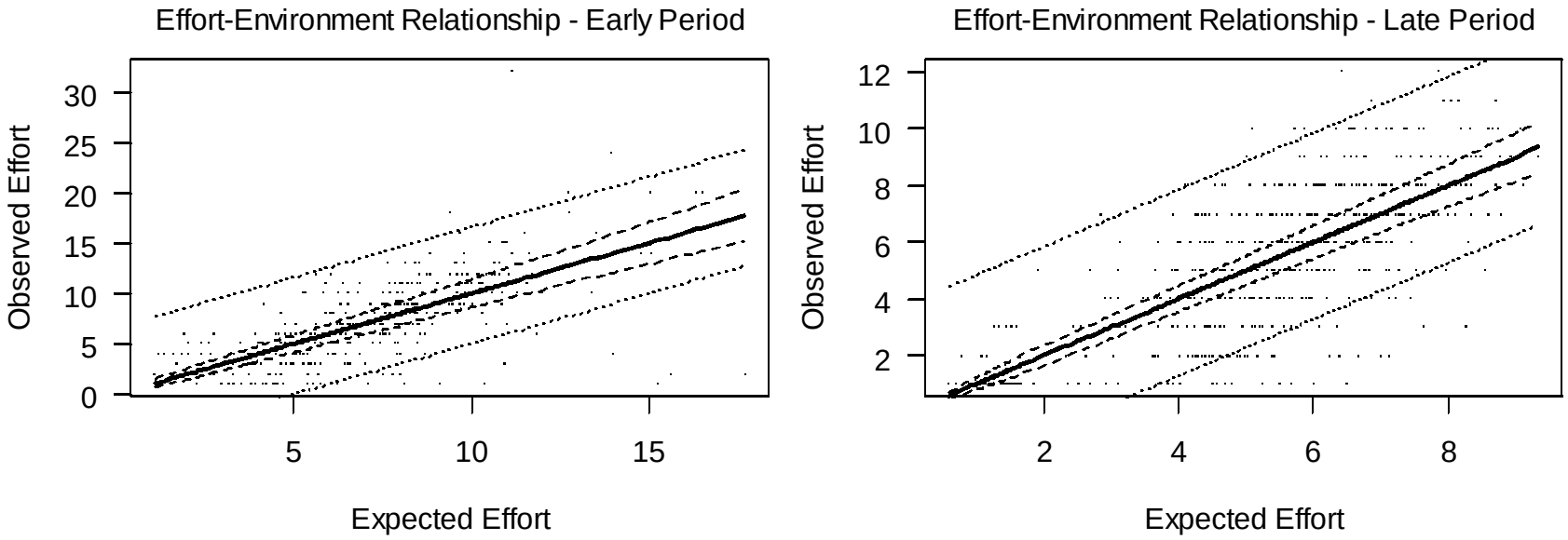

Figure 3.4 Effort-environment relationship (Riverton region, all regions displayed a similar form). The relationships were based on a generalized linear model with a log link function and a quasipoisson distribution. The 95 % estimation interval is represented by the dashed lines, while the 95 % prediction interval is depicted by the dotted lines. Effort had a statistically significant relationship with at least one variable in both periods and all regions. The variables included and their addition order for this and the remaining effort models are located in Appendix 4, Table A4.1. The model that relates the observed and expected effort shown above is a 1:1 relationship. The general form of the model used to generate the expected effort is given in equation 3.4.

Table 3.4 Strength and significance of the effort relationships. Table values are the percentage of the deviance explained by each variable. A reported value indicates statistical significance; the percentage of the deviance explained by the variable greater than or equal to 2 % (Maunder and Punt 2004). 'LI' indicates the variable is a measure of light intensity. The percentage of the deviance explained and the p-value for all of the statistically significant orders of the variables are provided in Appendix 4, Table A4.1 along with the variable addition order for each model.

Early Period	Gimli	Riverton	Selkirk	Traverse Bay	Wanipigow	South Basin
LI: Cloud Opacity						
LI: Visibility						
Pressure						
Red River Flow						
Temperature			6.6		3.5	
Wave Height		2.7	3.8			
Day	30.3	19.9	12.6	28.2	16.1	31.2
Year Factor	35.4	22.6	23.9	20.9	24.2	26.3
Total	65.7	45.2	46.9	49.1	43.8	57.5
Sample Size	375	352	342	348	151	399
Late Period						
LI: Cloud Opacity						
LI: Visibility						
Pressure						
Red River Flow						
Temperature	6.3			8.4		7.0
Wave Height		10.1			7.4	3.6
Day	8.6	8.5	25.1	12.5	15.3	17.6
Year Factor	6.1	36.4	12.8	7.4	7.9	1.9
Total	21.0	55.0	37.9	28.3	30.6	30.1
Sample Size	530	502	455	496	490	544

form of the relationships between effort and the variables found to be statistically significant are depicted in Figure 3.5 (all regions and periods for which the variable was statistically significant exhibited a similar form). The response value was dictated by the variable coefficients generated by the modeling process and show only the changes in effort magnitude in relation to the particular environmental variable. Only the variable of interest (all statistically significant orders) is plotted in each graph.

From Figure 3.5 it is apparent that high effort in the early period was related to low day values (concave down), while in the late period it was related to mid-range day values (concave down). The day variable always explained a larger percentage of the deviance than all of the other environmental variables combined (with the exception of the late period in the Riverton region, see Table 3.4). Regardless of fishery period, high effort was always partly related to high temperatures (monotonic increase) and low wave heights (monotonic decrease) when the individual variables were statistically significant in their respective models (see Table 3.4). The suitability of the models to the data was indicated by the residual variance, which differed from the ideal value of one (McCullagh and Nelder 1989) in 10 of the 12 models generated. In addition, the residual requirements of a normal distribution and an equal variance were not always met. Residual homoscedasticity was achieved in 6 of the 12 models, while a normal distribution was achieved in only 1 (residual histogram and scatterplot are shown in Figure 3.6, all regions and periods exhibited a similar form). Table 3.5 outlines the assumptions violated by each region and fishery period.

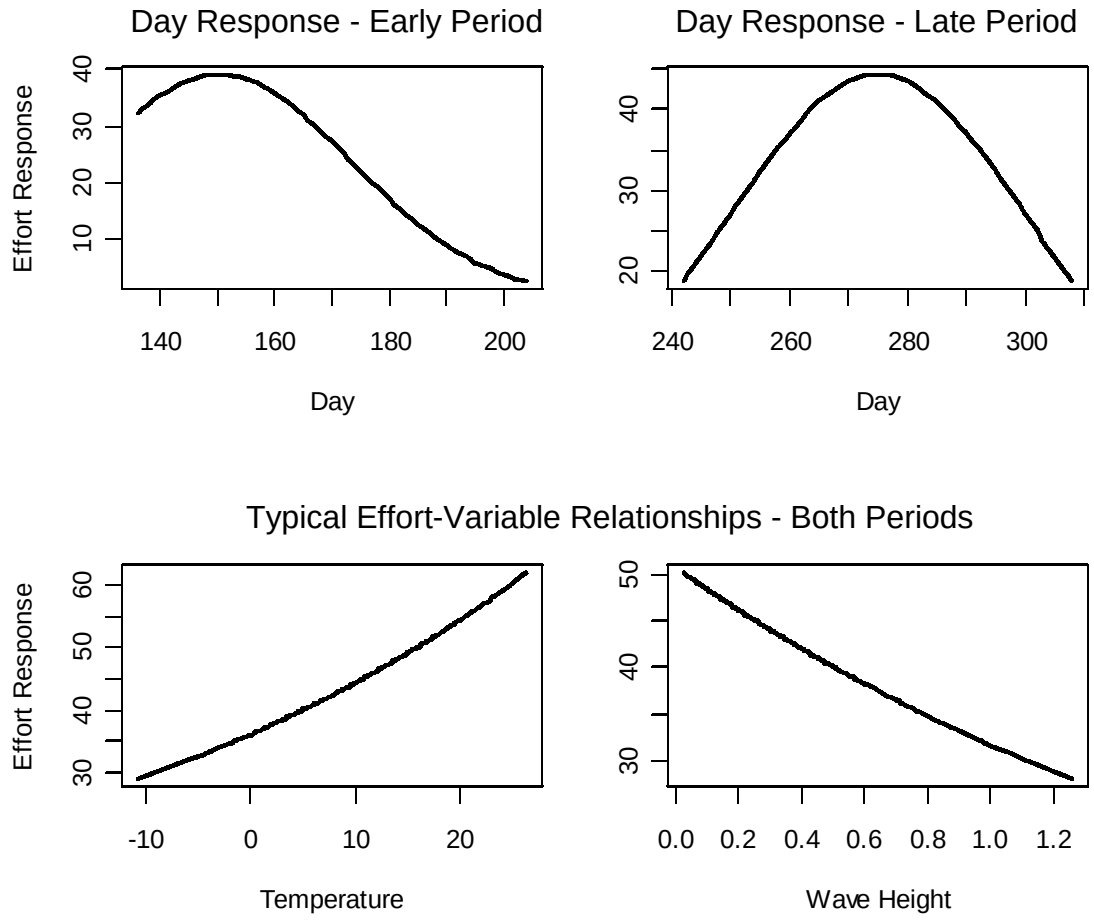

Figure 3.5 Typical effort-variable responses for both periods (south basin region). The temperature and wave height relationships were taken from the effort responses of the late period. However, they are typical of the effort responses in all periods in the other sub-regions within the south basin. Regression coefficients were taken directly from the model itself; the response variable is thus the change in effort associated with each variable. Day is day of the year (where January 1 of each year is day 1), temperature is dry bulb air temperature in degrees Celsius, and wave height is maximum significant wave height in meters.

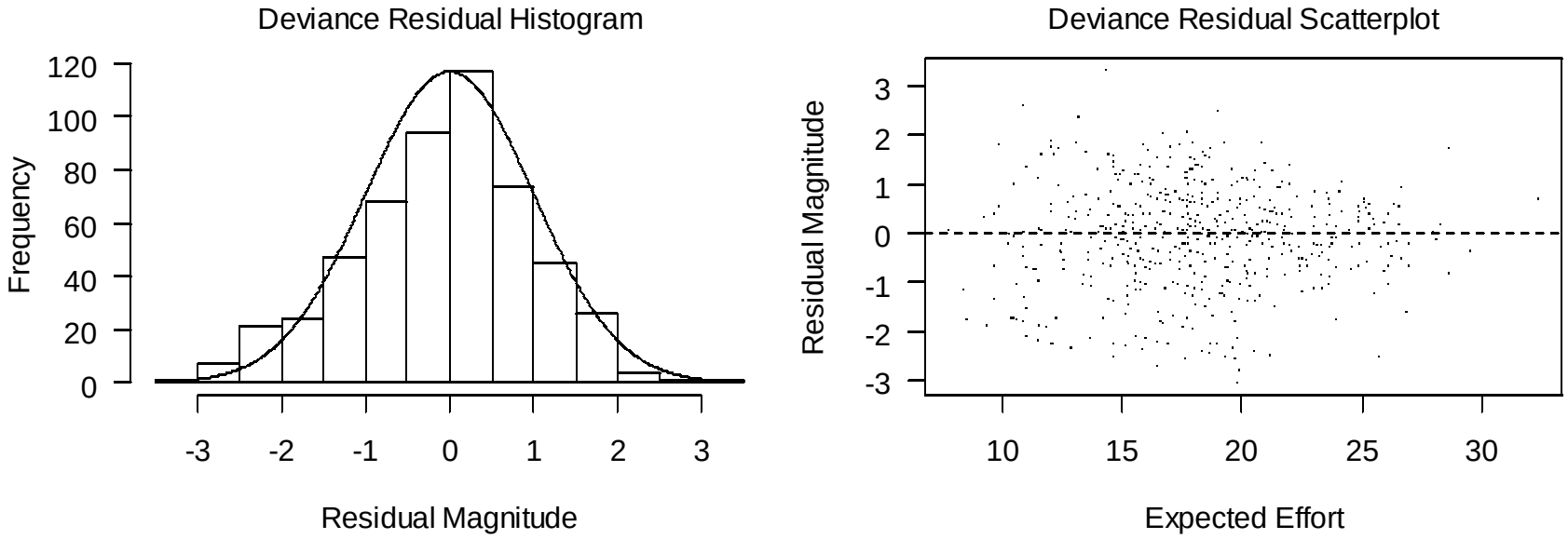

Figure 3.6 Informal effort model diagnostics - standardized studentized residual histogram and scatterplot. Data are from the typical Gimli region late fishery period model (sample size = 530); all other regions and periods displayed a similar form. The solid line on the histogram is the standard normal distribution used as a visual comparison with the observed residual distribution. These figures suggest that the model is appropriate for the data by visual inspection; the residuals appear normally distributed and the variance appears equal. Formal tests do not support this interpretation (see Table 3.5). However, given the form of the above figures the violations are not judged to be problematic.

Table 3.5 Formal effort model diagnostics using standardized studentized residuals. Table entries are p-values. Testing for normally distributed residuals was performed using a Lilliefors test; values less than 0.05 were judged to have a non-normal distribution by convention. Testing for equality of variance was performed using a Breusch-Pagan test; values less than 0.05 were judged to have an unequal variance. The suitability of the link function was tested using the variance of the residuals; values close to 1 support the link function chosen (McCullagh and Nelder 1989). Table values are from a chi-squared distribution with degrees of freedom 1 less than the sample size (Bhattacharyya and Johnson 1977); values less than 0.05 were judged to have an inappropriate link function. Residual homoscedasticity was observed in 6 of the 12 models generated, a suitable link function in 2, and a normal distribution was only present in 1. However, the appearance of the residual plots show that the departures listed below were unlikely to be problematic (see Figure 3.6).

Early Period

Model Assumption	Gimli	Riverton	Selkirk	Traverse Bay	Wanipigow	South Basin
Normal Distribution	0.026	< 0.001	0.002	0.019	0.488	< 0.001
Equal Variance	0.952	< 0.001	0.390	< 0.001	0.005	0.006
Suitable Link	0.040	0.008	0.007	0.004	1.000	< 0.001
Sample Size	375	352	342	348	151	399

Late Period

Model Assumption	Gimli	Riverton	Selkirk	Traverse Bay	Wanipigow	South Basin
Normal Distribution	0.003	< 0.001	< 0.001	0.020	0.003	< 0.001
Equal Variance	< 0.001	0.511	0.114	0.323	0.839	0.010
Suitable Link	0.008	0.031	0.001	0.097	0.015	< 0.001
Sample Size	530	502	455	496	490	544

III) CPUE Modeling

All regions exhibited a significant relationship between continuous CPUE and one or more of the variables examined (proportion of the deviance explained by the variable(s) was greater than or equal to 2 %, see Tables 3.6A and B). Figure 3.7 shows the relationship between CPUE and day. The percentage of the deviance explained and the p-value for each of the statistically significant orders of the variables are provided in Appendix 4, Table A4.2 along with the variable addition order for each model. The typical relationship between the observed and expected continuous CPUE data for both species are plotted in Figure 3.8; all regions displayed a similar form. The general form of the model used to generate expected CPUE is given in equation 3.5. See Appendix 4,

(3.5) $$\hat{y}_i = (\beta_0 + \beta_1 x_{i1} + ... + \beta_k x_{ik})^{-1}$$

Table A4.2 for the relevant variables and their addition order for each model. Table 3.6 values are the percentage of the deviance explained by a given environmental variable (all statistically significant orders); the inclusion of a value indicates that a polynomial order of the variable was statistically significant in the final model for that particular region. The results from the binary modeling process are not shown. They were judged to explain the data poorly because the probability of non-zero catch never differed appreciably from 1.0 (greater than 0.99) with each variable found to be statistically significant. This was true over the entire numerical range of the variables for any period, region, and species (the typical binary CPUE-variable relationship is shown in Figure 3.9.

Table 3.6A Strength and significance of the catch per unit effort (CPUE) relationships using the continuous walleye data. Table values are the percentage of the deviance explained by each variable. A reported value indicates statistical significance; the percentage of the deviance explained by the variable greater than or equal to 2 % (Maunder and Punt 2004). 'LI' indicates the variable is a measure of light intensity. The percentage of the deviance explained and the p-value for all of the statistically significant orders of the variables are provided in Appendix 4, Table A4.2 along with the variable addition order for each model.

Early Period	Gimli	Riverton	Selkirk	Traverse Bay	Wanipigow	South Basin
LI: Cloud Opacity						
LI: Visibility						
Pressure						
Red River Flow		2.3				
Temperature					2.3	
Wave Height						
Day	24.3	24.5	28.9	35.8		18.0
Year Factor	5.7	26.0	12.1	14.9	45.0	7.2
Total	30.0	52.8	41.0	50.7	47.3	25.2
Sample Size	373	352	334	361	151	398
Late Period						
LI: Cloud Opacity						
LI: Visibility						
Pressure						
Red River Flow						
Temperature			5.7			
Wave Height						
Day	18.0	31.8		12.4	23.9	30.8
Year Factor	8.4	22.8	20.2	11.2	23.2	11.2
Total	26.4	54.6	25.9	23.6	47.1	42.0
Sample Size	530	502	455	509	490	544

Table 3.6B Strength and significance of the catch per unit effort (CPUE) relationships using the continuous sauger data. Table values are the percentage of the deviance explained by each variable. A reported value indicates statistical significance; the percentage of the deviance explained by the variable greater than or equal to 2 % (Maunder and Punt 2004). 'LI' indicates the variable is a measure of light intensity. The percentage of the deviance explained and the p-value for all of the statistically significant orders of the variables are provided in Appendix 4, Table A4.2 along with the variable addition order for each model.

Early Period	Gimli	Riverton	Selkirk	Traverse Bay	Wanipigow	South Basin
LI: Cloud Opacity	4.7					2.2
LI: Visibility						
Pressure						
Red River Flow						7.0
Temperature		4.7		8.0		2.2
Wave Height					12.9	
Day	11.0	8.4	13.7	10.4		
Year Factor	9.7	19.7	10.4	13.4	68.8	1.6
Total	25.4	32.8	24.1	31.8	81.7	13.0
Sample Size	343	333	331	311	46	387
Late Period						
LI: Cloud Opacity						
LI: Visibility						
Pressure						
Red River Flow						
Temperature						
Wave Height						
Day						
Year Factor	41.6	59.9	34.3	39.8	43.6	56.9
Total	41.6	59.9	34.3	39.8	43.6	56.9
Sample Size	516	469	351	472	471	538

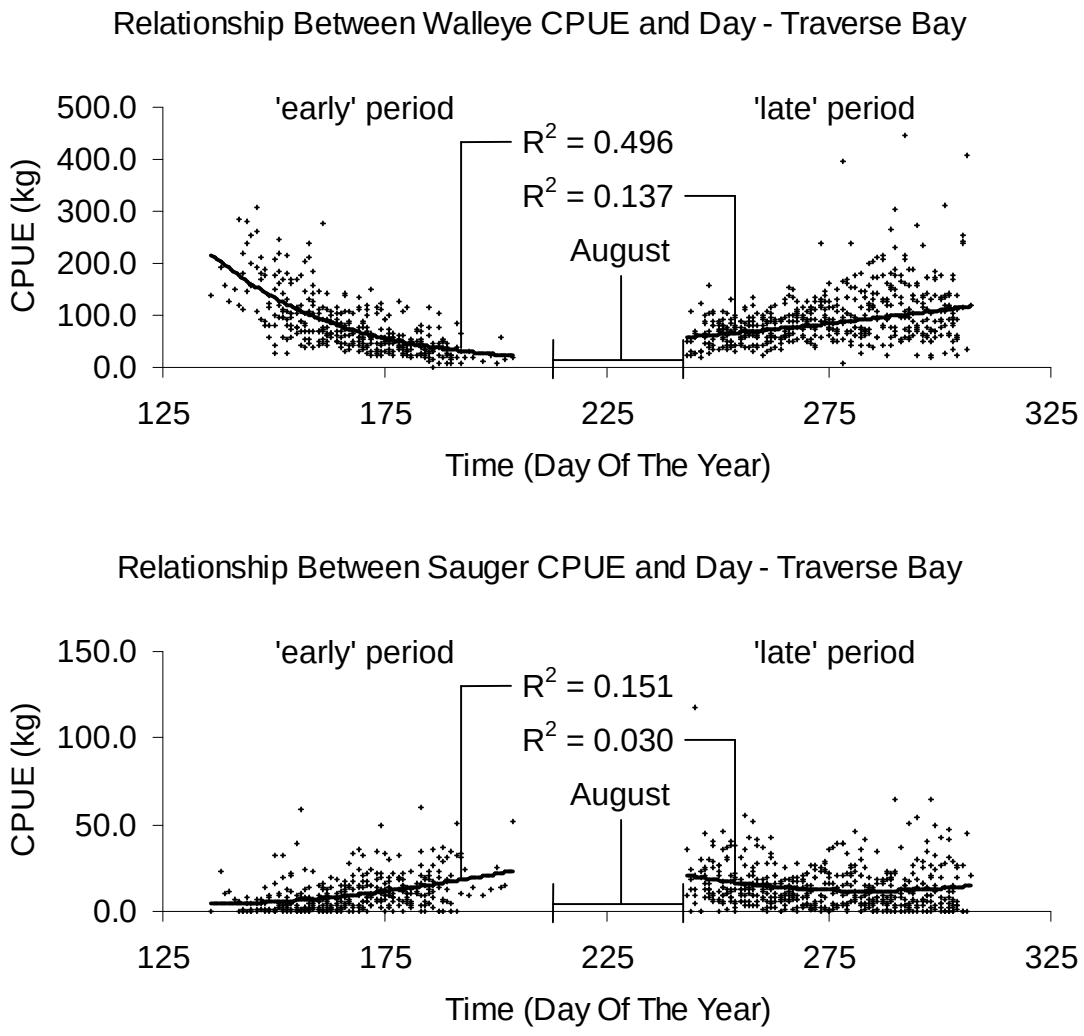

Figure 3.7 The relationship between day and catch per unit effort (CPUE) for the Traverse Bay region (1996-2004). Day was defined as the day of the year (where January 1 of each year was day 1). Other regions had similar functional forms but are not displayed for simplicity. The strength of this relationship lead to the inclusion of a 'day' variable when environmental impacts on CPUE were modeled in order to increase the explanatory power of the model. The data were divided into an 'early' and 'late' fishery period in order to maintain consistency with the effort data (see Figure 3.3).

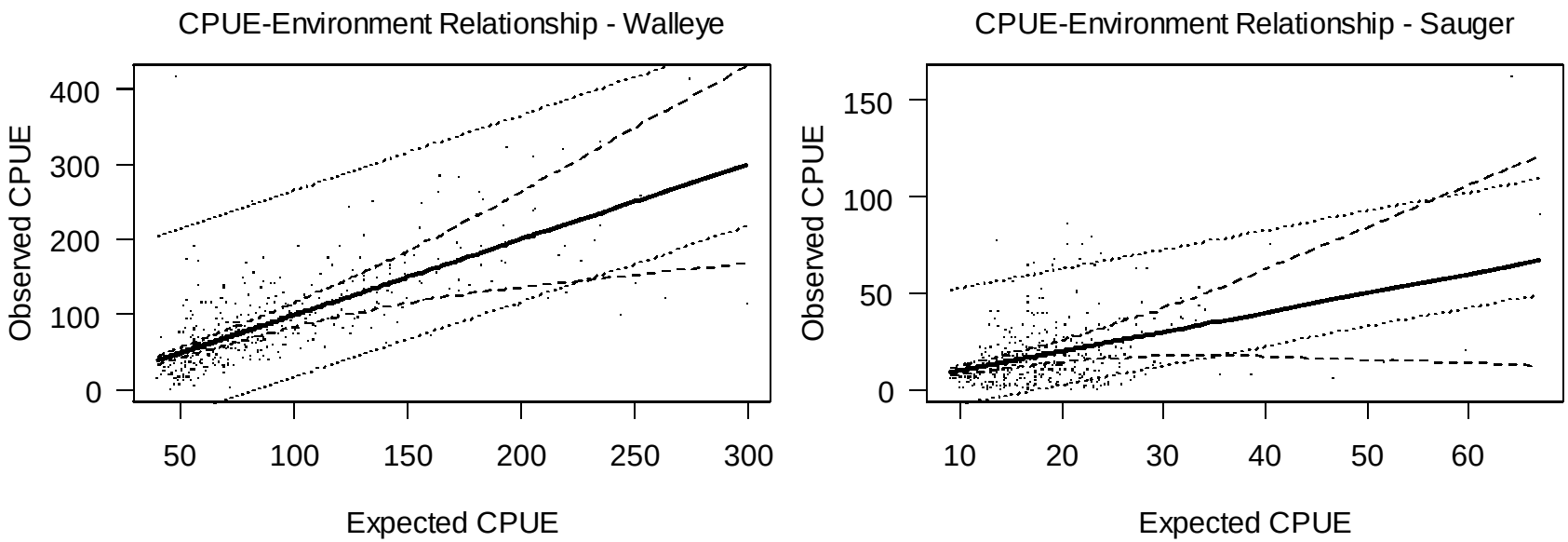

Figure 3.8 Continuous catch per unit effort (CPUE)-environment relationship (early period of the south basin region, all regions and periods displayed a similar form). The relationships were based on a generalized linear model with an inverse link function and a gamma distribution. The 95 % estimation interval is represented by the dashed lines, while the 95 % prediction interval is depicted by the dotted lines. The crossing of these two intervals at high expected CPUE indicates the model is not precise for predicting large CPUE values. The variables included and their addition order for this and the remaining effort models are located in Appendix 4, Table A4.2. The model that relates the observed and expected CPUE shown above is a 1:1 relationship. The general form of the model used to generate the expected effort is given in equation 3.5.

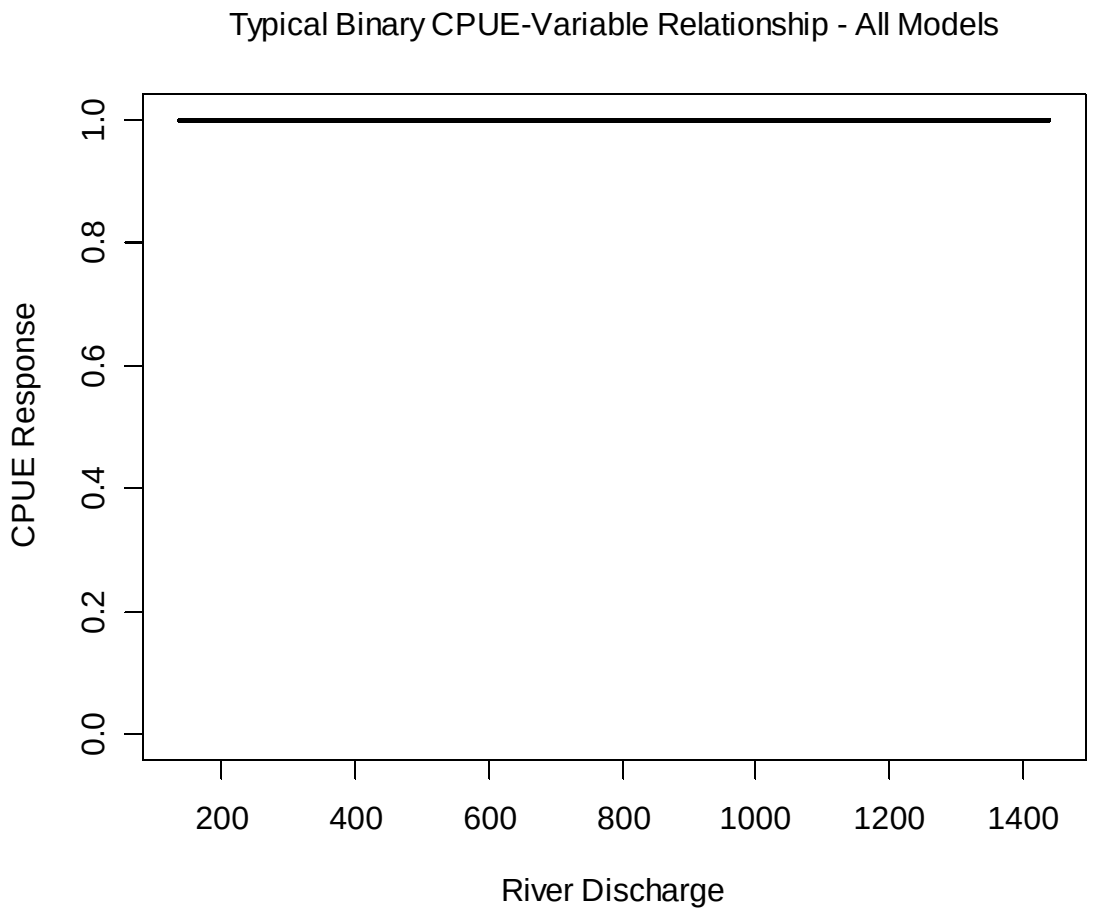

Figure 3.9 Typical binary catch per unit effort (CPUE)-variable response (early period walleye data for the Traverse Bay region). All regions, periods, variables, and species displayed a similar form. River discharge is discharge from the Red River in $cm^3 \cdot s^{-1}$. Regression coefficients were taken directly from the model itself; the response variable is thus the change in CPUE associated with each variable. The binary models were judged a poor descriptor of the binary CPUE data because all CPUE responses did not differ appreciably (less than 0.01) over the entire range of the predictor variables found to be statistically significant (river discharge in the above case).

Unless otherwise specified, all of the following discussions refer only to the continuous CPUE data.

As stated previously, the continuous CPUE data exhibited a statistically significant relationship with a number of the variables examined. The mean percentage of the deviance explained in all regions for the walleye data was 41.167 +/- 9.262 for the early period and 36.600 +/- 10.652 for the late period while for the sauger data it was 34.800 +/- 19.632 for the early period and 46.017 +/- 8.266 for the late period. As apparent from Table 3.6, analysis of deviance did not reveal any statistical significance with barometric pressure or atmospheric visibility. The 'day' temporal variable was statistically significant in the majority of the models generated with the exception of the sauger CPUE models for the late period - where none of the variables except year was statistically significant. The day variable always explained a larger percentage of the deviance than all of the other environmental variables combined when it was statistically significant (see Table 3.6). Although year was always included in the model regardless of statistical significance, it was statistically significant in all regions, periods, and species with the exception of the sauger CPUE model in the south basin during the early period (explained deviance < 2 %). The typical form of the relationships between the CPUE data and the variables found to be statistically significant are depicted in Figures 3.10A and 3.10B (all regions and periods for which the variable was statistically significant exhibited a similar form). The response value was dictated by the variable coefficients generated by the modeling process and show only the changes in CPUE magnitude in relation to the particular environmental variable. Only the variable of interest (all statistically significant orders) is plotted in each graph. In order to investigate the

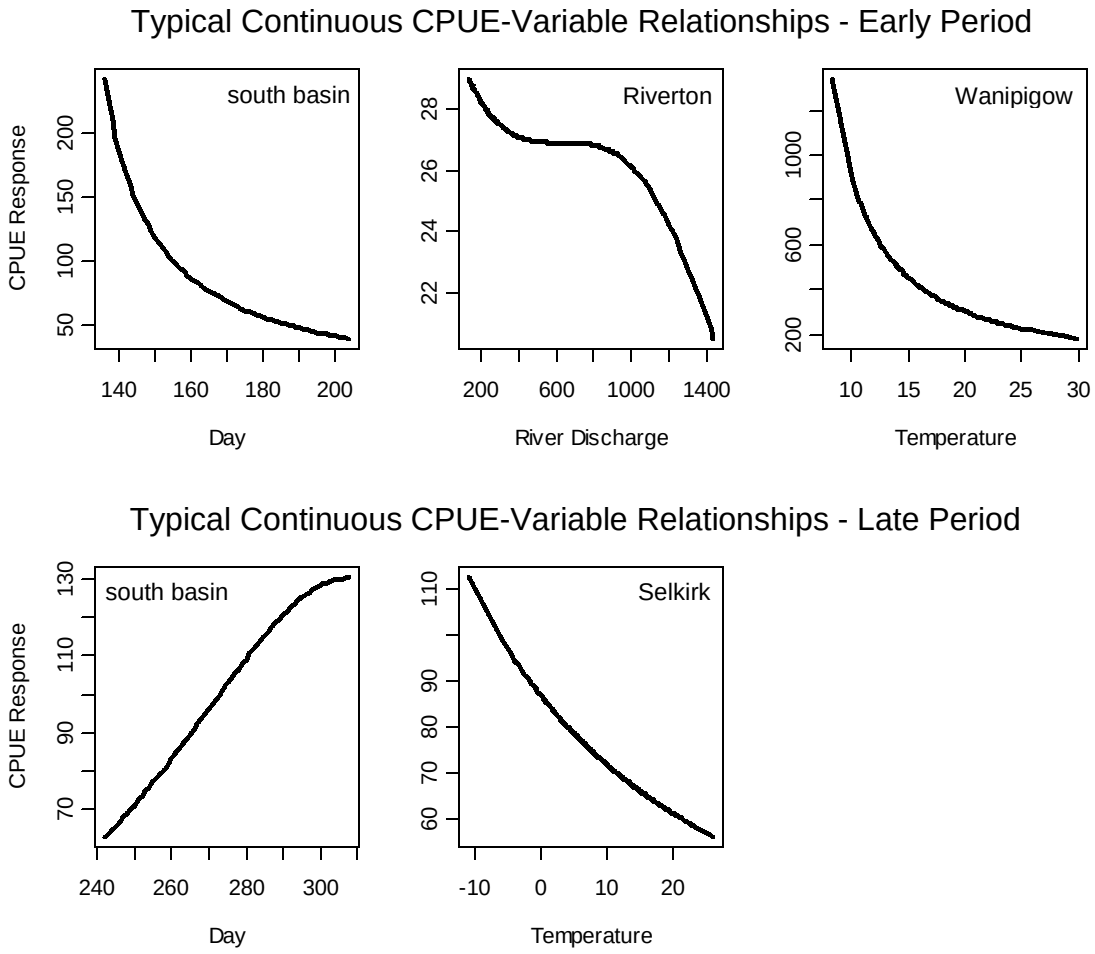

Figure 3.10A Typical catch per unit effort (CPUE)-variable responses for the continuous walleye data (originating region labeled inside graph). Regression coefficients were taken directly from the model itself; the response variable is thus the change in CPUE associated with each variable. Day is measured as the day of the year (where January 1 of each year was day 1), river discharge is discharge from the Red River in $cm^3 \cdot s^{-1}$, and temperature is dry bulb air temperature in degrees Celsius.

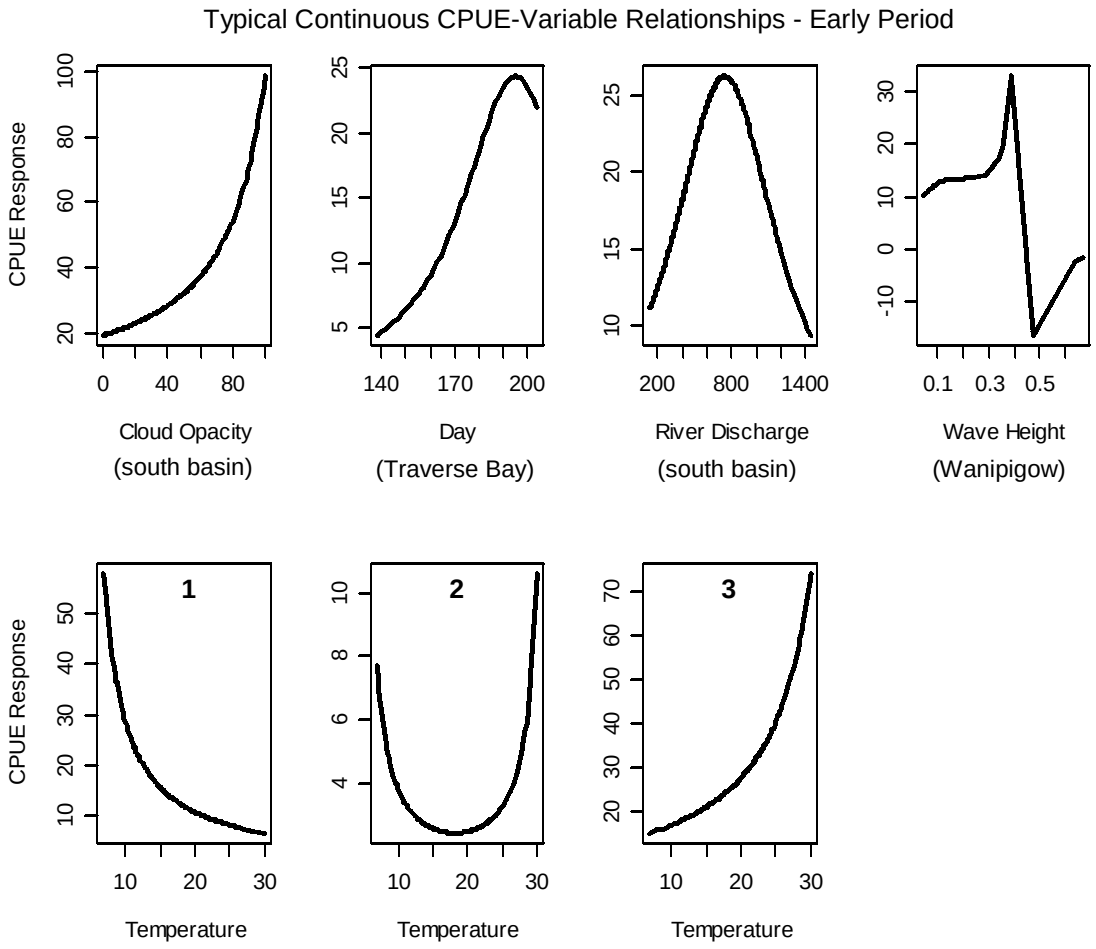

Figure 3.10B Typical catch per unit effort (CPUE)-variable responses for the continuous sauger data (originating region given in parentheses, only the early period was statistically significant with variables other than year). As in Figure 3.10A, the response variable is the change in CPUE associated with each variable. Cloud opacity is measured as a percentage and wave height is maximum significant wave height in meters. Other variable units are described in Figure 3.10A. Temperature took on 3 distinct forms depending upon region: Traverse Bay (1), Riverton (2), and the entire south basin (3). Temperature was not statistically significant in other regions.

possibility of preferential species discarding at high CPUE values, each period of daily walleye and sauger CPUE were plotted against each other with typical results depicted in Figure 3.11. The average coefficient of determination between all regions was 0.0436 +/- 0.0289 for the early period and 0.00641 +/- 0.00611 for the late period.

From Figure 3.10A it is apparent that high walleye CPUE was related to low day values in the early period (monotonic decrease), high day values in the late period (monotonic increase), high Red River discharge rates (concave down), and low temperatures (monotonic decrease) when the individual variables were statistically significant in their respective models (see Table 3.6A). From Figure 3.10B it is apparent that high sauger CPUE for the early period was related to high cloud opacity (monotonic increase), high day values (concave down), mid-range Red River discharge rates (concave down), extreme temperatures (various functional forms), and low wave heights (sinusoidal) when the individual variables were statistically significant in their respective models (see Table 3.6B). The relationship between temperature and sauger CPUE in the early period exhibited 3 distinct forms (shown in Figure 3.10B): high sauger CPUE was associated with low temperatures in Traverse Bay (monotonic decrease), extreme values in Riverton (concave up), and high temperatures in the south basin as a whole (monotonic increase).

Although using a delta approach incorporating generalized linear models did increase the number of relationships meeting the model assumptions compared to alternative methods (such as multiple regression analysis and alternative link functions), the residual requirements of a normal distribution and an equal variance were not always met (see Table 3.7). Residual homoscedasticity was achieved in 19 of the 24 of models, a

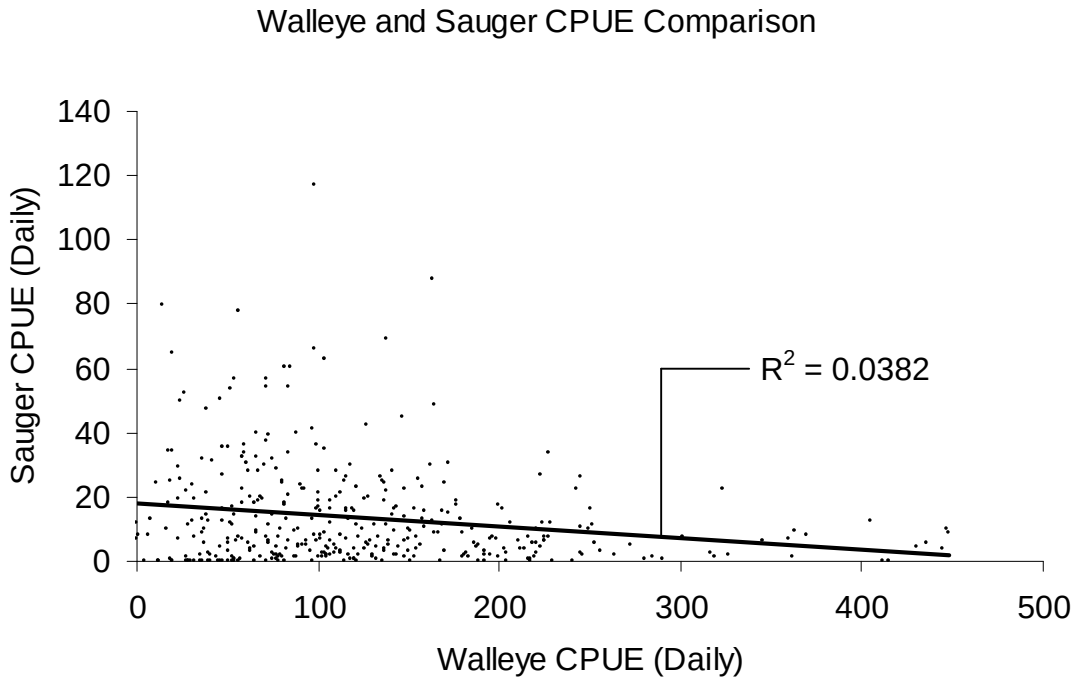

Figure 3.11 Comparison of daily walleye and sauger catch per unit effort (CPUE) values for the determination of discarding practices (early period of the Gimli region, all regions displayed a similar form). The low value of the coefficient of determination ($R^2 <$ 0.1) was judged to represent a lack of significant discarding practices between walleye and sauger. The average coefficient of determination between all regions in the south basin was also less than 0.1 at 0.0436 +/- 0.0289 for the early period and 0.00641 +/- 0.00611 for the late period (mean +/- 2 standard errors), which resulted in an identical conclusion for all fishery periods and regions of the basin.

Table 3.7 Formal catch per unit effort (CPUE) diagnostics using standardized studentized residuals from the continuous data. Tests for the continuous CPUE models are the same as those described for effort in Table 3.5. As shown in the table, residual homoscedasticity was observed in 19 of the 24 models generated, a normal distribution in 10, and a suitable link function in only 9. However, the appearance of the residual plots show that the departures listed below are unlikely to be problematic (see Figure 3.12).

Walleye (Early Period)

Model Assumption	Gimli	Riverton	Selkirk	Traverse Bay	Wanipigow	South Basin
Normal Distribution	0.019	0.007	< 0.001	< 0.001	0.739	< 0.001
Equal Variance	< 0.001	0.123	0.711	0.216	0.621	0.008
Suitable Link	< 0.001	0.328	< 0.001	< 0.001	0.602	< 0.001
Sample Size	373	352	334	361	151	398

Walleye (Late Period)

Model Assumption	Gimli	Riverton	Selkirk	Traverse Bay	Wanipigow	South Basin
Normal Distribution	< 0.001	0.011	0.185	0.005	0.109	< 0.001
Equal Variance	0.428	0.749	0.749	0.768	0.641	0.842
Suitable Link	< 0.001	< 0.001	0.030	< 0.001	0.281	0.061
Sample Size	530	502	455	509	490	544

Sauger (Early Period)

Model Assumption	Gimli	Riverton	Selkirk	Traverse Bay	Wanipigow	South Basin
Normal Distribution	0.828	0.710	0.018	0.239	0.403	0.007
Equal Variance	0.595	0.499	0.865	0.740	0.265	0.416
Suitable Link	0.148	0.975	< 0.001	0.224	0.923	0.048
Sample Size	343	333	331	311	46	387

Sauger (Late Period)

Model Assumption	Gimli	Riverton	Selkirk	Traverse Bay	Wanipigow	South Basin
Normal Distribution	< 0.001	0.002	0.706	0.835	0.717	< 0.001
Equal Variance	0.001	0.263	0.653	0.553	0.005	0.002
Suitable Link	< 0.001	0.004	0.039	0.163	0.005	0.007
Sample Size	516	469	351	472	471	538

normal distribution was achieved in 10, and an ideal variance was achieved in only 9 of the 24 models (residual scatterplot and histogram shown in Figure 3.12, all regions exhibited similar form).

3.4 Discussion

The results of this study illustrated that environmental effects on both catch and effort were prevalent in the south basin; 24 of the 36 models created using continuous data displayed statistical significance with at least one environmental variable. In support of the effort hypothesis, increases in wave height and decreases in temperature were associated with reduced effort and both are indicative of harsh weather conditions from a fishing perspective. However, other environmental variable values which indicated such harsh weather conditions did not reduce effort; only conditions which reduced walleye CPUE did so. Simply put, effort increased when the fishing was good and when the weather was good for fishing. The relationship between CPUE and temperature supported the CPUE hypothesis; sauger CPUE increased when temperature increased. However, in contrast with this hypothesis the opposite trend was observed in relation to walleye CPUE. This result was possibly explained by the temperature preferences of both species. In addition, sauger CPUE was found to increase with increasing cloud opacity; suggesting an affinity for conditions with lowered light levels. This conclusion supported the CPUE hypothesis as well. Further examination of these relationships is given in the following sections.

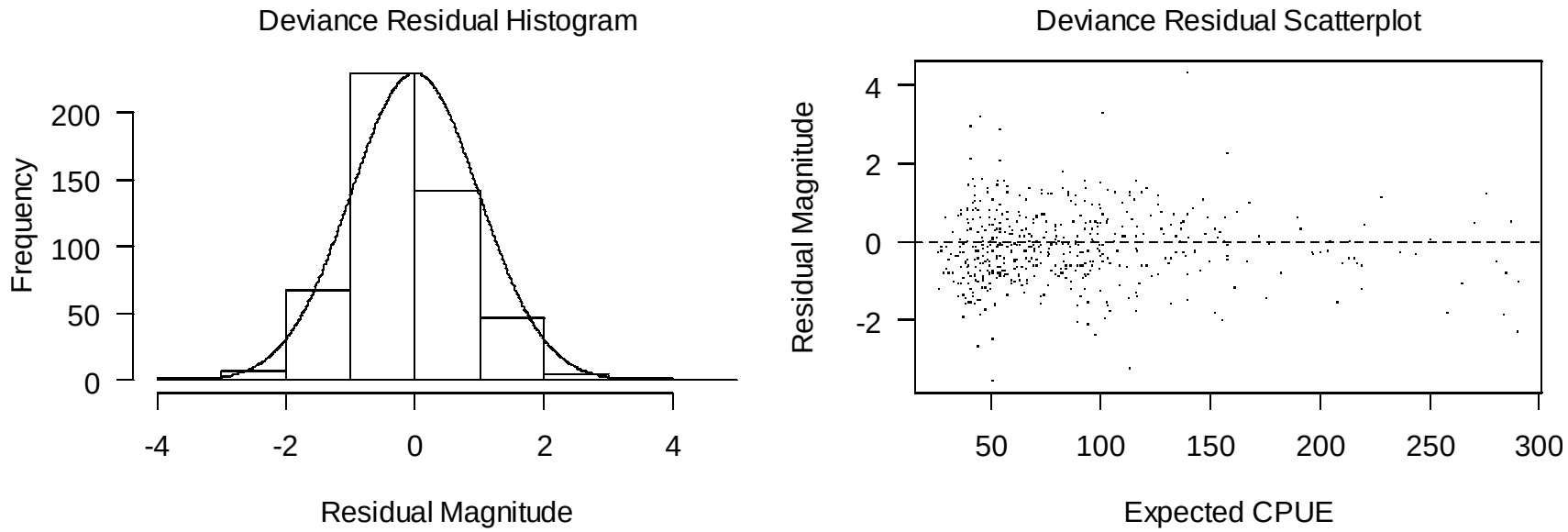

Figure 3.12 Informal catch per unit effort (CPUE) diagnostics - standardized studentized residual histogram and scatterplot. Data are from the typical Riverton region continuous walleye CPUE data (early period, sample size = 352); both species, periods and all other regions displayed a similar form. The solid line on the histogram is the standard normal distribution used as a visual comparison with the observed residual distribution. These figures suggest that the model is appropriate for the data by visual inspection; the residuals appear normally distributed and the variance appears equal. Formal tests do not support this interpretation (see Table 3.7). However, given the form of the above figures the violations are not judged to be problematic.

I) Wave Height Verification, Variable Multicollinearity, and Deviance Threshold Choice

A slope of 1 was not within the 95 % estimation interval between the calculated wave height and the observed wave height as recorded by the buoy. Thus wave height calculations were not an equivalent measure of true wave height. More importantly, the large proportion of the variability not explained by the relationship (as indicated by the coefficient of determination) suggested that the calculated wave height was a poor indictor of true wave height as recorded by the buoy. However, the buoy data are not flawless (as indicated by the associated quality control numbers). Additional discrepancies between the two measures of wave height may have resulted from the complex non-linear interactions between waves with different periods, wave trains moving in different directions, and/or shallow water wave dynamics. Similarly, there was no attempt to include pre-existing wave conditions on each occasion where wind direction shifted into a new direction division, as wave models incorporating wave-wave energy transfer, wave dissipation, and wind-wave generation are complex and remain incomplete theoretically (Sorensen 1997). Finally, the division of wind direction into 16 categories may have been excessive; wave trains typically move in a direction less than 90^{o} to wind direction (Sorensen 1997), thus a shift in wind direction less than 45^{o} from the initial direction may not have resulted in the degradation of the original wave train as originally assumed.

The analysis of multicollinearity between variables always produced a variance inflation factor (VIF) less than 4, where problematic multicollinearity is said to occur if VIF is 10 or larger by convention (Kutner et al. 2005). However, the variables examined

may have been inappropriate for making inferences about the relationship between environment and catch or effort. Using air temperature rather than water temperature was reasonable as both measures are highly correlated (Doan 1942). Air temperature has also been shown to relate to the biology of other fish species such as percids and gadids (Doan 1942; Criddle et al. 1998). In addition, the meteorological data supplied by the single weather station were unlikely to be representative of environmental conditions over the entire south basin. This is a cause for concern if attempting to attribute specific environmental variable values to catch and effort patterns, but not for attributing the relative environmental changes utilized in this study (Doan 1942) - provided that the relative changes are common across a broad geographical area such as the south basin.

The inclusion of a variable in the model if it explained at least 2 % of the null deviance was judged an appropriate threshold value. This variable selection technique applied a comparable penalty to the inclusion of a variable when compared to the more common BIC method. This supported the choice of the 2 % null deviance threshold for inferring variable statistical significance. In contrast, the AIC selection method selected models with p-values larger than 0.05 for accepted variables and was thus judged to be too liberal for comparison with the deviance threshold method.

II) Meteorological Influences on Effort

The large proportion of the deviance explained by all effort models indicated that environment had a statistically significant impact on effort in all periods and regions of the south basin, including the entire basin itself. The inclusion of the day variable was clearly justified as it was found to be statistically significant in all models. The day

variable also explained the greatest percentage of the null deviance relative to the other environmental variables (in all but one case) and was thus concluded to be the strongest predictor of effort relative to the other environmental variables. The 95 % prediction intervals were wide enough to limit the use of the model as a strong predictive tool. However, the relationships established were statistically significant over the range of environmental variables encountered. Increases in wave height and decreases in temperature coincided with decreased effort, a result which supported the effort hypothesis which predicted decreased effort in conjunction with hostile environmental conditions such as increased wave height and extreme temperatures. However, the spatial and temporal statistical significance of these variables was not consistent; they were often significant in one period but not in the other within the same region. Given that the difference in the mean wave height between periods was not statistically significant, the absence of a wave height effect in the same region in opposite periods and in the other regions in general may have resulted from the poor ability of the wave height function to indicate the true wave height as measured by the buoy. For temperature this phenomena was attributed to the low impact of the effect at less than 10 % of the null deviance in models where it was found to be statistically significant - the effect simply may not be as prevalent in different periods and regions depending upon the desire to fish and local variations in absolute temperature.

In contrast, other environmental variable values indicative of harsh meteorological conditions (such as low barometric pressure) did not effect effort in a statistically detectable fashion as hypothesized previously and were judged to have had little impact on effort in the south basin. Changes in effort were also attributed to

environmental conditions which influenced CPUE, although this theory did not explain all of the relationships observed. Low day values were indicative of both high effort and high walleye CPUE in the early period. However, high day values were associated with low sauger CPUE in the early period and may have indicated that fishers were specifically targeting walleye. This pattern was partially repeated in the late period; both effort and walleye CPUE increased with day. Effort then began to decrease while walleye CPUE continued to increase, suggesting that anthropogenic factors such as catch quota fulfillments asserted their effects. Despite this violation it was concluded that effort was not only influenced by harsh weather conditions from a fishing perspective but also by conditions which lead to higher walleye CPUE. The statistical significance of the year variable was attributed to changes in fishing strategies (Salas and Gaertner 2004) and fish abundance (Maunder and Punt 2004). Other environmental variables not considered in the analysis but which had a strong correlation (Kutner et al. 2005) with day (such as photoperiod) could also have been responsible for the strong statistically significant relationship observed between effort and day.

III) Discarding Behavior

The small value of the adjusted coefficient of determination and the lack of statistical significance in the ability of walleye CPUE to predict sauger CPUE suggested that prominent discarding behavior between walleye and sauger was unlikely. There appeared to be no preference for one species over the other in the catch statistics. This result was unusual considering that some estimates suggest that over 25 % of annual catch is discarded in other fisheries (Stratoudakis et al. 1998). The large range in CPUE

(over two orders of magnitude) also suggested the discarding of less valuable fish under conditions of high CPUE (Gillis et al. 1995); the 10-year average price of sauger (1996-2005) was approximately 18 % less than that of walleye (Freshwater Fish Marketing Corporation 2005). The small vessels which compose the south basin have limited hold capacity, making this form of discarding a potential concern. Discarding practices are also known to vary both spatially and temporally (Stratoudakis et al. 1998). In this study there was no evidence of this phenomena observed in the south basin.

IV) Meteorological Influences on CPUE

The large proportion of the deviance explained by all CPUE models indicated that environment had a statistically significant impact on CPUE in all periods and regions of the south basin, including the entire basin itself (with the exception of sauger CPUE in the late period). The inclusion of the day variable was clearly justified as it was found to be statistically significant in 14 of the 24 models. Where statistically significant, the day variable also explained the greatest percentage of the null deviance relative to the other environmental variables and was thus concluded to be the strongest predictor of CPUE relative to the other environmental variables. As with the effort models, the 95 % prediction interval was large and limits the use of the model as a strong predictive tool. The 95 % estimation interval of the line transected the prediction interval at higher CPUE values, illustrating that the model was inappropriate for estimating large CPUE. However, the relationships established were statistically significant over the range of environmental variables encountered. The models generated using the binary CPUE data predicted a constant, low probability of a CPUE = 0 record under any combination of

environmental variable values. This result could have been due to other variables not considered affecting the presence of either species or simply that both species were not regularly influenced to the point of exclusion by the meteorological conditions observed in the south basin during the study period. Consequently, these models were judged inadequate for identifying related factors for either species due to poor contrast and will not be discussed further. All subsequent discussions of CPUE refer to the continuous CPUE data only.

Significant relationships with CPUE were found for all variables examined with the exception of atmospheric visibility and barometric pressure, albeit in a sporadic fashion. In support of the CPUE hypothesis, low light intensity in the form of high cloud opacity was indicative of high sauger CPUE. This apparent lack of responsiveness of walleye to either visibility or cloud opacity was unexpected given that both walleye and sauger are known to be negatively phototropic (Ali et al. 1977), and that light intensity is the primary abiotic factor controlling the distribution of walleye (Lester et al. 2004). Given the high turbidity of the south basin (Brunskill et al. 1979), it was possible that high levels of atmospheric light intensity did not produce the higher light intensity levels below the water's surface which would have caused a behavioral response in walleye. This reasoning could also explain why cloud opacity was statistically significant in only 2 of the 12 sauger CPUE models; the south basin may have been simply be too turbid for variations in atmospheric light intensity to have had a measurable effect.

Similarly, wave height was only statistically significant in 1 of the 24 models generated. However, the response of CPUE to this variable was nonsensical and primarily dictated by a few data points. Consequently, the models could not support a statistically

significant relationship between wave height and CPUE. However, this study represented local wave height indirectly and may not have provided an accurate test of the CPUE hypothesis. It was also likely that the dominating amount of sediment introduced by the Red River (Allan and Brunskill 1977; Lake Winnipeg Research Consortium 2001) masked any increases in turbidity due to wave-induced sediment resuspension events. Similarly, the relationship between barometric pressure and CPUE was never statistically significant and consequently not likely to influence the CPUE of these two species. Other studies have found pressure to act as a stimulus for spawning behavior in rainbow trout (*Oncorhynchus mykiss*) (Peterson 1972), the activity of black crappie (*Pomoxis nigromaculatus*), and the depth distribution of sauger (Jeffrey and Edds 1999; Stoner 2004).

The observed relationship between walleye CPUE and temperature was also inconsistent with the CPUE hypothesis; walleye CPUE increased with decreasing air temperature. Walleye prefer a water temperature of 18^{o} C (Lester et al. 2004), while water temperatures in the south basin can exceed 20^{o} C in the summer (Torigai et al. 2000). Although temperature was statistically significant in only 2 of the 12 models generated using the walleye CPUE data, its effects were likely confounded by its relationship to the day variable which was statistically significant in 10 of the 12 models. The correlation between day and temperature was 0.363 and -0.775 for the early and late fishery periods, respectively. Walleye CPUE had a similar response to both day and temperature. Low day values in the early period were typified by both low temperatures and high walleye CPUE while high day values in the late period were associated with low

temperatures and high walleye CPUE once again. From these inter-relationships it may be concluded that temperature had an impact on walleye CPUE in all regions and periods.

The relationship between sauger CPUE and temperature was more complex. In support of the CPUE hypothesis, sauger CPUE increased with increasing air temperature in the entire south basin region during the early period. This result was once again potentially confounded by the relationship between temperature and day; high day values during the early period were associated with high temperatures and high sauger CPUE. This result was not surprising considering that sauger are known to prefer warmer water than walleye at 22^{o} C (Wahl and Nielsen 1985). The cause of the unusual response of sauger CPUE to temperature in the Riverton and Traverse Bay regions was unclear but may have stemmed from local water temperature changes brought about by the discharge from the Icelandic and Winnipeg rivers, respectively. This temperature effect is not restricted to walleye and sauger alone, numerous other fish species are known to respond to this environmental variable as well (Stoner 2004).

While not considered in the original hypotheses, discharge from the Red River had a significant impact on CPUE in 2 of the 24 models generated. As the largest source of suspended sediment in the south basin (Allan and Brunskill 1977; Lake Winnipeg Research Consortium 2001), increases in discharge suggest corresponding increases in south basin turbidity and turbidity is known to influence the distribution of both walleye and sauger (Nelson and Walburg 1977). Increased walleye CPUE in the Riverton region was associated with low-range discharge rates while increased sauger CPUE in the entire south basin region was associated with mid-range discharge rates (both during the early period). The reason that Red River discharge was statistically significant in only these

two instances was unclear, but it may have been the only occasions where turbidity as dictated by the discharge of the Red River had an obvious effect. Although both species are negatively phototropic (Ali et al. 1977), sauger prefer more turbid conditions than walleye (Nelson and Walburg 1977). This could explain the higher walleye CPUE observed at low discharges and the higher sauger CPUE observed at mid-range discharges. The drop in both species' CPUE at high discharges could have represented turbidities too high for either species which may have moved elsewhere or became inactive under these conditions. Other species have been shown to migrate away from highly turbid areas such as river plumes (Heege and Appenzeller 1998). However, the low prevalence of this variable in the fitted models suggested that it was in general of little practical significance in determining walleye and sauger CPUE.

The lack of statistical significance with any variables other than year in the late period of the sauger CPUE data indicated that the environmental conditions examined did not affect sauger CPUE during this time period. The statistical significance of the day and year effects for both species in general were accredited to other environmental variables unavailable to this analysis but which had a strong correlation with day (Kutner et al. 2005) as well as annual fluctuations in fish abundance (Maunder and Punt 2004), respectively. In addition, local fluctuations in environmental conditions and habitat could have been responsible for the variation observed in the relationship between CPUE and day.

Although numerous statistically significant relationships were found between CPUE and environment, there was the potential for a number of processes operating in the south basin to have increased the variation in the observed CPUE-environment

relationships. Gill net catch may not indicate changes in fish populations. For example, abundance has been significantly underestimated by gill net catch under high fish abundances (Olin et al. 2004). This is attributed to increased avoidance of the net by the detection of fish already caught, although this property should have been reduced under the conditions of high turbidity (Olin et al. 2004) found in the south basin. Furthermore, the re-allocation of fishing effort in response to spatially and temporally variable fish densities (Ives and Klopfer 1997) has the potential to bias CPUE-meteorological associations (Campbell 2004). This bias would arise if fishers systematically fish one area under one range of environmental conditions and fish another area under a different range of environmental conditions. In addition, other processes such as predator-prey dynamics can produce regional patterns of differing fish densities that confound the apparent associations between catch rate and environment (Ives and Klopfer 1997).

Several issues in the data collection and model building processes should be considered when interpreting these results. Only one meteorological station was used to characterize changes in environmental conditions. This could result in inaccurate representation of local conditions when weather patterns vary over a large region (Sundermeyer et al. 2005). Specifically, the assumption that the same weather between the northernmost region of Wanipigow and Gimli may have been overly simplistic. Finally, the generalized linear models used to construct the relationships generated residuals which exhibited homoscedasticity in 25 of the 36 models and a normal distribution in only 11 of the 36 models using the effort and continuous CPUE data. However, these violations of the model assumptions did not produce unreasonable residual distributions (Ortiz and Arocha 2004).

V) Conclusions

In conclusion, statistically significant relationships were prevalent between fishing effort and environment as well as between CPUE and environment throughout the south basin. Increases in effort were partially explained by decreases in wave height and increases in temperature, but were dominated by day values which increased the CPUE of walleye. Increases in walleye CPUE were partially explained by low temperatures and day values associated with that property. Increases in sauger CPUE were partially explained by increases in temperature and by day values indicative of this property in general as well as by increases in cloud opacity. Caution is advised when interpreting these conclusions as model assumptions were periodically violated. However, the methods employed here were superior to simple linear models, whose assumptions were violated to a greater extreme in all cases.

VI) Suggestions for Future Work

More complete knowledge of both environment and fisher behavior is required to strengthen the relationship between effort, CPUE, and environment. More detailed knowledge regarding the spatial and temporal variation in gill net placement would allow changes in CPUE due to changes in net location over time to be addressed. Similarly, quantification of reduced net fishing power due to gear saturation in the south basin may reduce under-estimation of catch rate. The incorporation of more direct measures of environmental conditions in each region such as percent cloud cover, photoperiod length, precipitation, water temperature, and wave height may increase the statistical significance

of environmental variables. Finally, knowledge regarding fish movement patterns in Lake Winnipeg would be useful in order to determine the sources of CPUE variation and the catch rate of walleye and sauger in general.

References

Ali, M.A., Ryder, R.A., and Anctil, M. 1977. Photoreceptors and visual pigments as related to behavioral responses and preferred habitats of perches (*Perca* spp.) and pikeperches (*Stizostedion* spp.). J. Fish. Res. Board Can. **34**: 1475-1480.

Allan, R.J., and Brunskill, G.J. 1977. Relative atomic variation (RAV) of elements in lake sediments: Lake Winnipeg and other Canadian lakes. Proc. Int. Symp. 1976: 108-120.

Agresti, A. 1996. An Introduction to Catagorical Data Analysis. John Wiley & Sons, Inc., N.Y.

Akritas, M.G., and Papadatos, N. 2004. Heteroscedastic One-way ANOVA and Lack-of-Fit Tests. J. Am. Stat. Assoc. **99**: 368-382.

Bhattacharyya, G.K., and Johnson, R.A. 1977. Statistical Concepts and Methods. John Wiley & Sons, Inc., N.Y.

Booth, A.J. 2000. Incorporating the spatial component of fisheries data into stock assessment models. ICES J. Mar. Sci. **57**: 858-865.

Brunskill, G.J., Schindler, D.W., Elliott, S.E.M., and Campbell, P. 1979. The attenuation of light in Lake Winnipeg Canada waters. Fish. Mar. Serv. Report 1522, Dep. Fish. Environ., Winnipeg, MB.

Campbell, R.A. 2004. CPUE standardisation and the construction of indices of stock abundance in a spatially varying fishery using general linear models. Fish. Res. **70**: 209-227.

Canada Department of Energy, Mines, and Resources, Canada Centre for Mapping. "Hecla, Manitoba" [map]. Edition 4. 1:250,000. Canada 1:250,000, sheet 62 P.

Ottawa: Canada Centre for Mapping, 1988.

Canada Department of Energy, Mines, and Resources, Canada Centre for Mapping. "Selkirk, Manitoba" [map]. Edition 7. 1:250,000. Canada 1:250,000, sheet 62-I. Ottawa: Canada Centre for Mapping, 1994.

Canada Department of Fisheries and Oceans, Canadian Hydrographic Service. "Canada, Manitoba, Lake Winnipeg, Red River To Berens River" [map]. Edition 8. 1:255,994. Canadian Hydrographic Service Map 6240. Ottawa: Canadian Hydrographic Service, 1995.

Conover, W.J. 1980. Practical Nonparametric Statistics. John Wiley and Sons, Inc., N.Y.

Criddle, K.R., Herrmann, M., Greenberg, J.A., and Feller, E.M. 1998. Climate fluctuation and revenue maximization in the eastern Bering Sea fishery for walleye pollock. N. Am. J. Fish. Manage. **18**: 1-10.

Doan, K.H. 1942. Some meteorological and limnological conditions as factors in the abundance of certain fishes in Lake Erie. Ecol. Monogr. **12**: 293-314.

Fox, J. 2002. An R and S-Plus Companion to Applied Regression. Sage Publications, Thousand Oaks, Calif.

Freshwater Fish Marketing Corporation. 2005. Freshwater Fish Marketing Corporation 2004-2005 Annual Report. Freshwater Fish Marketing Corporation, Winnipeg, MB.

Gillis, D.M., Pikitch, E.K., and Peterman, R.M. 1995. Dynamic discarding decisions: Foraging theory for high-grading in a trawl fishery. Behav. Ecol. **6**: 146-154.

Heege, T., and Appenzeller, A.R. 1998. Correlations of large-scale patterns of turbidity and pelagic fish biomass using satellite and acoustic methods. Arch. Hydrobiol.

Spec. Issues Advanc. Limnol. **53**: 489-503.

Hilborn, R. 1985. Fleet dynamics and individual variation: Why some people catch more fish than others. Can. J. Fish. Aquat. Sci. **42**: 2-13.

Ives, A.R., and Klopfer, E.D. 1997. Spatial variation in abundance created by stochastic temporal variation. Ecology **78**: 1907-1913.

Jeffrey, J.D., and Edds, D.R. 1999. Spring movements and spawning habitat of sauger (*Stizostedion canadense*) in a small midwestern USA reservoir. J. Fresh. Ecol. **14**: 385-397.

Kling, H.J. 1998. A summary of past and recent plankton of Lake Winnipeg, Canada using algal fossil remains. J. Paleolimnol. **19**: 297-307.

Kutner, M.H., Nachtsheim, C.J., Neter, J., and Li, W. 2005. Applied Linear Statistical Models, 5th Ed. McGraw-Hill Irwin, N.Y.

Lake Winnipeg Research Consortium. 2001. Report on the Health of the Lake Winnipeg Ecosystem and the Role of the Lake Winnipeg Research Consortium. Lake Winnipeg Research Consortium, Winnipeg, MB.

Lester, N.P., Dextrase, A.J., Kushneriuk, R.S., Rawson, M.R., and Ryan, P.A. 2004. Light and temperature: Key factors affecting walleye abundance and production. T. Am. Fish. Soc. **133**: 588-605.

Lysack, W. 1995. Mesh Size Effects in Lake Winnipeg's Commercial Fisheries. Manitoba Department of Natural Resources. Fisheries Branch MS Report No. 95-02.

Manitoba Conservation. 2003. A Profile of Manitoba's Commercial Fishery, Manitoba: Government of Manitoba.

Manitoba Conservation. 2006. Commercial Fishing Season Variance CFSV - 2006/1, Manitoba; Government of Manitoba.

Manly, B.F.J. 2001. Statistics for Environmental Science and Management. Chapman and Hall/CRC, Boca Raton, Fla.

Maunder, M.N., and Punt, A.E. 2004. Standardizing catch and effort data: A review of recent approaches. Fish. Res. **70**: 141-159.

McCullagh, P. and Nelder, J.A. 1989. Generalized Linear Models, 2nd Ed. Chapman and Hall/CRC, Boca Raton, Fla.

Nelson, W.R., and Walburg, C.H. 1977. Population dynamics of yellow perch (*Perca flavescens*), sauger (*Stizostedion canadense*), and walleye (*S. vitreum vitreum*) in four main stem Missouri River reservoirs. J. Fish. Res. Board Can. **34**: 1748-1763.

Olin, M., Kurkilahti, M., Peitola, P., and Ruuhijärvi, J. 2004. The effects of fish accumulation on the catchability of multimesh gillnet. Fish. Res. **70**: 135-147.

Ortiz, M., and Arocha, F. 2004. Alternative error distribution models for standardization of catch rates of non-target species from a pelagic longline fishery: Billfish species in the Venezuelan tuna longline fishery. Fish Res. **70**: 275-297.

Pennington, M. 1983. Efficient estimators of abundance, for fish and plankton surveys. Biometrics **39**: 281-286.

Peterson, D.A. 1972. Barometric pressure and its effect on spawning activities of rainbow trout. Prog. Fish Cult. **34**: 110-112.

Ryder, R.A. 1977. Effects of ambient light variations on behavior of yearling, subadult, and adult walleyes (*Stizostedion vitreum vitreum*). J. Fish. Res. Board Can. **34**:

1481-1491.

Salas, S., and Gaertner, D. 2004. The behavioural dynamics of fishers: Management implications. Fish and Fisheries **5**: 153-167.

Sorensen, R.M. 1997. Basic Coastal Engineering, 2nd Ed. Chapman and Hall, N.Y.

Stoner, A.W. 2004. Effects of environmental variables on fish feeding ecology: Implications for the performance of baited fishing gear and stock assessment. J. Fish. Biol. **65**: 1445-1471.

Stratoudakis, Y., Fryer, R.J., and Cook, R.M. 1998. Discarding practices for commercial gadoids in the North Sea. Can. J. Fish. Aquat. Sci. **55**: 1632-1644.

Sundermeyer, M.A., Rothschild, B.J., and Robinson, A.R. 2005. Using commercial landings data to identify environmental correlates with distributions of fish stocks. Fish. Oceanogr. **14**: 47-63.

Todd, B.J., Lewis, C.F.M., Thorleifson, L.H., Nielsen, E., and Last, W.M. 1998. Paleolimnology of Lake Winnipeg. J. Paleolimnol. **19**: 211-213.

Torigai, K., Schröder-Adams, C.J., and Burbidge, S.M. 2000. A variable lacustrine environment in Lake Winnipeg, Manitoba: Evidence from modern thecamoebian distribution. J. Paleolimnol. **23**: 305-318.

Vandenbyllaardt, L., Ward, F.J., Braekevelt, C.R., and McIntyre, D.B. 1991. Relationships between turbidity, piscivory, and development of the retina in juvenile walleyes. T. Am. Fish. Soc. **120**: 382-390.

Wahl, D.H., and Nielsen, L.A. 1985. Feeding ecology of the sauger (*Stizostedion canadense*) in a large river. Can. J. Fish. Aquat. Sci. **42**: 120-128.

Walters, C.J., and Collie, J.S. 1988. Is research on environmental factors useful to

fisheries management? Can. J. Fish. Aquat. Sci. **45**: 1848-1854.

Chapter Four: General Summary

The results of this study examined the degree to which environmental conditions influenced the effort allocation of fishers and the catch rate of walleye and sauger within the south basin of Lake Winnipeg. As expected, fishing effort declined when weather conditions made the act of fishing difficult - conditions such as low temperatures and high wave heights. However, these effects were not statistically significant in every region of the south basin. It was theorized that these conditions were simply not harsh enough by themselves to significantly inhibit fishing in all regions. In contrast, the limited predictive power of wave height was attributed to the poor ability of the method used to calculate wave height to predict true wave height. Actual wave height values from buoys would be of more use in future studies. In general, effort also increased when walleye CPUE was high; suggesting that fishers were specifically targeting walleye (as opposed to sauger) and fishing more when the CPUE for this species was high. However, more information on fisher behavior is needed to verify this. Specifically, knowledge regarding each fisher's target species and their variation in net placement throughout the open-water fishing season would allow more detailed inferences to be made regarding the fishing practices in the south basin as a whole.

Surprisingly, neither the CPUE of walleye nor sauger was affected in a statistically significant fashion by variations in turbidity front characteristics. This result suggested that the distribution of both species was not effected by turbidity in the south basin. This conclusion opposes those found in the primary literature. However, variation in water clarity measurements, the absence of local water clarity data, and the lack of universal algorithms for the conversion of satellite reflectance data to water clarity

measures may have injected sufficient variation into the data to obscure the relationship. In addition, the turbidity fronts established by the satellite may not have been representative of the turbidity throughout the majority of the water column as the satellite can only 'see' the turbidity of the uppermost portion of the water column. This limitation of the methodology may have once again obscured the relationship between turbidity and the distribution of walleye and sauger. Additional depth profiles need to be performed in order to determine whether turbidity differs significantly throughout the water column.

Of the remaining environmental variables examined, only temperature regularly exhibited a statistically significant relationship with walleye CPUE, while both temperature and cloud opacity regularly possessed a statistically significant relationship with sauger CPUE. The day variable was concluded to confound the effect of temperature because of its strong correlation with temperature. Walleye CPUE was found to decrease with increasing temperature while sauger CPUE was found to increase. Sauger CPUE was also found to increase with increasing cloud opacity. These results were consistent with the specific habitat requirements for each species detailed in the primary literature in the context of the range of habitats present in the south basin. However, caution is advised when interpreting these conclusions as model assumptions were periodically violated. In future studies of similar type, direct measures of specific environmental variables in each region such as the amount of precipitation, the percentage of cloud cover, and regional wave height observations may produce a stronger relationship between environment and the catch rate of these two fish species within Lake Winnipeg.

Appendix 1: Details on the Manipulation of Satellite Images

The location of all relevant features used either directly or indirectly in the manipulation of satellite images to define and quantify the turbidity fronts are listed in Table A1.1. The coordinates of each feature are described using the Universal Transverse Mercator (UTM) system in zone 14 U with a ten thousand meter grid (Canada Department of Energy, Mines and Resources 1988; Canada Department of Energy, Mines and Resources 1994). The regional boundaries were set by determining the approximate location from which the distance between one delivery location (around which the regions are centered) and its nearest neighbor were equal. The remainder of this appendix is composed of the annotated computer programming code used to manipulate the satellite images, subdivided into 3 sections: satellite image manipulation, turbidity front generation, and fractal dimension calculation. All computer code was written and used in MATLAB® version 6.5.0.180913a, release 13, incorporating the Image Processing Toolbox version 4.0, Mapping Toolbox version 1.3, and Statistics Toolbox version 4.0.

Table A1.1 Universal Transverse Mercator coordinates of the features used directly or indirectly in the manipulation of satellite images to define and quantify turbidity fronts. The ground truthing points were used to verify the accuracy of the satellite's georeferencing system while the depth profiles were used to verify the assumption that turbidity remained constant at depth. The start and end coordinates of the transect of the south basin used to verify the relationships between Secchi depth, turbidity, and satellite reflectance were identical to the western and eastern depth profile coordinates, respectively. Additional measurements of Secchi depth and surface turbidity were made every 250 m between these two coordinates, including at the start and end coordinates themselves.

Feature	Northing (m N)	Easting (m E)
Ground Truthing Point		
Chalet Beach	5 587 500	647 500
Elk Island (northernmost point)	5 628 500	674 250
Grand Beach (westernmost point)	5 603 000	667 300
Sandy Point (westernmost point)	5 653 150	648 300
Willow Point (easternmost point)	5 607 150	645 700
Depth Profile Location		
Western (W)	5 610 000	645 000
Eastern (E)	5 610 000	650 000

I) Satellite Image Manipulation

Loading MODIS Data

```
% Create a dialog box to load the data file and identify the file to be opened.
prompt={'MODIS File (Entire Path):'};dlg_title='Locate File';num_lines=1;
def={'e:'};filename=char(inputdlg(prompt,dlg_title,num_lines,def));
clear prompt def dlg_title num_lines

% Identify the file format of the filename: 'hdf' format, type 'eos'.
% 'eos' allows expression of the data in terms of swath and geolocation data.
info=hdfinfo(filename,'eos');

% Extract the swath information from the 'info' array and rename it. This is
% done so that in later functions just this component is examined.
swath=info.Swath;

% Transpose the array - column names are now row names.
{swath.DataFields.Name}';

% Extract reflectance data from the 'hdf' file:
% - 'filename' is the file
% - 'MODIS_SWATH_Type_L1B' is the dataset type
% - 'Fields' identifies which row to read, here the 'EV_250_RefSB' row
% - 'Box' defines the longitude and latitude to be displayed, here
%   longitude = -96.0 to 97.5 N and latitude as 50.0 to 51.5 W, a
%   range which encompasses the Lake Winnipeg area
% - 'AnyPoint' will display the reflectance data in the area defined as
%   long as any portion of the satellite's scan path enters that area
% - 'ExtMode' means that geolocation data must be taken in the same swath as
%   the reflectance data if set to 'Internal'
EV_250_RefSB=hdfread(filename,'MODIS_SWATH_Type_L1B','Fields',...
'EV_250_RefSB','Box',{[-96.0,-97.5],[50.0,51.5],'AnyPoint'},'ExtMode',...
'Internal');

% Load the latitude data with the same parameters as the reflectance data.
% However, 'GeolocationFields' fields are used instead of 'DataFields'.
Latitude=hdfread(filename,'MODIS_SWATH_Type_L1B','Fields','Latitude',...
'Box',{[-96.0,-97.5],[50.0,51.5],'AnyPoint'},'ExtMode','Internal');

% Load the longitude data in a similar fashion.
Longitude=hdfread(filename,'MODIS_SWATH_Type_L1B','Fields','Longitude',...
'Box',{[-96.0,-97.5],[50.0,51.5],'AnyPoint'},'ExtMode','Internal');
```

Locating and Subsetting the South Basin

```
% The entire dataset is too large to perform interpolation on it in its entirety.
% Thus a smaller dataset encompassing only the south basin must be created. Use
% only the band 1 data since it best illustrates suspended sediment. First this
% band must be extracted from the dataset. 'EV_250_RefSB' is a 3-dimensional
% array, with dimension 3 being band 2 and 1 in that order. Extracting only
% band 1 still yields a 3-dimensional array but with dimension 3 now of length
% 1 and can  thus be merged with band 1 to yield a 2-dimensional array. This is
% done with the 'squeeze' command. '(2,:,:)' means "extract 2nd array of 3rd
% dimension, merge the first and second dimensions with the 3rd dimension,
% which is now of length 1".
Band1=squeeze(EV_250_RefSB(2,:,:));

% Create a figure box and give it a number.
figure(1)

% Title the figure using the 'set' command.
set(1,'Name',' MODIS Band 1 0.620-0.670 um');

% Set the screensize and position of the figure.
scrsz=get(0,'ScreenSize');
set(1,'Position',[scrsz(3)*0.05 scrsz(4)*0.15 scrsz(3)*.9 scrsz(4)*0.7]);

% Plot the band 1 data using the 'imagesc' command.
imagesc(Band1);

% Note the row and column number which bound the south basin, these values
% must be divisible by 4 (explained later). The row range is the y-axis values from
% the figure and the appropriate column range is then the x-axis values. The subsetting
% syntax is StartRow:EndRow,  StartColumn:EndColumn. Add 1 to the start row and
% column numbers since the starting values are to be included in the subsetting
% procedure. 'R' and 'C' are the relevant row and column numbers, respectively.
subband=Band1(R+1:R,C+1:C);

% Next subset latitude using the same values as for 'Band1' but dividing by 4
% prior to adding 1. This is done because these geodetic arrays have one
% quarter the resolution as does the image array.
sublat=Latitude(R+1:R,C+1:C);

% Perform the same procedure with longitude, using the same numbers as in
% latitude.
sublon=Longitude(R+1:R,C+1:C);

% Increase the resolution of the geodetic arrays to match the image array.
% Image data are of 250 m pixel dimension, while geodetic data are of 1 000 m
```

```
% pixel dimension. These need to be the same scale for subsetting, therefore
% the geodetic arrays must be divided into a finer scale. This means that the
% geodetic arrays must have a step size of 0.25 the original step size. This
% correction will be first illustrated with latitude. First, create the
% appropriate grid size, in the format #columns,#rows. The grid is made using the
% 'meshgrid' command of format Start#:StepSize:End#. The end values will depend
% on the end value of the subsetted array. Use the 'size' command to generate
% these end values, creating an array that contains total rows in row 1 column
% 1 and the total columns in row 1 column 2.
sublatsize=size(sublat);

% Extract these values to create the grid.
[latx,laty]=meshgrid(1:1:sublatsize(1,2),1:1:sublatsize(1,1));

% Next create a finer grid for interpolation, starting at 0.25 since it is the
% first non-zero value on this finer scale.
[latxf,latyf]=meshgrid(0.25:0.25:sublatsize(1,2),0.25:0.25:sublatsize(1,1));

% Interpolation uses a lot of memory, thus it is wise to clear arrays which
% are no longer used but are taking up memory. This is done with the 'clear'.
clear Latitude Longitude EV_250_RefSB Band1

% Next interpolate using bicubic interpolation. Bicubic is chosen since it
% generates the smoothest transitions. The 'double' function is used to
% double the precision of the 'sublat' array calculation and is required for
% bicubic interpolation.
latfine=interp2(latx,laty,double(sublat),latxf,latyf,'bicubic');

% Repeat the process for longitude ('sublon') using the same values
% as for latitude ('sublat').
[lonx,lony]=meshgrid(1:1:sublatsize(1,2),1:1:sublatsize(1,1));
[lonxf,lonyf]= meshgrid(0.25:0.25:sublatsize(1,2),0.25:0.25:sublatsize(1,1));
lonfine=interp2(lonx,lony,double(sublon),lonxf,lonyf,'bicubic');

% Remove arrays no longer needed.
clear filename lonxf lonx scrsz lonyf lony latyf ans latx laty latxf
clear sublat sublon swath info sublatsize

% Convert the 'subband' array from 'unit16' to 'double' for plotting purposes.
subband=double(subband)+1;
```

Removing Image Distortion

```
% To remove distortion introduced during the satellite scanning process
% a function must be created. First open the programming window:
```

```
% -- Create the function: compress -- %
edit compress

% This function will remove non-numerical values from the geodetic arrays
% and remove distortion from the image array. The function is coded in two
% parts:

% A. Remove NaNs (non-numerical values) from the geodetic arrays and resize
% the image array to match. As an artifact of the subsetting procedure
% performed previously, the first three rows and columns of the geodetic arrays
% contain NaNs. These are easily removed:
array_dimension=size(latfine);
latfine2=latfine(4:array_dimension(1,1),4:array_dimension(1,2));
lonfine2=lonfine(4:array_dimension(1,1),4:array_dimension(1,2));
subband2=subband(4:array_dimension(1,1),4:array_dimension(1,2));
clear array_dimension

% The 'array_dimension' array is used to indicate the variable end row
% and column number since the size of the geodetic arrays are variable. The
% 'subband' array contains no NaN values, but must be resized to match the
% geodetic arrays. The rows and columns lost in this array are inconsequential
% since they do not represent portions of the south basin which will be
% examined.

% B. Remove distortion from the image array and resize the geodetic arrays to
% match. The image arrays often contain duplicated segments, an unavoidable
% consequence of the satellite scanning procedure. It is first necessary to
% locate the end row number of the last duplicated segment, 'end_value'. This
% can be done by entering the command 'imagesc(subband)' and performing
% a visual inspection of the image.
end_value=r; % the value of r changes with each image

% Some images contain no duplication. In these cases r is set to the total
% number of rows in the image array. Next determine the number of rows which
% compose a duplicated segment, again using 'imagesc' as before.
distseg=d; % the value of d changes with each image

% Some images contain no duplication. In these cases d=0. Set the length of
% non-duplicated segments, which in MODIS images is always 40.
trueseg=40;

% Create two variables for programming purposes, the purpose of each will be
% explained below.
x=1;y=1;
```

```
% To prevent accidental overwriting of the original arrays, duplicate and
% rename them:
trueband=subband2;latdist=latfine2;londist=lonfine2;

% Duplicated segments are only present in the row vectors, so only row numbers
% are relevant. The 'x' and 'y' variables set previously indicate if the
% duplicated segment currently being fixed extends back further then row 1.
% The purpose of this is to inform the program of a different action in this
% special case, as indicated by the 'if' statements within the 'for' loop.
% The following loop starts near the end row number and works toward row 1,
% removing duplicated segments in each cycle of the loop.

for r=1:50;
% 50 is an arbitrary number, since the images will never contain more then 50
% duplicated segments.

  x=end_value(1,1)-3-(distseg(1,1)-1)-trueseg(1,1)*(r-1);
% 'x' is equivalent to the start of the duplicated segments.

  y=end_value(1,1)-3-trueseg(1,1)*(r-1);
% 'y' is equivalent to the end of the duplicated segments.

  if x>0 & y>0 % i.e. segment is within the row limits of the array
    trueband((end_value(1,1)-3-(distseg(1,1)-1)-trueseg(1,1)...
    *(r-1)):(end_value(1,1)-3-trueseg(1,1)*(r-1)),:)=[];
    latdist((end_value(1,1)-3-(distseg(1,1)-1)-trueseg(1,1)...
    *(r-1)):(end_value(1,1)-3-trueseg(1,1)*(r-1)),:)=[];
    londist((end_value(1,1)-3-(distseg(1,1)-1)-trueseg(1,1)...
    *(r-1)):(end_value(1,1)-3-trueseg(1,1)*(r-1)),:)=[];
  end

% The same correction is applied to both geodetic and image arrays. This is
% done to maintain equal array size, even though the geodetic arrays contain no
% 'duplicated' segments, but do contain 'similar' segments which are erased in
% this step as well.

  if x<=0 & y>0 % i.e. duplicated segment extends further back then row 1
    trueband(1:end_value(1,1)-3-trueseg(1,1)*(r-1),:)=[];
    latdist(1:end_value(1,1)-3-trueseg(1,1)*(r-1),:)=[];
    londist(1:end_value(1,1)-3-trueseg(1,1)*(r-1),:)=[];
  end
end

% This is the special case where the start of the duplication is necessarily
% set to 1 since the arrays cannot have negative dimensions.
clear end_value distseg trueseg x y r subband2 latfine2 lonfine2
```

```
% The entire function is now complete (except for the image-specific
% parameters) and can be simply called upon with "compress". At this point
% the starting arrays (latfine, lonfine, and subband) are manually deleted.
% -- Function Complete -- %
```

Removing Geodetic Distortion and Creating the UTM Projection

```
% To remove distortion introduced during the satellite scanning process a
% function must be created. This function creates a universal transverse
% mercator grid with a cell resolution matching the MODIS data, then projects
% the MODIS geodetic data onto the UTM grid. First create the function:

% -- Create the Function: utmtrans -- %
edit utmtrans

% Find the latitude and longitude limits of the grid for plotting purposes.
latlim=[min(latdist(:)),max(latdist(:))];
lonlim=[min(londist(:)),max(londist(:))];

% Determine the size of the grid, again for map plotting purposes.
array_dimension=size(latdist);

% Create the utm grid, the size of which will vary depending upon the
% size of the array under examination. There is both a northing ('nrough')
% and easting ('erough') component.
nrough=zeros(array_dimension(1,1),array_dimension(1,2));
erough=zeros(array_dimension(1,1),array_dimension(1,2));

% Using the m_map toolbox, create the UTM system using 'm_proj'. m_map was
% created by Rich Pawlowicz, University of British Columbia whom can be
% contacted via email at rich@eos.ubc.ca.
% - 'UTM' is the system being used
% - lon and lat limits of the system are set by using 'lon' and 'lat'
% - a rectangular map (opposed to quadrangular) is set by setting 'rec' to 'on'
% - UTM zone is set to 14 by 'zon',14
% - northern hemisphere is selected by 'hem',0
% - world geodetic system 1984 ellipsoid is set by 'ell','wgs84' This
%   ellipsoid is chosen since it most accurately depicts the study region.
m_proj('UTM','lon',[lonlim(1,1) lonlim(1,2)],'lat',[latlim(1,1)...
latlim(1,2)],'rec','on','zon',14,'hem',0,'ell','wgs84');

% Create a filled contour map using the satellite data with 'm_contourf'.
m_contourf(londist,latdist,trueband);
```

```
% Use the 'mll2xy' function to translate the geodetic array data into
% the UTM grid (fill in values for 'easting' and 'northing' arrays).
[erough,nrough]=m_ll2xy(londist,latdist);

% At this point a figure is created which is not needed, so it is closed.
close figure no. 1

% Rename the image array so it is easier to understand what it represents.
band1=trueband;
clear latlim lonlim trueband londist latdist

% The utm arrays generated contain distortion present in the original MODIS
% geodetic arrays. This will be removed by choosing two non-distorted
% points and extrapolating the values over the distorted areas. The
% interval between rows is dependent on the column number. The row distance
% between 2 undistorted points must first be determined, this is done by
% creating the 'rdist' array. Row 1 is start row, row 2 is end row.
% Column 1 is 'nrough', column 2 is 'erough'.
rdist=zeros(2,2);imagesc(nrough)

% The size of the figure window is controlled by 'set' and 'Position'. The
% array following the 'Position' command dictates the size of the figure window
% in the format [distance from left of screen, distance from bottom of screen,
% width, height]. All measurements are in pixels.
set(1,'Position',[10,38,1005,653]);

% To prevent user confusion, a warning dialog ('warndlg') popup is created to
% guide user choices. The 'uiwait' command prevents the function from
% advancing until the user has performed the specified task. To select a
% desired point 'ginput' is used, a command which records the coordinates of
% the mouse cursor when the left mouse button is pressed.
warn=warndlg('Choose the middle of an undistorted segment near row 1',...
 'Northing Adjustment');
uiwait(warn);[c,r]=ginput(1);rdist(1,1)=round(r);
warn=warndlg('Choose the middle of an undistorted segment near end row',...
 'Northing Adjustment');
uiwait(warn);[c,r]=ginput(1);rdist(2,1)=round(r);
imagesc(erough)
warn=warndlg('Choose the middle of an undistorted segment near row 1',...
 'Easting Adjustment');
uiwait(warn);[c,r]=ginput(1);rdist(1,2)=round(r);
warn=warndlg('Choose the middle of an undistorted segment near end row',...
 'Easting Adjustment');
uiwait(warn);[c,r]=ginput(1);rdist(2,2)=round(r);
clear r c warn,close Figure No. 1
```

```
% Next overwrite the distorted areas. 'seg' refers to the row interval for
% each individual column. Column 1 is northing, 2 is easting.
seg=zeros(1,2);
for c=1:array_dimension(1,2);
  seg(1,1)=(nrough(rdist(2,1),c)-nrough(rdist(1,1),c))/(rdist(2,1)-rdist(1,1));
  seg(1,2)=(erough(rdist(2,2),c)-erough(rdist(1,2),c))/(rdist(2,2)-rdist(1,2));
  for r=1:array_dimension(1,1);
    nrough2(r,c)=nrough(rdist(1,1),c)+seg(1,1)*(r-rdist(1,1));
    erough2(r,c)=erough(rdist(1,2),c)+seg(1,2)*(r-rdist(1,2));
  end
end
nrough=nrough2;erough=erough2;
clear r c seg rdist array_dimension nrough2 erough2

% The function is complete and can be called with just 'utmtrans' in the
% future. The result is a UTM grid with corresponding image data.
% -- Function Complete -- %
```

Increasing Geodetic Array Accuracy

```
% The geodetic coordinates recorded by the MODIS satellite are not accurate
% enough to provide a solid foundation upon which to map locations. This
% function increases the accuracy of the utm arrays created in the previous
% function. First create the function:

% -- Create the Function: utmshift -- %
edit utmshift

% Select the file for examination and locate the central northern tip of
% Elk Island, which will be used as a common reference point. The actual
% coordinates of this point are subtracted from the observed coordinates
% (the 'shift' array). The result is then subtracted from the MODIS
% northing and easting arrays ('nrough' and 'erough' respectively) in order
% to increase accuracy.

imagesc(band1)
set(1,'Position',[10,38,1005,653]);
warn=warndlg('Zoom in on the central northern tip of Elk Island before pressing
OK','Manipulate Map');
uiwait(warn);[c,r]=ginput(1);
shift=[nrough(round(r),round(c))-5628500,erough(round(r),round(c))-674250];

% Set the Elk Island point to its correct coordinates and for every
% other point add on the appropriate distance, as determined in the 'shift'
% array. Column 1 is northing shift, column 2 is easting shift.
```

```
ad=size(nrough);
for r=1:ad(1,1);
  for c=1:ad(1,2);
    nrough2(r,c)=nrough(r,c)-shift(1,1);
    erough2(r,c)=erough(r,c)-shift(1,2);
  end
end
clear shift nrough erough

% Test these values against 4 points to determine array accuracy. Columns
% 1-4 represent Chalet Beach, Grand Beach Point, the western tip of Sandy
% Point, and Willow Point, respectively. 'err' rows 1-2 represent differences
% in terms of northing and easting. An extra column is included because the
% Elk Island point must be taken into consideration (0 error) when
% calculating the magnitude of adjustment (mean error) later. 'tpts' are
% the test point coordinates, with rows representing the points in
% alphabetical order. Column 1 is northing, 2 is easting.
tpts=[5587500,647500;5603000,667300;5653150,648300;5607150,645700];

err=zeros(2,5);imagesc(band1),set(1,'Position',[10,38,1005,653]);
warn=warndlg('Zoom in on Chalet Beach before pressing OK','Manipulate Map');
uiwait(warn);[c,r]=ginput(1);
err(1:2,1:1)=[tpts(1,1)-nrough2(round(r),round(c));tpts(1,2)...
 -erough2(round(r),round(c))];
warn=warndlg('Zoom in on Grand Beach Point before pressing OK',...
 'Manipulate Map');
uiwait(warn);[c,r]=ginput(1);
err(1:2,2:2)=[tpts(2,1)-nrough2(round(r),round(c));tpts(2,2)...
 -erough2(round(r),round(c))];
warn=warndlg('Zoom in on the western tip of Sandy Point before pressing OK',...
 'Manipulate Map');
uiwait(warn);[c,r]=ginput(1);
err(1:2,3:3)=[tpts(3,1)-nrough2(round(r),round(c));tpts(3,2)...
 -erough2(round(r),round(c))];
warn=warndlg('Zoom in on Willow Point before pressing OK','Manipulate Map');
uiwait(warn);[c,r]=ginput(1);
err(1:2,4:4)=[tpts(4,1)-nrough2(round(r),round(c));tpts(4,2)...
 -erough2(round(r),round(c))];
ans=1;clear tpts warn ans, close Figure No. 1

% Use the values calculated in 'err' to adjust the nrough and erough arrays
% based upon average error value for both northing and easting. Row 1 is
% the average of northing, row 2 is the average value of easting. These
% average values will be used as correction values in order to generate
% a final utm grid with variation centered around 0 meters.
adj=mean(err,2);
```

```
for r=1:ad(1,1);
  for c=1:ad(1,2);
    northing(r,c)=nrough2(r,c)-adj(1,1);
    easting(r,c)=erough2(r,c)-adj(2,1);
  end
end
clear ad r c nrough2 erough2

% Re-generate the error array including the adjustment values. Also
% generate an array demonstrating the pixel differences between actual and
% calculated northing and easting values. This uses 250 m as 1 pixel
% dimension, as detailed in the MODIS technical specifications.
error=[err(1:1,1:5)-adj(1,1);err(2:2,1:5)-adj(2,1)];
pixel_error=roundn(error/250,-1);
clear adj err

% The function is now complete and can be called with just 'utmshift' in the
% future. It is on this final workspace that all subsequent statistical,
% structural, and mapping operations will be performed.
% -- Function Complete -- %
```

II) Turbidity Front Generation

Plotting Hydrological Research Expedition Data

```
% This function maps the path of the Namao during its sampling trawls for
% correlation of turbidity and reflectance. First create the function:

% -- Create the Function: cruise -- %
edit cruise

% IMPORTANT: An array must be created BEFORE this function is run in order for
% it to work. This array must be 2x2, with rows representing start and end
% points, column 1 northing, and column 2 easting. Name this array 'pts'.
% IMPORTANT: Create a figure of the image first, using imagesc(band1). The
% 'd1' and 'd2' arrays are the euclidean distances from every cell in the
% utm arrays to the starting and ending trawl points, respectively.
ad=size(northing);d1=zeros(ad(1,1),ad(1,2));d2=zeros(ad(1,1),ad(1,2));
for r=1:ad(1,1);
  for c=1:ad(1,2);
    d1(r,c)=((pts(1,1)-northing(r,c))^2+(pts(1,2)-easting(r,c))^2)^0.5;
    d2(r,c)=((pts(2,1)-northing(r,c))^2+(pts(2,2)-easting(r,c))^2)^0.5;
  end
end
clear ad r c
```

```
% Find the smallest distance in these arrays and extract the row and column
% indices. Row 1 is start and end row values, row 2 is start and end
% column values. Plot these values on the image array.
rc=zeros(2,2);
[rc(1,1),rc(2,1)]=find(d1==min(d1(:)));[rc(1,2),rc(2,2)]=find(d2==min(d2(:)));
line(rc(2:2,1:2),rc(1:1,1:2),'Color','r','Marker','o')
clear d1 d2

% Extract the reflectance values over which the line lies. There are 4
% possible cases depending upon the direction the Namao moved during the
% sample. Each is outlined below. The 'tpath' array are the extracted
% values over the path rectangle. The exact reflectance value at any given
% point will be a combination of the values the path touches, The
% proportion of each must be estimated manually.
if rc(1,1)<=rc(1,2) & rc(2,1)<=rc(2,2)
  % ship moved north->south & west->east
  tpath=band1(rc(1,1):rc(1,2),rc(2,1):rc(2,2));
  helpdlg('cruise vector north --> south and west --> east',...
  'Namao Trawl Direction');
end
if rc(1,1)<=rc(1,2) & rc(2,1)>rc(2,2)
  % ship moved north->south & east->west
  tpath=band1(rc(1,1):rc(1,2),rc(2,2):rc(2,1));
  helpdlg('cruise vector north --> south and east --> west',...
  'Namao Trawl Direction');
end
if rc(1,1)>rc(1,2) & rc(2,1)<=rc(2,2)
  % ship moved from south->north & west->east
  tpath=band1(rc(1,2):rc(1,1),rc(2,1):rc(2,2));
  helpdlg('cruise vector south --> north and west --> east',...
  'Namao Trawl Direction');
end
if rc(1,1)>rc(1,2) & rc(2,1)>rc(2,2)
  % ship moved from south->north & east->west
  tpath=band1(rc(1,2):rc(1,1),rc(2,2):rc(2,1));
  helpdlg('cruise vector south --> north and east --> west',...
  'Namao Trawl Direction');
end
clear rc

% The 'openvar' command opens the array editor, in this case for 'tpath' so
% the values can be copied into Microsoft Excel for statistical manipulation.
openvar('tpath')

% The function is now complete and can be called on with just 'cruise' in the
```

```
% future.
% -- Function Complete -- %
```

Establishing the Turbidity Fronts

```
% This portion creates 4 figures (original image, thresholded image,
% shoreline view, and maximized contrast for ease of visual
% interpretation). The first step is to select the file to be examined.
% Once this function has been run the data are ready for the 'outline'
% function procedure described 'outline_s' and 'outline_t'.

% -- Create the Function: threshold1 -- %
edit threshold1
filename=uigetfile('*.mat','Open File');load(filename);
clear filename

% IMAGE 1 - THE ORIGINAL BAND 1 DATA %
% 'caxis' sets the minimum and maximum color values to be mapped when the
% figure is created. The 'colormap' function loads a specific color scheme
% under which the figure is created.
figure(1),set(1,'Name',' MODIS Band 1 0.620-0.670 um');
set(1,'Position',[10,440,499,253]);imagesc(band1)
caxis([182,3400]),load modismap,colormap(modismap)
clear modismap

% IMAGE 3 - SHORELINE VIEW %
% Create a shoreline image for visual validation of correct shoreline
% establishment by the function. Any reflectance values greater then the
% reflectance value at the maximum turbidity observed in all images is set
% to this level. This allows finer colormap resolution over the desired
% turbidity reflectance range. The image is then converted to a grayscale
% intensity image (i.e. having values only between 0-1). The 'mat2gray'
% function performs this task. This image is then converted to a binary
% image (having only values of 0 or 1, using 'im2bw') in order to plot the
% shoreline upon the intensity image. Because the reflectance-turbidity
% correlation is expressed in terms of *change in turbidity* the minimum
% reflectance for each image must be subtracted from all other reflectances
% in the image. The final 'for' loop gives the shoreline boundary specific
% values which can be looked for and colored appropriately by the chosen
% color scheme.
figure(3),set(3,'Name',' Shoreline Location');set(3,'Position',[10,38,499,327]);
ad=size(band1);bandclip=band1;
for r=1:ad(1,1);
  for c=1:ad(1,2);
    if band1(r,c)>3400;
```

```
      bandclip(r,c)=3400;
    end
  end
end
bandint_s=mat2gray(bandclip);
level_s=1.0; % alter this (0-1) to change shoreline characteristics
bandbw_s=im2bw(bandint_s,level_s);bandshore=bandclip;
for r=1:ad(1,1)-1;
  for c=1:ad(1,2)-1;
    if bandbw_s(r,c)+bandbw_s(r,c+1)==1 | bandbw_s(r,c)+bandbw_s(r+1,c)==1
      bandshore(r,c)=3450;
    end
  end
end
imagesc(bandshore),caxis([182,3460]),load shoremap,colormap(shoremap)
clear shoremap level_s bandint_s

% IMAGE 2 - THRESHOLDED IMAGE %
% This image displays the turbidity front (the value of which is selected
% using 'level_t') as a binary (0 or 1) image. It is upon this image that
% further analyses will be undertaken.
figure(2),set(2,'Name','  Thresholded Image');set(2,'Position',[517,440,499,253]);
bandclip_t=bandclip-min(band1(:));maxval=3400-min(band1(:));
bandint_t=mat2gray(bandclip_t);
level_t=0.0887; % alter this to desired turbidity
bandbw_t=im2bw(bandint_t,level_t);imagesc(bandbw_t)
load threshmap,colormap(threshmap)
clear threshmap level_t bandint_t bandclip

% IMAGE 4 - MAXIMIZED VISUAL CONTRAST %
% This image illustrates a broader colorscale over water, allowing for
% easier visual interpretation of water clarity. In this image land is
% shown as gray, shoreline in blue, turbidity front in white, and the
% continuity of water clarity from black through red to yellow. Black is
% water with the greatest clarity, yellow the greatest turbidity.
figure(4),set(4,'Name','  Amplified Contrast');set(4,'Position',[517,38,499,327]);
bandcont=bandshore;
for r=1:ad(1,1)-1;
  for c=1:ad(1,2)-1;
    if bandbw_t(r,c)+bandbw_t(r,c+1)==1 | bandbw_t(r,c)+bandbw_t(r+1,c)==1
      bandcont(r,c)=3460;
    end
  end
end
imagesc(bandcont),caxis([182,3510]),load contmap,colormap(contmap)
clear contmap ad r c error pixel_error
```

```
clear bandshore bandcont bandclip_t

% In the future this function can be called with simply 'threshold1'.
% -- Function Complete -- %

% Once this function has been run once, note the maxval value and determine
% the correct 'level' for the threshold image portion of the function (see
% 'Tresholding.xls, 'LevelCalc' worksheet. Run this function repeatedly under
% the multiple 'levels' required to extract turbidity front information for the
% relevant reflectance changes determined in the microsoft excel file 'LM
% Correlation.xls'.

% VARIATION - THRESHOLD1 INVERTED %

% This function is identical to 'threshold1' except that in the
% thresholding phase all 0's are converted to 1's and vice versa. The
% reason this function is performed over the other is that in this case the
% clear regions of water forms 'holes' which would not be picked up by
% 'threshold1'. Only the following is *added*:

% -- Create the Function: threshold1i -- %
edit threshold1i

% IMAGE 2 - THRESHOLDED IMAGE %
bandbw_t=im2bw(bandint_t,level_t); % break begins in 'threshold1' code
for r=1:ad(1,1); % first line of 'threshold1i' additional code
  for c=1:ad(1,2);
    if bandbw_t(r,c)==0
      bandbw_t(r,c)=1;
    else
      bandbw_t(r,c)=0;
    end
  end
end % last line of 'threshold1i' code
imagesc(bandbw_t) % break ends in 'threshold1' additional code

% in addition, replace 'load threshmap,colormap(threshmap)' with:
load threshmapi,colormap(threshmapi)

% In the future this function can be called with simply 'threshold1i'.
% -- Function Complete -- %
```

Mapping the Turbidity Fronts

```
% Once the 'threshold1'/'threshold1i' code has been run it is necessary to map
```

```
% the *boundaries* of these thresholds. This task is performed with the
% 'bwboundaries' command. The 'noholes' specification prevents the tracing of
% objects inside other objects which are surrounded by data labeled as
% 'background' (i.e. has a value of 0).

% Trace all the boundaries and open the resultant cell array for
% inspection. Cell arrays are essentially an array for which each cell
% contains information about another array. In this case, each cell maps
% the row and column indices for all boundary pixels in a particular
% 'object' (i.e. binary data with a value of 1).
bound_s=bwboundaries(bandbw_s,'noholes');

% Because only shoreline is desired, all boundaries with a perimeter less than 10
% pixels are discarded. This is done using the 'cellshrink' function:

% -- Create the Function: cellshrink_s -- %
edit cellshrink_s
ad=size(bound_s);x=1;

% Create the cell array 'bound_s2' by using the 'cell' command.
bound_s2=cell(1);
for r=1:ad(1,1);

% Extract each cell and examine its size.
  cad=size(bound_s{r});

% Alter the value of 'cad' to discard different total perimeter sizes.
  if cad(1,1)>=10
    bound_s2{x,1}=bound_s{r};
    x=x+1;
  end
end

% Overwrite the previously created shoreline boundary cell array.
bound_s=bound_s2;
clear ad x r cad bound_s2
% -- Function Complete -- %

% Call the function with:
cellshrink_s

% Use 'outline_s' to map the relevant objects onto the 'shoreline' array.
% The boundary pixels are set to have a value of 1. All objects left after
% 'cellshrink_s' has been run are mapped.

% -- Create the Function: outline_s -- %
```

```
edit outline_s
ad=size(band1);shoreline=zeros(ad(1,1),ad(1,2));

% For each cell in 'bound_s', extract the corresponding array and map.
adc=size(bound_s,1);
for r=1:adc
  test=bound_s{r};
  adtest=size(test);
  for r=1:adtest(1,1);
    shoreline(test(r,1),test(r,2))=1;
  end
end
figure,imagesc(shoreline)
clear ad adc adtest r r2 test
% -- Function Complete -- %

% Call the function with:
outline_s

% Load the correct colormap for ease of visualization:
load threshmap,colormap(threshmap)

% Trace the turbidity fronts.
bound_t=bwboundaries(bandbw_t,'noholes');

% Use 'cellshrink_t' to discard turbidity areas which are too small to be
% significant (perimeter less than 10 pixels). The function is identical
% to 'cellshrink_s' except for the specific arrays being examined.
cellshrink_t

% Use 'outline_t' to map the objects remaining after 'cellshrink_t' has been
% run. The function is identical to 'outline_s' except for the specific arrays
% being examined.
outline_t

% Load the correct colormap:
load threshmap,colormap(threshmap)

% Once all shoreline and turbidity objects have been located and mapped
% unnecessary arrays are deleted.
clear bandbw_s bandbw_t bound_s bound_t maxval threshmap
```

Turbidity Front Subdivision and Shoreline Correction

```
% This function compares the boundary characteristics created in 'outline'
```

```
% and determines the length of the turbidity front. This is done by
% assuming any turbidity boundary more then 1 pixel away from the shoreline
% boundary is truly part of the turbidity front.

% This first portion of the function creates an adjusted turbidity front,
% meaning that it is assumed to be a turbidity front if it lies more than 1
% pixel away from the shoreline. The length of this front is later
% translated into meters, given that 1 pixel dimension equals 250 meters,
% as detailed in the MODIS technical specifications.

% -- Create the Function: threshold2 -- %
edit threshold2
stfront=shoreline;ad=size(band1);tfront=zeros(ad(1,1),ad(1,2));
for r=2:ad(1,1)-1;
  for c=2:ad(1,2)-1;
    sltest=shoreline((r-1):(r+1),(c-1):(c+1));
    sumr=sum(sltest);,sumall=sum(sumr,2);
    if sumall==0 & turbidity(r,c)>0
      stfront(r,c)=2;
      tfront(r,c)=1;
    end
  end
end
figure(1),set(1,'Name','  Adjusted Turbidity Front');
set(1,'Position',[10,276,499,420]);imagesc(stfront)
load frontmap,colormap(frontmap)
clear r c sltest sumr sumall stfront frontmap

% Next the adjusted turbidity front (mapped in 'tfront') must be split up
% into specific unloading areas. These being Gimli, Riverton, Selkirk,
% Traverse Bay, and Wanipigow. The southern tip of Lake Winnipeg is used as
% a substitute for Selkirk since the ships don't travel over land. Any
% landing location-associated turbidity fronts in nonsensical regions (such
% as other lakes) or outside the south basin are removed in a the
% subsequent function 'refine.m'.

% The 'lpts' array lists the coordinates of the aforementioned locations,
% in alphabetical order by row. Column 1 is northing, column 2 is easting.
% Positions are obtained from searching 'Canadian Geographical Names',
% resulting in geodetic coordinates. Website:
% http://geonames.nrcan.gc.ca/search/search_e.php
% Geodetic coordinates are then translated into universal transverse mercator (UTM)
% values using the 'GeoTrans' software application (see the 'extra applications'
% folder for details.

landings_info=zeros(5,2);
```

```
stdivide=shoreline;
lpts=[5611361.73,642565.99;5656799.36,647054.46;5584000.00,660000.00;5616229.75,
682820.16;5674692.04,688522.11];
for r=1:ad(1,1);
  for c=1:ad(1,2);
    if tfront(r,c)==1
      dist(1,1)=sqrt((lpts(1,1)-northing(r,c))^2+(lpts(1,2)-easting(r,c))^2); % gimli
      dist(2,1)=sqrt((lpts(2,1)-northing(r,c))^2+(lpts(2,2)-easting(r,c))^2); % riverton
      dist(3,1)=sqrt((lpts(3,1)-northing(r,c))^2+(lpts(3,2)-easting(r,c))^2); % selkirk
      dist(4,1)=sqrt((lpts(4,1)-northing(r,c))^2+(lpts(4,2)-easting(r,c))^2); % traverse bay
      dist(5,1)=sqrt((lpts(5,1)-northing(r,c))^2+(lpts(5,2)-easting(r,c))^2); % wanipigow
      [rmin,cmin]=find(dist==min(dist(:)));
    end
    if tfront(r,c)==1 & rmin==1
      landings_info(1,1)=landings_info(1,1)+1;
      stdivide(r,c)=2;
    elseif tfront(r,c)==1 & rmin==2
      landings_info(2,1)=landings_info(2,1)+1;
      stdivide(r,c)=3;
    elseif tfront(r,c)==1 & rmin==3
      landings_info(3,1)=landings_info(3,1)+1;
      stdivide(r,c)=4;
    elseif tfront(r,c)==1 & rmin==4
      landings_info(4,1)=landings_info(4,1)+1;
      stdivide(r,c)=5;
    elseif tfront(r,c)==1 & rmin==5
      landings_info(5,1)=landings_info(5,1)+1;
      stdivide(r,c)=6;
    end
  end
end
landings_info(1,2)=landings_info(1,1)*0.25;
landings_info(2,2)=landings_info(2,1)*0.25;
landings_info(3,2)=landings_info(3,1)*0.25;
landings_info(4,2)=landings_info(4,1)*0.25;
landings_info(5,2)=landings_info(5,1)*0.25;
figure(2),set(2,'Name','  Regional Turbidity Fronts');set(2,'Position',[517,276,499,420]);
imagesc(stdivide),load dividemap,colormap(dividemap)
clear lpts ad r c dist rmin cmin dividemap tfront turbidity

% The function can now be called with simply 'threshold2'.
% -- Function Complete -- %

% For each visibility level completed (0.25, 0.50, and 1.00 m) the workspace is
% archived in the following manner. 'divided_###' is the array containing the
% turbidity thresholds subdivided by landing point and corrected for proximity
```

```
% to the shoreline. 'fronts_###' is the array containing the length of the
% turbidity front. Rows represent the landing points chosen in alphabetical
% order. Column 1 is the number of pixels composing the front while Column 2
% is the corresponding length in kilometers. The '###' portion of the
% previously mentioned arrays indicates which visibility the array contains
% information on. For example, 'fronts_025' is 0.25 m visibility information.
divided_###=stdivide;
fronts_###=landings_info;
clear stdivide landings_info

% Once all visibilities have been archived in the above fashion the array
% containing solely the shoreline data can be deleted.
clear shoreline
```

III) Fractal Dimension Calculation

Calculation of the Turbidity Front's Fractal Dimension

```
% -- Create the Function: boxcount -- %
edit boxcount

% This function calculates the fractal dimension of each turbidity front
% visibility (0.25 and 0.50 m) via the box counting technique. Five
% different box sizes have been chosen: 1, 2, 4, 8, and 16 pixels per side,
% creating a square. The first step is to open the workspace to be
% examined.

filename=uigetfile('*.mat','Open File');
load(filename);
clear filename

% The 'x' variable denotes box size, 2 pixel is chosen as the starting
% point. The 'boxlim' array determines the maximum size of the front arrays
% which will fit all box sizes equally. If this task is not performed there
% will be disproportionately more boxes overlaid onto the array as box size
% decreases.
x=1;ad=size(band1);boxlim=fix(ad./16);

% Create an array to keep track of the number of boxes containing part of
% the turbidity front for all visibilities. Column number is increasing
% visibility (0.25 and 0.50 m from left to right) and row number is
% increasing box size (1, 2, 4, 8, and 16 from top to bottom).
bcount=zeros(5,2);

% Create an array to keep track of the relative size of the boxes, based on
```

```
% the number that will *equally* fit into the column dimension of the front
% arrays.
s=zeros(1,5);

% The 'z' variable allows the function to run five times; once at each box
% size. 'nboxr' and 'nboxc' indicate how many boxes will fit *entirely* on
% the turbidity front arrays. 's' is the size of the boxes, defined by how
% many will fit across the *width* of the front arrays, thus they are
% always fractional.
for z=1:5;
  nboxr=boxlim(1,1)*16/x;
  nboxc=boxlim(1,2)*16/x;
  s(1,z)=1/nboxc;

% Overlay the boxes onto the front arrays. The '###box' arrays are individual boxes
% repeated in all possible locations without overlap. The formula contained
% within the parentheses indicate the start & end row & column number of
% each new box.
  for r=1:nboxr;
    for c=1:nboxc;
      box025=divided_025(r*x-x+1:r*x,c*x-x+1:c*x);
      box050=divided_050(r*x-x+1:r*x,c*x-x+1:c*x);
      nbox025=find(box025>1);nbox050=find(box050>1);

% Count the number of boxes containing a portion of the front for each of
% the 2 visibilities.
      if size(nbox025,1)>0
        bcount(z,1)=bcount(z,1)+1;
      end
      if size(nbox050,1)>0
        bcount(z,2)=bcount(z,2)+1;
      end
    end
  end
% Increase the size of the boxes and repeat.
  x=x*2;
end
clear ad box025 box050 c nboxc nboxr r nbox025 nbox050 x z boxlim

% Compute the base 10 log of the count arrays and for 1/s for later ease of
% use in the fractal dimension calculation. The 'warning off all' line is
% used to suppress warnings generated by matlab when attempting to take the
% log base 10 of 0, which occurs when there are 0 counts in any category.
warning off all
cntlog=log10(bcount);sfrac=s.^-1;s_log=log10(sfrac);
clear bcount sfrac s
```

```
warning on all

% Next perform linear regression to get an estimate of slope, which is the
% equivalent of the box counting fractal dimension. The final array,
% entitled 'fractal' will contain the fractal dimension for increasing
% visibility (column number, from left to right) for all landing points in
% that particular visibility.

% In order to properly implement the linear regression function 'regress'
% some arrays need to be transposed. This ensures the variables are in the
% correct order for the regression function and is brought about with the
% '." command. Use the 'find' command to determine if any of the values
% for the particular box size and visibility are the log base 10 of 0,
% which matlab represents as negative infinity, or '-Inf'. If these
% values are found that particular calculation is skipped, leaving a 0 in
% the corresponding fractal array cell. The chance of generating a 0 from
% the regression equation is remote because only turbidity fronts with
% a minimum of 10 pixels were mapped, and of these the chance of getting a
% perfectly square point (a 'point', which has 0 dimension) is unlikely.
fractal=zeros(1,2);st=s_log.';
clear s_log
for vis=1:2;
  findinf=find(cntlog(1:5,vis:vis)==-Inf);
  if vis==1 & size(findinf,1)==0
    fractal(1,vis)=regress(cntlog(1:5,vis:vis),st);
  elseif vis==2 & size(findinf,1)==0
    fractal(1,vis)=regress(cntlog(1:5,vis:vis),st);
  end
end
clear cntlog findinf st vis

% For simplicity, compress related variables into single arrays. If this is
% desired, press 'Yes' on the question dialog box created by 'questdlg'.
% 'utm_values' contains the utm coordinates of band1, with page 1 (:,:,1)
% being northing and page 2 being easting. 'front_maps' contain the mapped
% turbidity fronts and their associated landing points. Page 1 is the 0.25
% m visibility and page 2 0.50. 'front_values' contain the
% turbidity front lengths associated with the landing points in
% alphabetical (row number) in both pixels (column 1) and distance as
% meters (column 2). The pages contain the visibilities in the same order
% as specified in 'front_maps'.
q=questdlg('Compress related information into 3-dimensional arrays?','Perform
Task','Yes','No','No');
if strcmp(q,'Yes')
  utm_values=northing;,utm_values(:,:,2)=easting;
  front_maps=divided_025;front_maps(:,:,2)=divided_050;
```

```
  front_values=fronts_025;front_values(:,:,2)=fronts_050;
  clear divided_025 divided_050 easting fronts_025 fronts_050 northing
end
clear q
openvar('fractal')

% The function can now be called simply with 'boxcount'.
% -- Function Complete -- %
```

Refinement of Turbidity Front Characteristics

```
% For the function below to work the desired visibility must be extracted from the
% 3-dimensional 'front_maps' and 'front_values' arrays to form one 2-dimensional array
% from each 3-dimensional array, composed of only the data from the desired visibility.
% These extracted arrays must be named 'front_maps' and 'front_values', respectively.
% Name the 3-dimensional arrays something else and recombine all visibilities to form
% new 3-dimensional arrays once all desired visibilities have been refined.

% -- Create the Function: refine -- %
edit refine

% This function removes non-south basin turbidity fronts from the satellite
% image. All removals are done manually and this function can be run
% as many times as desired. Turbidity front lengths are recalculated and
% overwritten previous values after a correction is applied to nullify the
% effect of varying resolution in the image due to original image location
% in the satellite's 'snapshot'. The fractal dimension is also
% recalculated, but the correction to nullify varying resolution is not applied to it because
% the fractal dimension calculation using box counting is relative to image size.

% 'cfactor' is the correction factor applied to the distances, with the
% third column of the 'front_values' array being the corrected distances.
% Column 1 is uncorrected distance in pixels, 2 uncorrected distance in
% kilometers. Rows are landing points in alphabetical order.

% IMPORTANT: The 'dividemap' workspace must be in the same directory as
% this function.

% View the image:
figure(1),set(1,'Name','  Regional Turbidity Fronts');set(1,'Position',[10,38,1005,653]);
imagesc(front_maps),load dividemap,colormap(dividemap),caxis([0 6]);

% Select the region where turbidity front is to be deleted.
% If no region is to be deleted simply select an area containing no
% turbidity front information and click 'yes' on the next question.
```

```
warn=warndlg('Click on upper-left & lower-right of region to be deleted','Select Region');
uiwait(warn);[c,r]=ginput(2);r=round(r);,c=round(c);
for rr=r(1,1):r(2,1);
  for cc=c(1,1):c(2,1);
    if front_maps(rr,cc)>1
      front_maps(rr,cc)=0;
    end
  end
end
clear c cc r rr warn
imagesc(front_maps),colormap(dividemap),caxis([0 6]);
clear dividemap

% Recalculate all measures of turbidity if all necessary deletions have
% been made:
q=questdlg('Recalculate front length and fractal dimension?','Perform
Task','Yes','No','No');
if strcmp(q,'Yes')
  front_values=zeros(5,3);
  ad=size(front_maps);
  % Recalculate turbidity front lengths.
  % Note that the new lengths are in kilometers.
  for r=1:ad(1,1);
    for c=1:ad(1,2);
      for lp=2:6;
        if front_maps(r,c)==lp
          front_values(lp-1,1)=front_values(lp-1,1)+1;
        end
      end
    end
  end
  front_values(:,2)=front_values(:,1).*0.25;
  clear c lp r

  % Set correction factor, given that the distance between the north tip of
  % elk island and willow point is 36 000 meters.
  warn=warndlg('Zoom in on Willow Point before pressing OK','Manipulate Map');
  uiwait(warn);
  [c(1,1),r(1,1)]=ginput(1);
  warn=warndlg('Zoom in on the northern tip of Elk Island before pressing
OK','Manipulate Map');
  uiwait(warn);
  [c(2,1),r(2,1)]=ginput(1);
  close 1
  d=(sqrt((c(2,1)-c(1,1))^2+(r(1,1)-r(2,1))^2))*250;
  cfactor=36000/d;
```

```
 front_values(:,3)=front_values(:,2).*cfactor;
 clear c d r warn

 % Recalculate the fractal dimension using the box counting technique.
 % See the 'boxcount' function for a description of the process.
 x=1;
 boxlim=fix(ad./16);
 bcount=zeros(5,1);
 s=zeros(1,5);
 for z=1:5;
  nboxr=boxlim(1,1)*16/x;
  nboxc=boxlim(1,2)*16/x;
  s(1,z)=1/nboxc;
  for r=1:nboxr;
   for c=1:nboxc;
    box025=front_maps(r*x-x+1:r*x,c*x-x+1:c*x);
    nbox025=find(box025>1);
    if size(nbox025,1)>0
     bcount(z,1)=bcount(z,1)+1;
    end
   end
  end
  x=x*2;
 end
 clear ad box025 c nboxc nboxr r nbox025 x z boxlim
 warning off all
 cntlog=log10(bcount);
 sfrac=s.^-1;
 s_log=log10(sfrac);
 clear bcount sfrac s
 warning on all
 fractal=0;
 st=s_log.';
 clear s_log
 findinf=find(cntlog(1:5,1)==-Inf);
 if size(findinf,1)==0
  fractal=regress(cntlog(1:5,1),st);
 end
 front_map=front_maps;
 clear cntlog findinf front_maps st
 openvar('fractal'),openvar('front_values')
else
 close 1
end
clear q
```

```
% The function can now be called simply with 'refine'.
% -- Function Complete -- %

% It is upon the refined turbidity front lengths and fractal dimensions that the
% relationships with CPUE were established.
```

Appendix 2: Location of Important Features in the South Basin

The location of the open-water centers (hereafter referred to as 'centers') and all associated fetches for each region and the south basin buoy are listed in the following tables. Table A2.1 lists the fetches for each region's center and the buoy while Table A2.2 lists the location of the centers and the buoy. The coordinates of each feature are described using the Universal Transverse Mercator (UTM) system in zone 14 U with a ten thousand meter grid (Canada Department of Energy, Mines and Resources 1988; Canada Department of Energy, Mines and Resources 1994). The regional boundaries were set by determining the approximate location from which the distance between one delivery location (around which the regions are centered) and its nearest neighbor were equal. The center of each region was then estimated. The fetches for the maximum significant wave height calculations were then measured from these centers.

Table A2.1 Fetches from the open water center of each region and the south basin buoy. Fetches are in meters; the associated compass heading and direction are given in the first two columns, respectively. Compass direction is in degrees.

Compass	Compass	Center or Item Fetch (meters)						
Heading	Direction (degrees)	Gimli	Riverton	Selkirk	Traverse Bay	Wanipigow	South Basin	Buoy C45140
N	360.0	36 250	23 000	63 500	30 500	11 250	40 500	26 750
NNE	22.5	66 250	28 750	35 250	11 000	13 500	43 250	48 250
NE	45.0	39 000	21 500	14 250	8 500	13 250	26 250	32 500
ENE	67.5	32 750	19 000	12 750	5 750	7 250	21 500	27 000
E	90.0	14 000	20 000	12 750	5 250	8 000	21 500	25 250
ESE	112.5	15 250	24 750	10 000	6 750	10 750	21 500	11 750
SE	135.0	16 500	30 500	8 500	7 000	14 250	24 250	18 000
SSE	157.5	30 750	21 000	7 000	19 250	36 750	15 000	26 000
S	180.0	30 500	60 500	6 750	16 500	33 500	45 000	44 250
SSW	202.5	27 750	51 250	6 500	13 500	69 750	47 000	38 000
SW	225.0	18 750	30 000	8 250	10 000	37 500	30 000	24 750
WSW	247.5	14 750	23 750	11 500	6 000	14 250	24 250	19 250
W	270.0	14 750	20 000	13 500	37 750	10 250	21 500	17 500
WNW	292.5	15 500	20 500	16 000	40 000	9 500	25 750	19 250
NW	315.0	19 250	9 750	22 000	32 500	11 750	27 250	22 750
NNW	337.5	31 750	10 750	41 750	43 000	14 500	23 500	36 250

Table A2.2 Universal Transverse Mercator coordinates of each regions' open water center and the location of the south basin buoy. Coordinates are in meters north (m N or 'northing') and meters east (m E or 'easting').

Region	Northing (m N)	Easting (m E)
Gimli	5 615 750	656 250
Riverton	5 645 500	664 000
Selkirk	5 591 000	658 875
Traverse Bay	5 630 000	680 750
Wanipigow	5 680 125	673 125
South Basin	5 630 000	664 625
Buoy C45140	5 628 929	659 995

Appendix 3: Details on the Construction of Generalized Linear Models

This appendix contains the annotated computer programming code used to construct typical generalized linear models (GLMs) utilized as the modeling tool for relating effort and CPUE to the environmental variables. All three modeling processes are described under their own respective headings: effort model construction, binary CPUE model construction, and continuous CPUE model construction. All computer code was written and used in R® version 2.1.1.

Effort Model Construction

```
# Read in the data; the first row should contain column headings with no quotation
# marks. To adjust for autocorrelation include the centered day of the year values.
# Centering is done by subtracting the day of the year median. Create the polynomials;
# they must be defined as separate variables in order to see a reduction in deviance due to
# each order. 'day' refers to the centered day of the year. Also create and center the
# environmental polynomials and express the 'year' variable as a factor.
day=julian-median(julian);day2=day^2;day3=day^3
vis=vis-mean(vis);vis2=vis^2;vis3=vis^3
temp=temp-mean(temp);temp2=temp^2;temp3=temp^3
press=press-mean(press);press2=press^2;press3=press^3
copac=copac-mean(copac);copac2=copac^2;copac3=copac^3
wave=wave-mean(wave);wave2=wave^2;wave3=wave^3
redf=redf-mean(redf);redf2=redf^2;redf3=redf^3
yearF=factor(year)

# Use a generalized linear model with a quasipoisson distribution and a log link. The
# log link is typical for this type of data but the quasipoisson family must be used instead
# of the conventional poisson distribution because the dispersion parameter is not 1.
# Select the statistically significant variables. This is done using a table of deviance. Only
# retain the polynomials which explain at least 2% of the null deviance. However,
# the year factor should always be included in the model (regardless of its statistical
# significance) for standardization purposes.

# Add and remove each variable individually to see what percentage of the null deviance
# it explains. The year factor is included at the start as stated previously. First create
# and name an array with all the polynomials in it.
vars=as.data.frame(cbind(day,day2,day3,vis,vis2,vis3,temp,temp2,temp3,press,press2,
press3,copac,copac2,copac3,wave,wave2,wave3,redf,redf2,redf3,yearF))
colnames(vars)=c("day","day2","day3","vis","vis2","vis3","temp","temp2","temp3",
"press","press2","press3","copac","copac2","copac3","wave","wave2","wave3","redf",
"redf2","redf3","yearF")
model.null=glm(ndeliv~yearF,family=quasipoisson(link="log"))
null.deviance=model.null$null.deviance

# Create an index specifying the number of variables to set the starting point at the null
# model with the year factor included (effort ~ constant + yearF).
varIndex=1:dim(vars)[2]
model.now=model.null

# Run the code below to determine the percentage of deviance each variable explains.
# Add the variable which explains the greatest percentage (fill in ?? after the 'update'
# command) and run the code again. Do this until no variables explain more than the
# threshold value. Note that once a variable is included in the 'update' line it is
# still examined in the loop but it has no impact because it is already included in the
```

```
# model. Once the final variable is included, the model generation step is complete.
devImp=as.numeric(NULL)
for (i in 1:length(varIndex)) {
  model.try=update(model.now,.~.+vars[,i])
  devImp=c(devImp,(model.now$deviance-model.try$deviance)/null.deviance*100)
}
names(devImp)=colnames(vars)
cbind(devImp);max(devImp)
model.now=update(model.now,.~.+??)

# Define the final model and create a summary.
j.glm=model.now;summary(j.glm);anova(j.glm)

# The suitability of model is estimated by the form of the standardized studentized
# deviance residuals - which should have a normal distribution. Extract the deviance
# residuals and standardize them by dividing by phi, the dispersion parameter, and 1-h,
# one minus the diagonal hat matrix entries. phi is returned in the summary(glm object)
# command.
j.phi=summary(j.glm)$dispersion

# Create the denominator for standardizing as above.
j.denom=sqrt(j.phi)*sqrt(1-hatvalues(j.glm))

# Extract the deviance residuals and standardize.
j.Dres=residuals(j.glm,type="deviance")/j.denom
```

Binary CPUE Model Construction

```
# Read in the binary data. To adjust for autocorrelation include the centered day of the
# year values. Centering is done by subtracting the day of the year median. Create the
# polynomials; they must be defined as separate variables in order to see a reduction in
# deviance due to each order. 'day' refers to the centered day of the year. Also create and
# center the environmental polynomials and express the 'year' variable as a factor.
day=julian-median(julian);day2=day^2;day3=day^3
vis=vis-mean(vis);vis2=vis^2;vis3=vis^3
temp=temp-mean(temp);temp2=temp^2;temp3=temp^3
press=press-mean(press);press2=press^2;press3=press^3
copac=copac-mean(copac);copac2=copac^2;copac3=copac^3
wave=wave-mean(wave);wave2=wave^2;wave3=wave^3
redf=redf-mean(redf);redf2=redf^2;redf3=redf^3
yearF=factor(year)

# For binomial data a generalized linear model is used with the binomial family and
# a complimentary log-log (cloglog) link function. The cloglog link is used because the
# scarcity of zeros and absence of extreme variable values suggests an asymmetrical
# relationship between the linear predictors and the observed values - the default logit
```

```
# link is symmetrical at the mean linear predictor value around the line y=x line. The
# quasibinomial family is used instead because the dispersion parameter estimate of 1 for
# the binomal family is not reasonable. Use a table of deviance to determine the deviance
# explained by the model. Record the null deviance for later use. Only retain polynomials
# which explain at least 2% of the null deviance. However, the year factor should always
# be included in the model (regardless of its statistical significance) for standardization
# purposes.

# Add and remove each variable individually to see what percentage of the null deviance
# it explains. The year factor is included at the start as stated previously. First create
# and name an array with all the polynomials in it.
vars=as.data.frame(cbind(day,day2,day3,vis,vis2,vis3,temp,temp2,temp3,press,press2,
press3,copac,copac2,copac3,wave,wave2,wave3,redf,redf2,redf3,yearF))
colnames(vars)=c("day","day2","day3","vis","vis2","vis3","temp","temp2","temp3",
"press","press2","press3","copac","copac2","copac3","wave","wave2","wave3","redf",
"redf2","redf3","yearF")
model.null=glm(cpue~yearF,family=quasibinomial(link="cloglog"))
null.deviance=model.null$null.deviance

# Create an index specifying the number of variables to set the starting point at the null
# model with the year factor included (cpue ~ constant + yearF).
varIndex=1:dim(vars)[2]
model.now=model.null

# Run the code below to determine the percentage of deviance each variable explains.
# Add the variable which explains the greatest percentage (fill in ?? after the 'update'
# command) and run the code again. Do this until no variables explain more than the
# threshold value. Note that once a variable is included in the 'update' line it is
# still examined in the loop but it has no impact because it is already included in
# the model. Once the final variable is included the model generation step is complete.
devImp=as.numeric(NULL)
for (i in 1:length(varIndex)) {
  model.try=update(model.now,.~.+vars[,i])
  devImp=c(devImp,(model.now$deviance-model.try$deviance)/null.deviance*100)
}
names(devImp)=colnames(vars)
cbind(devImp);max(devImp)
model.now=update(model.now,.~.+??)

# Define the final model and create a summary.
j.glm=model.now;summary(j.glm);anova(j.glm)

# Residuals are not tested because they are not informative for binomial models. Instead
# the hosmer-lemeshow test for goodness-of-fit is performed. If the resultant p-value is
# greater than 5% (by convention) then the model is appropriate for the data. It is first
# necessary to create the function.
```

```
HosmerLemeshow=function(y,pie) {
  o=order(pie);pie=pie[o];y=y[o];n=length(y)
  decY=rep(0,10);decPi=rep(0,10);decN=rep(0,10)
  decile=quantile(pie,probs=c(.1,.2,.3,.4,.5,.6,.7,.8,.9,1))
  decY[1]=sum(y[pie<=decile[1]])
  decPi[1]=mean(pie[pie<=decile[1]])
  decN[1]=length(y[pie<=decile[1]])
  for ( i in 2:10) {
    decY[i]=sum(y[pie>decile[i-1] & pie<=decile[i]])
    decPi[i]=mean(pie[pie>decile[i-1] & pie<=decile[i]])
    decN[i]=length(y[pie>decile[i-1] & pie<=decile[i]])
  }
  ChatNum=((decY-decN*decPi)^2);ChatDen=decN*decPi*(1-decPi)
  Chat=sum(ChatNum/ChatDen);df=8
  Xsq=qchisq(.95,8);pValue=pchisq(Chat,8,lower.tail=FALSE)
  list(Chat=Chat,df=df,Xsq=Xsq,pValue=pValue,decY=decY,decPi=decPi,decN=decN)
}

# Perform the test.
HosmerLemeshow(cpue,j.glm$fitted.values)

# Compare with the model using instead a logit link function. Ideally the logit model
# should have a lower p-value than the cloglog link function, but as long as the cloglog
# link function has a p-value>0.05 it is still appropriate. The reason for using a cloglog
# link is described above. First re-define the model using a logit link.
jL.glm=glm(cpue~,family=quasibinomial(link="logit"))

# Perform the test.
HosmerLemeshow(cpue,jL.glm$fitted.values)
```

Continuous CPUE Model Construction

```
# Read in the continuous data. To adjust for autocorrelation include the centered day of
# the year values. Centering is done by subtracting the day of the year median. Create the
# polynomials; they must be defined as separate variables in order to see a reduction in
# deviance due to each order. 'day' refers to the centered day of the year. Also create and
# center the environmental polynomials and express the 'year' variable as a factor.
day=julian-median(julian);day2=day^2;day3=day^3
vis=vis-mean(vis);vis2=vis^2;vis3=vis^3
temp=temp-mean(temp);temp2=temp^2;temp3=temp^3
press=press-mean(press);press2=press^2;press3=press^3
copac=copac-mean(copac);copac2=copac^2;copac3=copac^3
wave=wave-mean(wave);wave2=wave^2;wave3=wave^3
redf=redf-mean(redf);redf2=redf^2;redf3=redf^3
yearF=factor(year)
```

```
# Use a gamma distribution because the mean varies with the standard deviation as
# opposed to the variance and an inverse link function because this combination makes
# the standardized studentized deviance residuals the "most normal". Use a table of
# deviance to determine the deviance explained by the model. Record the null deviance
# for later use. Only retain the polynomials which explain at least 2% of the null
# deviance. However, the year factor should always be included in the model (regardless
# of its statistical significance) for standardization purposes.

# Add and remove each variable individually to see what percentage of the null deviance
# it explains. The year factor is included at the start as stated previously. First create
# and name an array with all the polynomials in it.
vars=as.data.frame(cbind(day,day2,day3,vis,vis2,vis3,temp,temp2,temp3,press,press2,
press3,copac,copac2,copac3,wave,wave2,wave3,redf,redf2,redf3,yearF))
colnames(vars)=c("day","day2","day3","vis","vis2","vis3","temp","temp2","temp3",
"press","press2","press3","copac","copac2","copac3","wave","wave2","wave3","redf",
"redf2","redf3","yearF")
model.null=glm(cpue~yearF,family=Gamma(link="inverse"))
null.deviance=model.null$null.deviance

# Create an index specifying the number of variables to set the starting point at the null
# model with the year factor included (cpue ~ constant + yearF).
varIndex=1:dim(vars)[2]
model.now=model.null

# Run the code below to determine the percentage of deviance each variable explains.
# Add the variable which explains the greatest percentage (fill in ?? after the 'update'
# command) and run the code again. Do this until no variables explain more than the
# threshold value. Note that once a variable is included in the 'update' line it is
# still examined in the loop but it has no impact because it is already included in
# the model. Once the final variable is included the model generation step is complete.
devImp=as.numeric(NULL)
for (i in 1:length(varIndex)) {
  model.try=update(model.now,.~.+vars[,i])
  devImp=c(devImp,(model.now$deviance-model.try$deviance)/null.deviance*100)
}
names(devImp)=colnames(vars)
cbind(devImp);max(devImp)
model.now=update(model.now,.~.+??)

# Define the final model and create a summary.
j.glm=model.now;summary(j.glm);anova(j.glm)

# The suitability of model is estimated by the form of the standardized studentized
# deviance residuals - which should have a normal distribution. Extract the deviance
# residuals and standardize them by dividing by phi, the dispersion parameter, and 1-h,
# one minus the diagonal hat matrix entries. phi is returned in the summary(glm object)
```

```
# command.
j.phi=summary(j.glm)$dispersion

# Create the denominator for standardizing as above.
j.denom=sqrt(j.phi)*sqrt(1-hatvalues(j.glm))

# Extract the deviance residuals and standardize.
j.Dres=residuals(j.glm,type="deviance")/j.denom
```

Appendix 4: Effort and Catch per Unit Effort Full Models

This appendix contains information on the effort and CPUE models generated for each region. The regression coefficient, Wald test p-value, and percentage of the null deviance explained (identified as "Dev Exp %") by each statistically significant variable and polynomial order are listed. The variables are listed in the order by which they were added to the model (from first to last). A given variable order was said to be statistically significant if it explained at least 2 % of the null deviance. Although not used as a statistical significance criterion directly, the Wald test p-values are supplied for comparison with the significance inferred by the deviance. The Wald test was chosen because of its superior performance under heteroscedastic conditions (Akritas and Papadatos 2004) which result from periodic deviations from the chosen distribution (see Tables 3.5 and 3.7).

Table A4.1 contains information on the effort models while Table A4.2 contains information on the continuous CPUE data models (Table A4.2A lists the walleye models while Table A4.2B lists the sauger models). Binary CPUE models were not informative and are not shown. Variable abbreviations are as follows: copac = cloud opacity, temp = dry bulb temperature, redf = Red River flow, wave = maximum significant wave height, and year = year factor. For all models 'day' was defined as the day of the year (where January 1 of each year was day 1). The number after the variable name indicates the polynomial order of the variable (no number for order 1). For example, 'temp2' is the squared temperature term.

Table A4.1 Effort models by region.

Early Period				Late Period			
GIMLI REGION							
Variable	Coefficient	p-value	Dev Exp (%)	Variable	Coefficient	p-value	Dev Exp (%)
intercept	2.190E+00	< 0.001		intercept	2.990E+00	< 0.001	
year		< 0.001	35.361	year		< 0.001	6.122
day	-5.290E-02	< 0.001	27.500	day2	-6.060E-04	< 0.001	8.633
day3	4.090E-05	< 0.001	2.834	temp	2.080E-02	< 0.001	6.256
RIVERTON REGION							
Variable	Coefficient	p-value	Dev Exp (%)	Variable	Coefficient	p-value	Dev Exp (%)
intercept	1.641E+00	< 0.001		intercept	3.870E-01	< 0.001	
year		< 0.001	22.590	year		< 0.001	36.408
day	-2.348E-02	< 0.001	16.834	wave	-9.860E-01	< 0.001	10.115
day2	-6.285E-04	< 0.001	3.053	day2	-6.340E-04	< 0.001	8.525
wave	-5.392E-01	< 0.001	2.718				
SELKIRK REGION							
Variable	Coefficient	p-value	Dev Exp (%)	Variable	Coefficient	p-value	Dev Exp (%)
intercept	1.670E+00	< 0.001		intercept	1.805E+00	< 0.001	
year		< 0.001	23.861	year		< 0.001	12.755
day	-1.410E-02	< 0.001	12.564	day2	-7.401E-04	< 0.001	16.044
temp3	4.700E-04	< 0.001	6.580	day	-8.865E-03	< 0.001	9.124
wave2	-2.110E+00	< 0.001	3.756				
TRAVERSE BAY REGION							
Variable	Coefficient	p-value	Dev Exp (%)	Variable	Coefficient	p-value	Dev Exp (%)
intercept	2.239E+00	< 0.001		intercept	2.480E+00	< 0.001	
year		< 0.001	20.890	year		< 0.001	7.374
day	-2.945E-02	< 0.001	23.342	day2	-7.570E-04	< 0.001	12.484
day2	-8.024E-04	< 0.001	4.877	temp	2.530E-02	< 0.001	8.444

Table A4.1 Effort models by region (continued).

Early Period				Late Period			
WANIPIGOW REGION							
Variable	Coefficient	p-value	Dev Exp (%)	Variable	Coefficient	p-value	Dev Exp (%)
intercept	1.936E-01	0.483		intercept	1.900E+00	< 0.001	
year		< 0.001	24.198	year		< 0.001	7.933
day2	-1.660E-03	< 0.001	10.411	day2	-8.010E-04	< 0.001	15.316
day	-2.037E-02	< 0.001	5.674	wave	-8.250E-01	< 0.001	7.445
temp	2.881E-02	0.003	3.481				
SOUTH BASIN REGION							
Variable	Coefficient	p-value	Dev Exp (%)	Variable	Coefficient	p-value	Dev Exp (%)
intercept	3.341E+00	< 0.001		intercept	3.790E+00	< 0.001	
year		< 0.001	26.300	year		0.097	1.923
day	-3.490E-02	< 0.001	25.717	day2	-7.900E-04	< 0.001	17.594
day2	-9.357E-04	< 0.001	5.455	temp	2.040E-02	< 0.001	7.022
				wave	-4.690E-01	< 0.001	3.627

Table A4.2A Continuous walleye CPUE models by region.

Continuous Walleye (Early Period)				Continuous Walleye (Late Period)			
GIMLI REGION							
Variable	Coefficient	p-value	Dev Exp (%)	Variable	Coefficient	p-value	Dev Exp (%)
intercept	9.810E-03	< 0.001		intercept	8.260E-03	< 0.001	
year		0.017	5.666	year		< 0.001	8.397
day	2.220E-04	< 0.001	24.316	day	-7.690E-05	< 0.001	18.038
RIVERTON REGION							
Variable	Coefficient	p-value	Dev Exp (%)	Variable	Coefficient	p-value	Dev Exp (%)
intercept	3.720E-02	< 0.001		intercept	1.430E-02	< 0.001	
year		< 0.001	25.984	year		< 0.001	22.802
day	3.920E-04	< 0.001	24.544	day	-3.320E-04	< 0.001	28.434
redf3	2.190E-11	< 0.001	2.293	day2	5.920E-06	< 0.001	3.371
SELKIRK REGION							
Variable	Coefficient	p-value	Dev Exp (%)	Variable	Coefficient	p-value	Dev Exp (%)
intercept	1.960E-02	< 0.001		intercept	1.410E-02	< 0.001	
year		< 0.001	12.085	year		< 0.001	20.209
day	6.100E-04	< 0.001	28.933	temp	2.420E-04	< 0.001	5.661
TRAVERSE BAY REGION							
Variable	Coefficient	p-value	Dev Exp (%)	Variable	Coefficient	p-value	Dev Exp (%)
intercept	1.470E-02	< 0.001		intercept	1.240E-02	< 0.001	
year		< 0.001	14.880	year		< 0.001	11.199
day	3.910E-04	< 0.001	35.753	day	-9.690E-05	< 0.001	12.389

Table A4.2A Continuous walleye CPUE models by region (continued).

Continuous Walleye (Early Period)				Continuous Walleye (Late Period)			
WANIPIGOW REGION							
Variable	Coefficient	p-value	Dev Exp (%)	Variable	Coefficient	p-value	Dev Exp (%)
intercept	2.880E-03	0.001	0.001	intercept	1.410E-02	< 0.001	
year		< 0.001	44.983	year		< 0.001	23.179
temp	2.180E-04	0.011	2.262	day	-1.900E-04	< 0.001	18.154
				day2	5.860E-06	< 0.001	5.707
SOUTH BASIN REGION							
Variable	Coefficient	p-value	Dev Exp (%)	Variable	Coefficient	p-value	Dev Exp (%)
intercept	1.430E-02	< 0.001		intercept	9.720E-03	< 0.001	
year		< 0.001	12.702	year		< 0.001	11.244
day	3.070E-04	< 0.001	32.029	day	-1.240E-04	< 0.001	28.802
				day2	1.880E-06	< 0.001	2.026

Table A4.2B Continuous sauger CPUE models by region.

Continuous Sauger (Early Period)				Continuous Sauger (Late Period)			
GIMLI REGION							
Variable	Coefficient	p-value	Dev Exp (%)	Variable	Coefficient	p-value	Dev Exp (%)
intercept	1.512E-01	< 0.001		intercept	2.251E-02	< 0.001	
year		< 0.001	9.730	year		< 0.001	41.622
day	-2.034E-03	< 0.001	10.967				
copac	-4.621E-04	< 0.001	4.714				
RIVERTON REGION							
Variable	Coefficient	p-value	Dev Exp (%)	Variable	Coefficient	p-value	Dev Exp (%)
intercept	4.090E-01	< 0.001		intercept	2.505E-02	< 0.001	
year		< 0.001	19.691	year		< 0.001	59.911
day	-8.180E-03	< 0.001	5.198				
temp2	-2.230E-03	< 0.001	4.725				
day2	3.410E-04	< 0.001	3.152				
SELKIRK REGION							
Variable	Coefficient	p-value	Dev Exp (%)	Variable	Coefficient	p-value	Dev Exp (%)
intercept	2.700E-02	< 0.001		intercept	5.746E-02	< 0.001	
year		< 0.001	10.427	year		< 0.001	34.299
day	-4.450E-04	< 0.001	13.727				
TRAVERSE BAY REGION							
Variable	Coefficient	p-value	Dev Exp (%)	Variable	Coefficient	p-value	Dev Exp (%)
intercept	8.210E-02	< 0.001		intercept	4.021E-02	< 0.001	
year		< 0.001	13.399	year		< 0.001	39.752
day	-3.050E-03	< 0.001	8.367				
temp	5.780E-03	< 0.001	8.046				
day2	5.650E-05	0.003	2.009				

Table A4.2B Continuous sauger CPUE models by region (continued).

Continuous Sauger (Early Period)				Continuous Sauger (Late Period)			
WANIPIGOW REGION							
Variable	Coefficient	p-value	Dev Exp (%)	Variable	Coefficient	p-value	Dev Exp (%)
intercept	7.411E-02	0.022		intercept	3.605E-02	< 0.001	
year		< 0.001	68.799	year		< 0.001	43.559
wave3	-6.092E+00	0.006	12.924				
SOUTH BASIN REGION							
Variable	Coefficient	p-value	Dev Exp (%)	Variable	Coefficient	p-value	Dev Exp (%)
intercept	4.000E-02	< 0.001		intercept	2.837E-02	< 0.001	
year		0.002	1.587	year		< 0.001	56.852
redf2	1.400E-07	< 0.001	4.707				
redf	-3.170E-05	0.002	2.318				
copac	-4.170E-04	< 0.001	2.208				
temp	-2.250E-03	0.001	2.164				